Doctoral Dissertation

Doctoral Program in Bioengineering and Medical-Surgical Sciences

(32nd Cycle)

Magneto-plasmonic nanoparticles for photothermal therapy

Cristina Multari

Supervisors

Prof. Enrica Vernè

Prof. Marta Miola, Co-Supervisor

Politecnico di Torino

November, 2020

A mio figlio Guglielmo

I hereby declare that, the contents and organisation of this dissertation constitute my own original work and does not compromise in any way the rights of third parties, including those relating to the security of personal data.

……..

Cristina Multari

Turin, July 29, 2020

Summary

The activities performed during the present PhD thesis were mainly focused on the synthesis, optimization process and characterization of magneto-plasmonic nanoparticles (MPNPs) composed by a magnetic core (SPIONs) and an external gold or silver nanoparticles decoration (Au and Ag NPs respectively), that could be used as advanced system in magneto-photothermal therapy and diagnosis of cancer.

The aim was to produce these MPNPs-Au/Ag with the innovative use of tannic acid (TA), an organic compound with antioxidant, antiviral, anti-inflammatory, and anticarcinogenic properties, maintaining the peculiar characteristics of both nanomaterials. This allowed to generate a hybrid nanosystem that could act as drug delivery system and contrast agent for magnetic resonance (directly reaching the tumor site), while concurrently allowing photothermal therapy.

In particular, the MPNPs-Au/Ag were synthetized through two different route:

- In the first route the nanoplatforms were synthetized through a simple co-precipitation method in which the citric acid was used as stabilizing agent and APTES as functionalizantion to immobilize the TA reduced Au NPs or Ag NPs.
- In the second routes, the efforts were devoted to improve the preparation of MPNPs-Au/Ag usying the TA as reducing and stabilizing agent, avoiding the use of any other reagents. This allow to obtain the nanoplatforms through a new, simple and green synthesis method.

For both synthesis routes, the correct formations of MPNPs-Au/Ag were detected by physical, chemical and morphological characterization methods demonstrating the good dispersion and the correct grafting of metal nanoparticles on SPIONs surface. Then, the magneto-plasmonic properties were detected with magnetic and optical characterization which confirm their ability to maintain the peculiar properties of both nanomaterials.

Moreover, the ability of the as-synthetized MPNPs-Au/Ag to produce heat, was studied by irradiating the samples with a laser light, confirming the capability of the metal NPs to generate heating in the surrounding fluid and therefore to be potentially used for photothermal therapy.

A cytotoxicity study was also performed to preliminary asses the biocompatibility of the NPs and to establish the MPNPs concentration that would not damage the healthy cells. For this purpose, the effect of MPNPs-Au/Ag were detected both on healthy and cancer cells.

Finally, in order to analyze the efficacy of MPNPs in contact with healthy and cancer cells, a green laser source was used to evaluate the ability of Au NPs to convert absorbed light into thermal energy. Cell tests confirmed that MPNPs-Au causes an important damage of cancer cells, if exposed to laser light; while is not resulting dangerous in normal cells. This indicate that the MPNPs-Au allows to convert the light received into heating which can destroy cancer cells, due to their high heat sensitivity.

In conclusion, the synergy and the combined effect of SPIONs and metal NPs allows us to maintain the possibility of precisely driving the MPNPs to a specific tumour site using an external magnetic field, due to their superparamagnetic response, and to produce heat by converting the light received from laser irradiation into thermal energy, due to the Au NPs' decoration.

Thus, these hybrid nanoplatforms have great potential for use in photothermal therapy in cancer.

Table of Contents

List of Tables

List of Figures

Chapter 1

Introduction and aim of the work

In recent years, much research have focused on the field of cancer treatment because the world mortality data for cancer diseases indicate a necessity for novel therapeutic approaches and new pharmaceutical agents to overcome cancer[1]. Many studies have concentrated on new-generation cancer medicines that offer good alternatives to conventional cytotoxic compound-based chemotherapy.

One of new therapeutic approaches that has aroused great interest is photothermal therapy. Compared to other conventional therapies (such as, chemotherapy, radiotherapy and surgery) it shows repeatable results, no toxicity and reduced invasiveness; moreover, its efficacy has been demonstrated in different types of cancer[2].

Despite this promising background, photothermal therapy still suffers from several limitations[3–5], such as low selectivity of tumors, low bioavailability and low tissue penetration. In this therapy, many common photosensitizers must be activated with visible light, generally in the window (620-750 nm). This window is characterized by a low depth of penetration in tissues and therefore the clinical application of phototherapy is currently limited to superficial and flat lesions.

The purpose of the present project is to overcome this limitation of phototherapy with the support of nanotechnology. Due to the innovative improvements of

nanotechnological techniques, it is possible to develop new nano-sized materials for biomedical applications.

In particular, the idea is to combine different kinds of nanoparticles (NPs) obtained from eco-friendly materials and develop hybrid nanoplatforms, thus creating an innovative approach for the magneto-photothermal therapy of cancer.

NPs have attracted huge attention recently because of their excellent aptitude to be used as nanocarriers for many therapeutic strategies[6], such as delivering therapeutic payloads at tumour site, carrying different theranostic agents or providing a non-invasive imaging of a specific tumor. Much attention has been paid to superparamagnetic iron oxide nanoparticles (SPIONs), gold nanoparticles (Au NPs) and silver nanoparticles (Ag NPs) because they possess unique properties, which make them very attractive for the developement of hybrid nanoplatform.

SPIONs are known for their ability to be used in different biomedical applications, such as contrast agents in magnetic resonance imaging (MRI), heat sources for hyperthermia and vectors for drug delivery, especially in cancer therapy[7,8]. Moreover, these materials are suitable for therapeutic and diagnostic purposes thanks to their well-known chemical-physical properties, in fact, they possess the great ability to be activated through an external magnetic field without retaining any magnetism once the field has been removed[9]. Thanks to these exceptionl physical, chemical and magnetic properties, SPIONs are one of the most promising candidates in cancer theranostic. Furthermore, they demonstrate high biocompatibility, low toxicity and biodegradability.

Au NPs have received large attention in cancer research due to their high stability, ease of synthesis and surface modification and excellent biocompatibility, in fact, even at high concentration, they present very low toxicity. Moreover, thanks to their particular chemical, physical and morphological characteristic it has been selected as one of the best candidate to works as photosensitizers[10]. They present a unique photo-physical phenomenon, called surface plasmon resonance (SPR), resulting from the interaction with light radiation. This allow Au NPs to be externally activated and controlled by using a light stimulus. Thanks to the SPR effect, Au NPs can be used as non-conventional dye in photothermal therapy: when Au NPs are irradiated with a laser light in a specific wavelength, they can transform the radiation into thermal energy by producing heat. This bring cancer cells into apoptosis, due to their increased heat sensitivity[10].

Ag NPs have been broadly used as antibacterial and anticancer agents due to their intrinsic cytotoxicity given by their high degree of toxicity against cells. Thanks to their distinctive physiochemical properties and anti-inflammatory, antibacterial functional features, Ag NPs play an important role in the development of novel biomedical applications. Moreover, Ag NPs are also plasmonic structure and possess the exceptional ability to scatter visible light thanks to the SPR effect so they are able to absorb light and scatter to a specific wavelength, this makes them a suitable approach for cancer theranostic.

Thanks to the attractive physico-chemical properties and excellent ability of SPIONs, Au NPs and Ag NPs described above, these nanoparticles were selected to create a hybrid nano-sized structure. The structures are capable of maintaining the peculiar abilities of each nanomaterial and thus represent an innovative approach in magneto-photothermal therapy of cancer.

The magneto-plasmonic nanoplatform (MPNPs) are composed of a magnetic core and external gold or silver NPs decoration (MPNPs-Au and MPNPs-Ag) acting in synergy. The MPNPs simultaneously possess both magnetic and plasmonic properties. The magnetic properties allow drug delivery and imaging while the thermal action occurs as a result of the SPR absorption of Au NPs or Ag NPs.

During the thesis work the two nanostructures MPNPs-Au and MPNPs-Ag are developed and characterized with the same approach through highly performing techniques in order to explore both routes and evaluate which was the best performing solution.

One of the major challenge and novelty of this work is to optimize the MPNPs procedure in terms of materials, properties, scalability and cost-efficiency by means of the innovative use of tannic acid (TA). TA, a polyphenolic compound extracted from plants, is proposed as stabilizing and reducing agent to create a new, simple and green synthetized MPNPs. In this project, TA is successfully used as eco-friendly agent capable of reducing Au or Ag NPs directly on SPIONs surface while ensuring a good stabilization of the dispersion. In recent years, many studies[11–15] have concentrated on the use of polyphenolic compounds as green routes to stabilize or reduce NPs, but to the author best knowledge, this is the first study on the ability of TA to act simultaneously within few minutes as reducing agent for Au

or Ag NP and stabilizing agent for MPNPs-Au and MPNPs-Ag hybrid nanoplatforms.

An additional aim is to investigate the cytotoxicity of the as-prepared MPNPs-Au and MPNPs-Ag in contact with different healthy and cancer cells. This allow to study the ability of the nanoplatforms to work as phototherapy system in contact with cancer cells evaluating their potential use for biomedical application.

Thus, due to the tailored optimization that the present thesis work will offer, the final hybrid nanoplatforms that will be selected among the other syntheses, will offer a great improvement in cancer therapy over existing pure magnetic or plasmonic nanoparticles. These nanoplatforms give the possibility of precisely driving the MPNPs to a specific tumour site using an external magnetic field and contemporaneously produce heat by converting the light received from laser irradiation into thermal energy.

1. Stewart BW, Kleihues P. World cancer report. 2003.
2. Sibata CH, Colussi VC, Oleinick NL, Kinsella TJ. Photodynamic therapy in oncology. *Expert Opin Pharmacother*. 2001;2(6):917-927. doi:10.1517/14656566.2.6.917.
3. Oleinick NL, Evans HH. The photobiology of photodynamic therapy: cellular targets and mechanisms. *Radiat Res*. 1998;150(5 Suppl):S146-56.
4. Ricchelli F. Photophysical properties of porphyrins in biological membranes. *J Photochem Photobiol B*. 1995;29(2-3):109-118. doi:10.1016/1011-1344(95)07155-u.
5. Dougherty TJ, Gomer CJ, Henderson BW, et al. Photodynamic therapy. *J Natl Cancer Inst*. 1998;90(12):889-905. doi:10.1093/jnci/90.12.889.
6. Martinelli C, Pucci C, Ciofani G. Nanostructured carriers as innovative tools for cancer diagnosis and therapy. *APL Bioeng*. 2019;3(1):11502. doi:10.1063/1.5079943.
7. Tefft BJ, Uthamaraj S, Harburn JJ, Klabusay M, Dragomir-Daescu D, Sandhu GS. Cell Labeling and Targeting with Superparamagnetic Iron Oxide Nanoparticles. *J Vis Exp*. 2015;(105):e53099. doi:10.3791/53099.
8. Pietronave S, Iafisco M, Locarno D, Rimondini L, Maria Prat M. Functionalized nanomaterials for diagnosis and therapy of cancer. *J Appl Biomater & Biomech JABB*. 2009;7(2):77-89. http://europepmc.org/abstract/MED/20799167.
9. Conde J, Dias JT, Grazú V, Moros M, Baptista P V, de la Fuente JM. Revisiting 30 years of biofunctionalization and surface chemistry of inorganic nanoparticles for nanomedicine. *Front Chem*. 2014;2:48. doi:10.3389/fchem.2014.00048.
10. Menon JU, Jadeja P, Tambe P, Vu K, Yuan B, Nguyen KT. Nanomaterials for Photo-Based Diagnostic and Therapeutic Applications. *Theranostics*. 2013;3:152-166. doi:10.7150/thno.5327.
11. Zhang J, Chen D, Han D, et al. Tannic acid mediated induction of apoptosis in human glioma Hs 683 cells. *Oncol Lett*. 2018;15(5):6845-6850.
12. Dong G, Liu H, Yu X, et al. Antimicrobial and anti-biofilm activity of tannic acid against Staphylococcus aureus. *Nat Prod Res*. 2018;32(18):2225-2228. doi:10.1080/14786419.2017.1366485.
13. Veisi H, Moradi SB, Saljooqi A, Safarimehr P. Silver nanoparticle-decorated

on tannic acid-modified magnetite nanoparticles (Fe3O4@TA/Ag) for highly active catalytic reduction of 4-nitrophenol, Rhodamine B and Methylene blue. *Mater Sci Eng C*. 2019;100:445-452. doi:https://doi.org/10.1016/j.msec.2019.03.036.

14. Ahmad T. Reviewing the Tannic Acid Mediated Synthesis of Metal Nanoparticles. Thundat T, ed. *J Nanotechnol*. 2014;2014:954206. doi:10.1155/2014/954206.
15. Aromal SA, Philip D. Facile one-pot synthesis of gold nanoparticles using tannic acid and its application in catalysis. *Phys E Low-dimensional Syst Nanostructures*. 2012;44(7-8):1692-1696. doi:10.1016/j.physe.2012.04.022.

Chapter 2

Nanotechnology

Nanotechnology is a rapidly expanding field which involves various sectors, including engineering, electronics, materials sciences and biomedicine[1]. In fact, nanotechnologies represent a well-established reality in the scientific world as they allow to study and produce materials, structures and devices with innovative properties and functionalities[2]. They are based on a set of technologies and processes that require a multidisciplinary approach involving numerous research fields ranging from supramolecular chemistry to quantum physics, from material science to molecular biology, from mechanical to chemical or electronic engineering. The term 'nanotechnology' first appeared in1974 in the paper "On the basic concept of Nano-Technology" written by N. Taniguchi in which he wrote: "'Nano-technology mainly consists of the processing of separation, consolidation, and deformation of materials by one atom or one molecule"[3]. This is the first scientific publication in which the feasibility of nanotechnology was demonstrated. The revolutionary perspectives associated with nanotechnologies derive from the fact that behaviors and characteristics of matter in the colloidal state have drastically different dimensions from those observed in macro dimensions[4]. In fact, nanotechnology use the properties developed by a material at its nanometric scale which differ in terms of properties from the same material at a bigger scale[4–6].

Nanotechnologies find application in many productive sectors[7]: here are reported some of many current or potential applications in the scientific and technological fields (figure 2.1)[5,6,8].

Figure 2. 1 Nanotechnologies applications

Nanoelectronics

Nanotechnology can improve the characteristics of electronic devices by reducing their weight and energy dissipation, improving their capacity through the increase of memory chip density and decreasing the size of transistors used in integrated circuits in order to create smaller and more powerful devices[9].

Environment

Nanotechnology can help reduce both air and water pollution[10].

The air quality can be improved by acting, for example, on the performance of the catalysts used to transform the vapors escaping from automobiles or industrial plants into harmless gases. The greater surface area of nanotechnological catalysts

allows them to interact simultaneously with more chemicals, demonstrating greater efficacy than the conventionally used counterpart.

In improving water quality, on the other hand, nanotechnology is being sought to develop solutions to different problems. A challenge is the removal of industrial water pollution using nanoparticles to convert the contaminant, through chemical reactions, and make it harmless. Another challenge is the removal of salt or metals from water[11]: deionization methods based on electrodes composed of nanometric fibers are promising in reducing costs and energy requirements for transforming salt water into drinking water[12].

Chemical sensors

Carbon nanotubes, zinc oxide nanowires or palladium nanoparticles can be used as sensing elements in nanotechnological sensors. The operating principle is based on changing the electrical characteristics, such as resistance or capacity, of the sensitive element following the absorption of few gas molecules; this allows to detect even very low concentrations of chemical vapors[13,14].

A possible application could be the assembly of these sensors in places where you want to check for the presence of vapors emitted by explosive devices, in order to guarantee safety[15].

Textile industry

The textile production of fabrics containing particles or fibers at nanometric dimensions allows an improvement of the properties without a significant increase in weight, thickness or stiffness[16]. Current applications concern, among others, the use of nanowhiskers for the production of water repellent and stain-resistant pants or the use of silver nanoparticles in order to kill bacteria and make garments odor-free[17].

Agribusiness

Nanotechnology can influence different aspects of food science, from how food is grown to how it is packaged, but also food safety or the health benefits offered by food[18].

An application under development consists of the use of nanosensors able to detect bacteria and other contaminants in packaging plants. This would allow

frequent testing at a lower cost than sending samples to an analytical laboratory and as a consequence, would significantly reduce the risk of contaminated food.

Sport

Nanotechnology is also able to offer advantages in the sports sector by improving not only the equipment, but also the athlete's performance level in order to reduce the risk of injuries and make the sporting experience more enjoyable for athletes and spectators.

Some of the current applications include the addition of nanoparticles to the frame of the tennis rackets which allow better control and greater power when hitting the ball, or filling with silica nanoparticles the spaces between the carbon fibers in the fishing rods, in order to strengthen them without increasing their weight[19].

Nanomedicine

It deals with diagnosing, monitoring, treating and preventing diseases in order to improve and make existing treatments more effective and develop new therapies[20].

The contribution of nanotechnologies in the medical sector is very broad and includes new diagnostic tools, agents and imaging methods, systems for administering drugs, therapies, implants and constructs capable of repairing and regenerating tissues and organs[21,22].

This is made possible by the manipulation of atoms and molecules at the nanoscale level to produce structures with desired properties and of dimensions comparable to those of biomolecules, able to interact with the cells of the human body.

2.1 Nanotechnology in medicine

Nanomedicine is the application of nanotechnology to achieve innovation in clinics, which studies the biological effect that takes place inside the cells and uses this information for the engineering of nanomaterials and biosensors and the development of increasingly sophisticated medical therapies[20,23,24].

Nanomedicine deals specifically with the development of nanotechnologies for pharmacological and medical applications and its goal is to obtain drugs and devices of exactly controlled structure and composition and with dimensions comparable to those of the biomolecules which they must interact with. Nanomedicine is emerging in many areas thanks to the development of new materials that are changing the operative methods with new applications in the surgical field, supplying prostheses that are always better tolerated and more biocompatible[25]. The use of systems comparable in size to those of a virus that can easily penetrate cells allows the development of systems for earlier and more accurate diagnosis. In therapy, nanotechnologies can lead to benefits with regards to the use of drugs with inadequate chemical-physical and biopharmaceutical properties (biopharmaceutical class II, III and IV drugs). For example, it is possible to obtain drugs with improved solubility characteristics or to encapsulate the drug in a suitable lipid and polymeric coating that allows to overcome the gastrointestinal barriers and to quickly reach the circulation. In any other field the effects of nanotechnologies have been as relevant as in oncology because they allow to exploit some peculiarities of the tumor tissue such as vessel permeability and retention in tumor tissues. Modified proteins, liposomes, polymeric micelles, nanoparticles and nanogels have already entered the market or are undergoing clinical trials[26].

One of the mayor applications developed by nanomedicine is the use of nanoparticles which are capable of conveying drugs, heat or other substances within our body in a targeted manner, i.e. directed to specific cells. In fact, regardless of the severity of the disease, systemic administration of drug molecules produces side effects (or in more serious cases toxic effects) related to therapy[27]. Nanomedicine offer improvements both in terms of selectivity towards the diseased tissue or cell, and in the administration of hardly soluble active ingredients as well as degradation stability[26].

European Science Foundation (ESF) Forward Look Nanomedicine defined, through a consensus conference, nanomedicine in the following way: "Nanomedicine is the discipline that uses nanometric tools for the diagnosis, prevention and treatment of diseases and for having a greater understanding of the complex physiopathological mechanisms underlying diseases. Therefore, the ultimate goal is to improve the quality of life. "

2.1.1 Nanomedicine in cancer treatment

One of the main goals of nanomedicine is the development of new and more efficient cancer treatments that are able to improve the efficiency of the currently available chemo-therapeutic agents and allow an early pre-symptomatic diagnosis of cancer. In fact, conventional therapies for treating cancer such as surgery, radiotherapy, chemotherapy and immunotherapy, are still ineffective in some cases[19] and in addition they can have serious side effect as well as different drawbacks as non-selectivity, high toxicity and invasiveness[27]. Moreover, the patient's tolerable level of toxicity to radiotherapy or chemotherapy limits their applications and therefore their beneficial effect.

Hence, nanomedicine compared with traditional therapy and chemotherapeutic drugs, offers the opportunity to combine multiple function in a single system that is able to target, monitor and treat cancer: this aptitude is known as “theranostic” effect, which is the ability to combine diagnostic and therapeutic capability in a single system (figure 2.2).

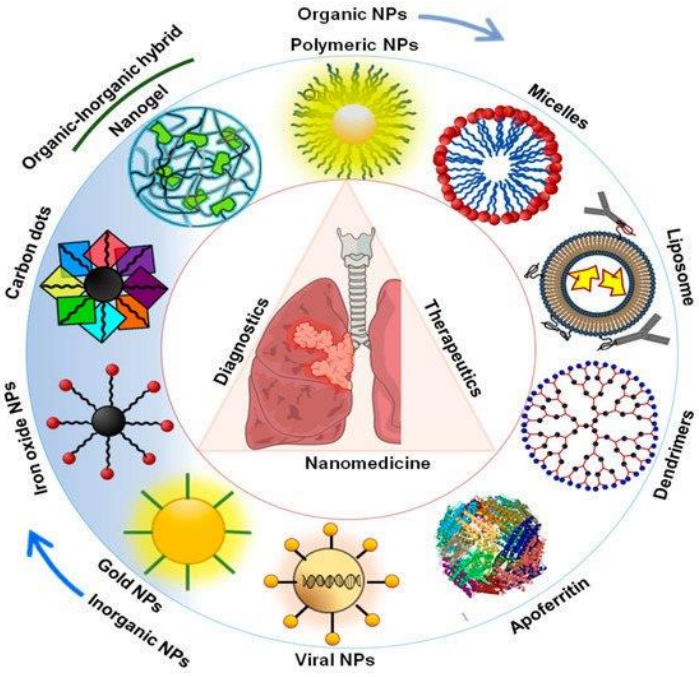

Figure 2. 2 Representation of different nanomedicine approaches in lung cancer theranostic.[28]

Another important advantage of nanomedicine is that allow the delivery of a drug in a protected nanosystem through the biological barriers with a high degree

of transport and protection from the immune system, in this way the efficacy of therapy is improved[29]. In fact, thanks to drug delivery is possible to have a controlled transport of a drugs in a specific site and release it in a time-dependent way, without affecting healthy organs. This allow to obtain different advantaged such as the reduction of the drug's dose to be administrated, the minimization of the undesirable side effects and so the improvement of therapeutic index.

Drug delivery solves the problem attributed to the poor solubility of drugs in water and consequently the low absorption of the drug by the body.

Specifically addressing the drugs to the desired site of action, in particular the anticancer drugs to tumors, is becoming a challenge that is currently being addressed. Nowadays, the challenge is to design a theranostic nanovector combining the use of biocompatible materials to exploit their properties and peculiarities in order to achieve structures that can increase the therapeutic effects and the efficiency of diagnosis while controlling that the two mechanisms occur at different times of action.

Here are reported some nanomaterials gained approval by Food and Drug Administration (FDA) and are commonly used in medicine nowadays (Table 2.1).

Table 2. 1 Nanomaterials undergoing clinical trials or FDA approved[21]

Table 1. Examples of Nanomaterials in Clinical Use.*

Nanomaterial	Trade Name	Application	Target	Adverse Effects	Manufacturer	Current Status
Metallic						
Iron oxide	Feridex	MRI contrast	Liver	Back pain, vasodilatation	Bayer Schering	FDA approved
	Resovist	MRI contrast	Liver	None	Bayer Schering	FDA approved
	Combidex	MRI contrast	Lymph nodes	None	Advanced Magnetics	In phase 3 clinical trials
	NanoTherm	Cancer therapy	Various forms	Acute urinary retention	MagForce	In phase 3 clinical trials
Gold	Verigene	In vitro diagnostics	Genetic	Not applicable	Nanosphere	FDA approved
	Aurimmune	Cancer therapy	Various forms	Fever	CytImmune Sciences	In phase 2 clinical trials
Nanoshells	Auroshell	Cancer therapy	Head and neck	Under investigation	Nanospectra Biosciences	In phase 1 clinical trials
Semiconductor						
Quantum dot	Qdots, EviTags, semiconductor nanocrystals	Fluorescent contrast, in vitro diagnostics	Tumors, cells, tissues, and molecular sensing structures	Not applicable	Life Technologies, eBioscience, Nanoco, CrystalPlex, Cytodiagnostics	Research use only
Organic						
Protein	Abraxane	Cancer therapy	Breast	Cytopenia	Abraxis Bioscience	FDA approved
Liposome	Doxil/Caelyx	Cancer therapy	Various forms	Hand–foot syndrome, stomatitis	Ortho Biotech	FDA approved
Polymer	Oncaspar	Cancer therapy	Acute lymphoblastic leukemia	Urticaria, rash	Rhône-Poulenc Rorer	FDA approved
	CALAA-01	Cancer therapy	Various forms	Mild renal toxicity	Calando	In phase 2 clinical trials
Dendrimer	VivaGel	Microbicide	Cervicovaginal	Abdominal pain, dysuria	Starpharma	In phase 2 clinical trials
Micelle	Genexol-PM	Cancer therapy	Various forms	Peripheral sensory neuropathy, neutropenia	Samyang	For phase 4 clinical trials

* MRI denotes magnetic resonance imaging.

In the specific case of cancer treatment, several nanomaterials such as liposome, polymeric micelles or iron oxide NPs have been approved for cancer treatment and many others are under clinical investigation (table 2.2), moreover, due to the complexity of tumor biology and patient heterogeneity, cancer nanomedicine require for novel approach to improve the nano-bio interaction and develop novel and more effective therapeutic NPs. In fact, the properties of nanomaterials such as shape, size, composition and surface ligand can highly influence the biological process determining the final therapeutic effects.

Table 2. 2 Examples of clinical-stage nanomedicines for cancer therapy[30]

Therapy modality	Generic name and/or proprietary name	Nanotechnology platform	Active pharmaceutical ingredients	Cancer type	Status
Chemotherapy: non-targeted delivery	Liposomal doxorubicin (Doxil)	Pegylated liposome	Doxorubicin	HIV-related Kaposi sarcoma, ovarian cancer, and multiple myeloma	Approved by FDA
	Liposomal daunorubicin (DaunoXome)	Liposome	Daunorubicin	HIV-related Kaposi sarcoma	Approved by FDA
	Liposomal vincristine (Marqibo)	Liposome	Vincristine sulfate	Acute lymphoblastic leukaemia	Approved by FDA
	Liposomal irinotecan (Onivyde or MM-398)	Pegylated liposome	Irinotecan	Post-gemcitabine metastatic pancreatic cancer	Approved by FDA
	Liposomal doxorubicin (Myocet)	Liposome	Doxorubicin	Metastatic breast cancer	Approved in Europe and Canada
	Mifamurtide (Mepact)	Liposome	Muramyl tripeptide phosphatidyl-ethanolamine	Nonmetastatic, resectable osteosarcoma	Approved in Europe
	Nab-paclitaxel (Abraxane)	Albumin NP	Paclitaxel	Breast, lung and pancreatic cancer	Approved by FDA
	SMANCS	Polymer conjugate	Neocarzinostatin	Liver and renal cancer	Approved in Japan
	Polymeric micelle paclitaxel (Genexol-PM)	Polymeric micelle	Paclitaxel	Breast cancer and NSCLC	Approved in Korea
	Liposomal cisplatin (Lipoplatin)	Pegylated liposome	Cisplatin	NSCLC	Phase III
	NK-105	Polymeric micelle	Paclitaxel	Metastatic or recurrent breast cancer	Phase III
	Liposomal paclitaxel (EndoTAG-1)	Liposome	Paclitaxel	Pancreatic cancer, liver metastases and HER2 negative and triple-negative breast cancer	Phase II
	Nab-rapamycin (ABI-009)	Albumin NP	Rapamycin	Advanced malignant PEComa and advanced cancer with mTOR mutations	Phase II
	CRLX 101	Polymeric NP	Camptothecin	NSCLC, metastatic renal cell carcinoma and recurrent ovarian, tubal or peritoneal cancer	Phase II
Chemotherapy: targeted delivery	MM-302	HER2 targeting liposome	Doxorubicin	HER2-positive breast cancer	Phase II/III
	BIND-014	PSMA-targeting polymeric NP	Docetaxel	NSCLC and mCRPC	Phase II
	MBP-426	TfR targeting liposome	Oxaliplatin	Gastric, oesophageal and gastro-oesophageal adenocarcinoma	Phase I/II
	Anti EGFR immunoliposomes loaded with doxorubicin	EGFR targeting liposome	Doxorubicin	Solid tumours	Phase I
Chemotherapy: stimuli-responsive delivery	ThermoDox	Liposome	Doxorubicin	Hepatocellular carcinoma	Phase III
Chemotherapy: combinatorial delivery	Liposomal cytarabine–daunorubicin (CPX-351 or Vyxeos)	Liposome	Cytarabine and daunorubicin (5:1)	High-risk acute myeloid leukaemia	Phase III
	CPX-1	Liposome	Irinotecan and floxuridine (1:1)	Advanced colorectal cancer	Phase II
Hyperthermia	NanoTherm	Iron oxide NP	NA	Glioblastoma	Approved in Europe
	AuroLase	Silica core with a gold nanoshell	NA	Head and neck cancer, and primary and metastatic lung tumours	Pilot study
Radiotherapy	NBTXR3	Hafnium oxide NP	NA	Adult soft tissue sarcoma	Phase II/III
Gene or RNAi therapy	SGT53	TfR targeting liposome	Plasmid encoding normal human wild-type p53 DNA	Recurrent glioblastoma and metastatic pancreatic cancer	Phase II
	PNT2258	Liposome	DNA oligonucleotide against BCL-2	Relapsed or refractory non-Hodgkin lymphoma and diffuse large B-cell lymphoma	Phase II
	SNS01-T	Polyethylenimine NP	siRNA against eIF5A and plasmid expressing eIF5A K50R	Relapsed or refractory B cell malignancies	Phase I/II
	Atu027	Liposome	siRNA against protein kinase N3	Advanced or metastatic pancreatic cancer	Phase I/II

Therapy modality	Generic name and/or proprietary name	Nanotechnology platform	Active pharmaceutical ingredients	Cancer type	Status
	TKM-080301	Lipid NP	siRNA against PLK1	Neuroendocrine tumours, adrenocortical carcinoma and advanced hepatocellular carcinoma	Phase I/II
	DCR MYC	Lipid NP	Dicer-substrate siRNA against MYC	Hepatocellular carcinoma	Phase I/II
	MRX34	Liposome	miR 34 mimic	Primary liver cancer, solid tumours and haematological malignancies	Phase I
	CALAA-01	TfR targeting polymeric NP	siRNA against ribonucleotide reductase M2	Solid tumours	Phase I
	ALN-VSP02	Lipid NP	siRNAs against KSP and VEGFA	Solid tumours	Phase I
	siRNA EPHA2 DOPC	Liposome	siRNA against EPHA2	Advanced cancers	Phase I
	pbi shRNA STMN1 LP	Lipid NP	shRNA against stathmin 1	Advanced and/or metastatic cancer	Phase I
Immunotherapy	Tecemotide	Liposome	MUC1 antigen	NSCLC	Phase III
	dHER2 + AS15	Liposome	Recombinant HER2 (dHER2) antigen and AS15 adjuvant	Metastatic breast cancer	Phase I/II
	DPX-0907	Liposome	Multi-tumour associated antigens	HLA-A2-positive advanced stage ovarian, breast and prostate cancer	Phase I
	Lipovaxin-MM	Liposome	Melanoma antigens	Malignant melanoma	Phase I
	JVRS 100	Lipid NP	Plasmid DNA	Relapsed or refractory leukaemia	Phase I
	CYT 6091	Colloidal gold NP	TNF	Advanced solid tumours	Phase I

2.2 Type of nanomaterials

Nanomedicine uses the properties developed by a material at its nanometric scale 10^{-9} m (figure 2.3) which differ in terms of chemistry, physics or biology from the same material at a bigger scale[4]. The term "nanomaterials" identifies particulate nanostructures, which may have various shapes, but which have at least one dimension in the nanometric scale. Nanomaterials can be spherical or tubular, filamentous or irregularly shaped, can be formed from various materials, and can exist in the dispersed state or in a melted, aggregated and agglomerated form.

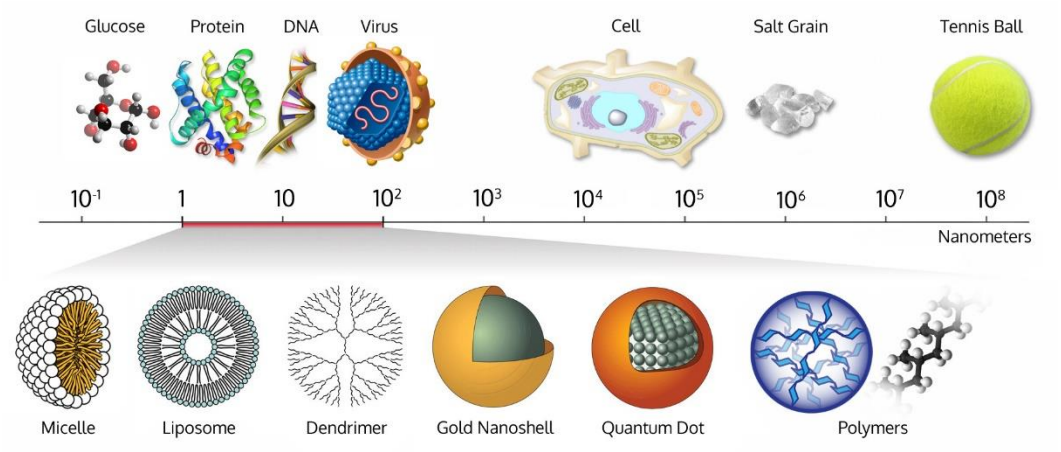

Figure 2. 3 Different nanoparticle types and their size in the context of various biological components [31]

A common characteristic of nanoparticles (NP) is that, due to their size, they possess different properties and characteristics from those of the parental chemical species. In fact, NPs have a much greater exposed surface area for the same mass compared to the same material in the form of a macroparticle and this exponentially increases their chemical and biological reactivity.

Nanomaterials (NMs) can have natural origin, such as those produced by natural combustion processes (volcanoes, spontaneous fires) or have anthropogenic origins [32]. In this case, is possible to distinguish those produced unintentionally (originating from vehicular traffic in particular from diesel engines, incinerators, industries and domestic heating) and those voluntarily produced. To this last category belong artificial NMs, or engineered NMs, that are specifically produced by nanotechnologies to carry out technological purposes at various levels and in various scientific and industrial fields [33]. Today, the most produced NMs by nanotechnology are titanium, silicon, aluminum, metals and carbon.

A common classification divides nanomaterials into 4 groups:

I) Carbon NMs, composed mainly of carbon, usually in the form of hollow spheres, ellipsoids or tubes. Spherical or ellipsoid carbon nanomaterials are called "fullerenes", while cylindrical ones are called "nanotubes".

II) Metals NMs, which include quantum dots, nanogolds, nanosilvers and metal oxides such as titanium dioxide (TiO2).

III) Dendrimers and polymers of “nano” dimentions, consisting of branched units. These can be used for the selective and controlled transport of drugs, markers

and oligonucleotides since they contain internal cavities in which molecules can be easily incorporated.

IV) Composites NMs, obtained by combining different types of solids which often are made up of a matrix (metallic, polymeric or ceramic) reinforced with nanometric particles. This union allows to obtain hybrid systems with mechanical, thermal and electrical properties intermediate to those of the single constituents and therefore more resistant and light materials, not sensitive to corrosion and to abrasive wear.

In general, the peculiar properties of nanomaterials are due to the fact that, due to their size, they follow the physical laws found between classical physics and quantum physics; in fact, the surface / volume ratio is very high, halfway between that of atoms and that of materials over micron in size. The characteristics that allows to change the NMs properties are essentially the composition, the size and the surface and all these parameters must be controlled when thinking about the technical application which they are designed for. On the other hand, the undesirable effects of NMs seem to be due precisely to those characteristics that make them so interesting, such as a large surface area and high surface reactivity. Many studies have also shown that changes in surface charge strongly influence biological responses to NPs, such as phagocytosis, genotoxicity and inflammation [34].

2.2.1 NMs synthesis

As already stated, the essence of Nanotechnologies is to build new materials and objects on the nanometric scale. To achieve this goal, it is not possible to simply use miniaturization techniques for the starting materials, but various production techniques are required which can be classified and summarized in the "Top-down" and "Bottom-up" strategies (figure 2.4).

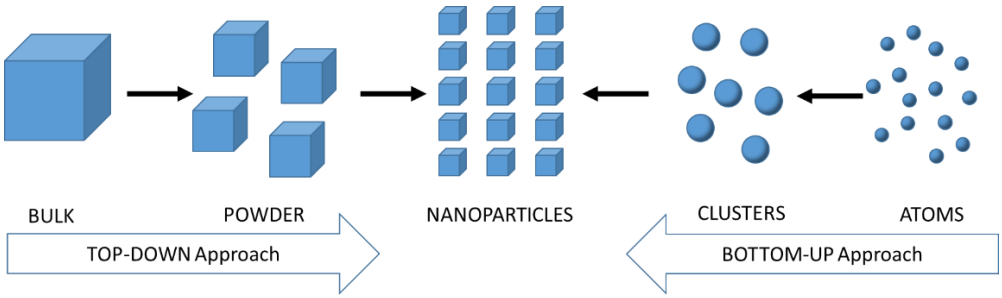

Figure 2. 4 Top-down and bottom-up approaches for the synthesis of nanoparticles.

The Top-down approach consists in starting from a bulk material obtaining the nanostructure by progressive removal of matter. The main peculiarity of this production strategy is the reproducibility, the reliability and the complexity of the objects that can be obtained; on the other hand, is a technique with high energy impact and that produce greater production waste than other. The Top-down production strategy is realized through the use of precision engineering and lithography techniques, which have allowed the production of most of the electronic and optical devices available today.

The Bottom-up strategy, instead, consists in the creation of more complex structures starting from the assembly of single atoms or molecules; this is normally achieved with the natural manifestation of interaction between the constituent elements, which organize themselves to form the desired structure. The techniques that work according to this strategy are substantially three: chemical synthesis, Self-assembly, and "positional assembly". Through chemical synthesis we can obtain nanostructures in two ways. The first is to produce and manipulate the bulk material until the desired structure is achieved. The second way is to produce the elements forming the structure at a higher level of organization than the various bulk materials (for example molecules), which will then be assembled to form the nanostructure using one of the two remaining Bottom-up production strategies.

With the self-assembly process, atoms and molecules spontaneously organize themselves to obtain nanostructures, in fact, they are able to establish characteristic physical and chemical local interactions that guide their assembly and recognition. This is a reversible process, which can be controlled by an appropriate components design, by the environment in which the process takes place, and by the forces that guide it. Although this process is exploited in an extremely efficient way by nature (just think about the coupling of nitrogenous bases to form the double helix of DNA,

the folding of a polypeptide chain to obtain a specific protein, or the double phospholipid layer of biological membranes) the industrial application of this technique is still limited, but extremely attractive from an environmental and economic point of view due to the low energy impact and waste production. The "positional assembly" technique is the direct manipulation of atoms, molecules or aggregates to form the desired nanostructure. This technique can be exploited to create structures on a surface using Scanning probe microscopy (SPM), or in three dimensions by exploiting the technology of Optical tweezers; however, there are still extremely laborious techniques that cannot be applied on an industrial level.

An interesting consideration to taking into account is how over the years the Top-down and Bottom-up production strategies have evolved in terms of capacity to manufacture nanostructures with increasingly smaller dimensions for the Top-down approach, and larger for the Bottom-up ones. This growth has led to an overlap of the dimensional limits achievable with the two strategies [35], and to the development of techniques for the construction of hybrid nanostructures constituted by the union of NP (of any origin) with biopolymers [36].

Due to the numerous problems that chemical and physical NPs synthesis procedures present, there is an essential need to develop more environmentally friendly procedures. This new awareness has led to the development of an ecological approach for the synthesis of NP that has various advantages such as simplicity, cost-effectiveness, compatibility for biomedical and pharmaceutical applications, as well as large-scale commercial production [37]. A promising approach to achieve this goal is to exploit the wide range of biological resources. In fact, over the last few years, plants, algae, fungi, bacteria and viruses have been used for the metallic NPs production with a low-cost, low energy dissipation and non-toxic method[38].

The synthesis and assembly of NPs would benefit from the development of "clean", non-toxic and environmentally friendly technologies that go under the name of "Green Chemistry". Green chemistry “aims to less use or avoid using hazardous substances in a chemical process. In fact, green chemistry is a movement to find alternatives to the use of hazardous chemicals such as feedstock, reagents, solvents, products, and byproducts in the production processes. Moreover, it concerns about sustainability of using raw materials and energy sources for manufacturing.”[38]

The use of Green Chemistry in nanosciences allows obtaining high precision in the synthesis and low production of waste, enormous benefits in production on a

commercial scale, for society and the environment[39]. The use of low-cost chemicals, non-toxic and biodegradable solvents is essential for the synthesis of non-dangerous materials for both the environment and humans. The reducing agent, the reaction medium and the stabilizing agent are the three key factors for the synthesis and stability of metal nanoparticles[40].

Therefore, green chemistry plays a crucial role in the synthesis of NPs for biomedical application because the materials used come from biological pathways (eg. plants or natural polymers) and are therefore safe to be consumed by humans thanks to their high biocompatibility and biodegradability. Furthermore, the biological compounds present in these materials, can act both as reducing, capping and stabilizing agents during the NPs synthesis process allowing to control the size and shape of the NPs[41].

A "clean" method to synthesize gold and silver NPs for example, involves the use of AuCl4 and AgNO3 that undergo reduction with heparin and hyaluronic acid, that are reducing and stabilizers agents. The NPs thus obtained show stability under physiological conditions and have important biological activities (such as anti-inflammatory and anticoagulant efficacy) demonstrated by in vivo and in vitro studies[42]. Recently an active field of research study the incorporation of carbohydrates on nanomaterials. Jiang and colleagues synthesized hybrid NPs of poly (glucosamine) chitosan-Au using chitosan and ethylenediaminetetraacetic acid (EDTA); they obtained the reduction in situ of the Au ions in polymeric spheres using EDTA as a reducing agent [43]. Gorges and co-workers have used glucose as a reducing agent to form NPs using chlorinated ions trapped in a film of amines and lipids in turn trapped on a glass substrate[44].

Raveendran et al. used β-D-glucose as a reducing agent and starch as an encapsulating agent to obtain silver NPs [45]. Recently an eco-friendly method has been developed, thanks to which is possible to prepare silver nanoparticles in natural polymeric media. Nano silver particles were synthesized in an aqueous solution containing silver nitrate, glucose as a reducing agent and gelatin as a stabilizing agent. The NPs were found to be uniform, with an average diameter of 5 nm and, of course, adhered to the gelatin matrix. This type of method can be used for the synthesis of other metallic nanoparticles such as those of gold, palladium and platinum nanoparticles[40].

1. Schaming, D. & Remita, H. Nanotechnology: from the ancient time to nowadays. *Found. Chem.* **17,** 187–205 (2015).
2. Sanchez, F. & Sobolev, K. Nanotechnology in concrete – A review. *Constr. Build. Mater.* **24,** 2060–2071 (2010).
3. Taniguchi, N., Arakawa, C. & Kobayashi, T. On the basic concept of 'nano-technology'. in *International Conference on Production Engineering* 18–23 (1974).
4. Sanvicens, N. & Marco, M. P. Multifunctional nanoparticles – properties and prospects for their use in human medicine. *Trends Biotechnol.* **26,** 425–433 (2008).
5. Xia, Y., Xiong, Y., Lim, B. & Skrabalak, S. E. Shape-Controlled Synthesis of Metal Nanocrystals : Simple Chemistry Meets Complex Physics ? Angewandte. *Angew Chem Int Ed Engl* **48,** 60–103 (2009).
6. Hong, S. & Farokhzad, O. C. Nanocarriers as an emerging platform for cancer therapy. *Nat. Nanotechnol.* **2,** 751–60 (2007).
7. Sozer, N. & Kokini, J. L. Nanotechnology and its applications in the food sector. *Trends Biotechnol.* **27,** 82–89 (2009).
8. Hameed, J. & Saeed, A. *Applications of Nanotechnology in Solar Energy and Energy Storage Sectors*. (2019).
9. Daniels-Race, T. 12 - Nanodevices: fabrication, prospects for low dimensional devices and applications. in (ed. Feldman, M. B. T.-N.) 399–423 (Woodhead Publishing, 2014). doi:https://doi.org/10.1533/9780857098757.399
10. Palit, S. & Hussain, C. M. Nanomaterials for Environmental Science: A Recent and Future Perspective. *Nanotechnology in Environmental Science* 1–18 (2018). doi:doi:10.1002/9783527808854.ch1
11. Kanchi, S., Sabela, M. I. & Bisetty, K. Analytical Applications of Nanoscale Materials for Water Treatment: A Review. *Nanotechnology in Environmental Science* 71–124 (2018). doi:doi:10.1002/9783527808854.ch4
12. Singh, P. P. Nanotechnology: Greener Approach for Sustainable Environment. *Nanotechnology in Environmental Science* 805–824 (2018). doi:doi:10.1002/9783527808854.ch25
13. Helmus, M., Gammel, P., Allen, F. & Migliorato, P. Nanotechnology-

enabled chemical sensors and biosensors. *Am. Lab.* **38,** 34 (2006).

14. Patni, N., Pillai, S. & Mehta, T. NANO TECHNOLOGY IN CHEMICAL SENSORS. in *Nanotechnology, Novel Perspectives and Prospects* 6 (2015).
15. Li, J. & Lu, Y. Nanostructure-engineered chemical sensors for hazardous gas and vapor detection. *Proc SPIE* **5593,** (2004).
16. Patra, J. K. & Gouda, S. Application of nanotechnology in textile engineering : An overview. *J. Eng. Technol. Res.* **5,** 104–111 (2013).
17. Ravindra, S., Murali Mohan, Y., Narayana Reddy, N. & Mohana Raju, K. Fabrication of antibacterial cotton fibres loaded with silver nanoparticles via 'Green Approach'. *Colloids Surfaces A Physicochem. Eng. Asp.* **367,** 31–40 (2010).
18. King, T., Osmond-McLeod, M. J. & Duffy, L. L. Nanotechnology in the food sector and potential applications for the poultry industry. *Trends Food Sci. Technol.* **72,** 62–73 (2018).
19. Baronzio, G. *et al.* A Brief Overview of Hyperthermia in Cancer Treatment. *Integr. Oncol.* **3,** (2014).
20. Nikalje, A. P. Nanotechnology and its Applications in Medicine. **5,** 81–89 (2015).
21. Kim, B. Y. S. Nanomedicine. *N. Engl. J. Med.* **363,** 2434–43 (2010).
22. Saini, R., Saini, S. & Sharma, S. Nanotechnology: the future medicine. *J. Cutan. Aesthet. Surg.* **3,** 32–33 (2010).
23. Jabir, N. R. *et al.* Nanotechnology-based approaches in anticancer research. TL - 7. *Int. J. Nanomedicine* **7 VN-re,** 4391–4408 (2012).
24. Holm, B. A. *et al.* Nanotechnology in BioMedical Applications. **1406,** (2017).
25. Boisseau, P. & Loubaton, B. Nanomedicine , nanotechnology in medicine. *Comptes Rendus Phys.* **12,** 620–636 (2011).
26. Mukherjee, A. *et al.* Lipid-polymer hybrid nanoparticles as a next-generation drug delivery platform: state of the art, emerging technologies, and perspectives. *Int. J. Nanomedicine* **14,** 1937–1952 (2019).
27. Brannon-Peppas, L. & Blanchette, J. O. Nanoparticle and targeted systems for cancer therapy. *Adv. Drug Deliv. Rev.* **56,** 1649–1659 (2004).
28. Mukherjee, A. & Paul, M. Recent Progress in the Theranostics Application of. *Cancers (Basel).* **11,** (2019).

29. Patra, J. K. *et al.* Nano based drug delivery systems: recent developments and future prospects. *J. Nanobiotechnology* **16,** 71 (2018).
30. Shi, J., Kantoff, P. W., Wooster, R. & Farokhzad, O. C. Cancer nanomedicine: progress, challenges and opportunities. *Nat. Rev. Cancer* **17,** 20–37 (2017).
31. Hulkoti, N. I. & Taranath, T. C. Biosynthesis of nanoparticles using microbes — A review. *Colloids Surfaces B Biointerfaces* **121,** 474–483 (2014).
32. Stern, S. T. & Mcneil, S. E. Nanotechnology Safety Concerns Revisited. *Toxicol. Sci.* **101,** 4–21 (2008).
33. Borm, P. J. A. *et al.* The potential risks of nanomaterials: a review carried out for ECETOC. *Part. Fibre Toxicol.* **3,** 1–35 (2006).
34. Borm, P. J. A. & Kreyling, W. Toxicological hazards of inhaled nanoparticles--potential implications for drug delivery. *J. Nanosci. Nanotechnol.* **4,** 521–531 (2004).
35. Whatmore, R. W. Nanotechnology — what is it ? Should we be worried ? *Occup. Med. (Chic. Ill).* **56,** 295–299. (2006).
36. Niemeyer, C. Nanoparticles, proteins, and nucleic acids: biotechnology meets materials science. *Angew. Chemie Int. Ed.* **40,** 4128–4158 (2001).
37. Filippo, E., Serra, A., Buccolieri, A. & Manno, D. Green synthesis of silver nanoparticles with sucrose and maltose : Morphological and structural characterization. *J. Non. Cryst. Solids* **356,** 344–350 (2010).
38. Thakkar, K. N., Mhatre, S. S. & Parikh, R. Y. Biological synthesis of metallic nanoparticles. *Nanomedicine Nanotechnology, Biol. Med.* **6,** 257–262 (2010).
39. Dahl, J. A., Maddux, B. L. S. & Hutchison, J. E. Toward greener nanosynthesis. *Chem. Rev.* **107,** 2228–2269 (2007).
40. Darroudi, M., Ahmad, M. B., Zamiri, R. & Zak, A. K. Time-dependent effect in green synthesis of silver nanoparticles. *Int J Nanomedicine* **6,** 677–681 (2011).
41. Pin, Y. *et al.* Green biosynthesis of superparamagnetic magnetite Fe 3 O 4 nanoparticles and biomedical applications in targeted anticancer drug delivery system : A review. *Arab. J. Chem.* **13,** 2287–2308 (2020).
42. Kemp, M. M. *et al.* Synthesis of gold and silver nanoparticles stabilized with glycosaminoglycans having distinctive biological activities.

Biomacromolecules **10,** 589–595 (2009).

43. Guo, R., Zhang, L., Zhu, Z. & Jiang, X. Direct Facile Approach to the Fabrication of Chitosan−Gold Hybrid Nanospheres. *Langmuir* **24,** 3459–3464 (2008).
44. Gole, A., Kumar, A., Phadtare, S., B. Mandale, A. & Sastry, M. Glucose induced in-situ reduction of chloroaurate ions entrapped in a fatty amine film: formation of gold nanoparticle–lipid composites. *PhysChemComm* **4,** 92–95 (2001).
45. Raveendran, P., Fu, J. & Wallen, S. L. Completely 'Green' Synthesis and Stabilization of Metal Nanoparticles. *J. Am. Chem. Soc.* **125,** 13940–13941 (2003).

Chapter 3

Nanoparticles

As anticipated in the previous chapter, one of the mayor applications developed by nanotechnology is the use of nanoparticles in medical field. In fact, technological progresses in NPs synthesis and functionalization are generating important advances in patient screening, diagnosis, monitoring and treatment. Thanks to the development of new multifunctional targeting devices, novel imaging agents and innovative monitoring sensors, the efficiency of the processes are improved while minimizing the costs[1–4].

There are different types of nanoparticles, each of which present certain characteristics based on their different nature. NPs can be prepared with polymers or organic materials (organic nanoparticles) or with inorganic elements (inorganic nanoparticles).

Among the organic nanoparticles we find liposomes and micelles, dendrimers and carbon nanotubes.

- Liposomes are phospholipid vesicles with dimension between 50-100 nm composed by a bilayer membrane structure which is similar to the biological ones. Thanks to their amphiphilic properties they are generally used as carriers in which the hydrophilic molecules can be encapsulated in the internal aqueous phase, while the hydrophobic molecules transported in the lipid bilayer. The chemical-physical

properties of liposomes can be accurately modified simply by mixing different lipid molecules, varying the surface charge, functionality and size in order to increase their delivery specificity.

- Dendrimers are highly branched synthetic polymers (<15 nm) with a layered architecture consisting of three parts: a multifunctional core, branching units and surface functional groups, which determine its characteristics. Thanks to the modification of their multiple terminal groups they are excellent drug and imaging diagnosis agent carriers.
- Carbon nanotubes are cylinders of coaxial graphite sheets whith a dimension <100 nm, they have excellent strength and electrical properties and are efficient heat conductors. Carbon nanotubes can be used as drug carriers, biosensors and tissue-repairs scaffolds.

Among the inorganic nanoparticles there are: quantum dots, metallic and magnetic nanoparticles; these possess a central core made of inorganic material which defines the magnetic, fluorescent, electronic and optical properties.

- A quantum dot is a semiconductor crystal highly packed by hundreds or thousands of atoms, and whose dimensions are in the order of a few nanometers (from 1 to 100nm). By varying the size of the quantum dots, they change their optical properties, and are typically used for their ability to emit different florescence. Moreover, they are characterized by high resistance to photobleaching and photo-chemical degradation. For this reason, they are excellent tools for contrast agent in biomedical imaging and label for bioassays.
- Metallic nanoparticles: Metallic particles of nanometric dimensions present a unique photo-physical phenomenon, called localized surface plasmon resonance (LSPR), they are able to absorb light and emit photons with the same frequency in all direction. Thanks to this property they are used for biomedical imaging because can be easily detectable with different techniques as optic absorption and fluorescence. Moreover, they are able to change their properties by varying their size, shape and dimension.
- Magnetic nanoparticles: spherical nanocrystals (10-20 nm), typically based on magnetic iron oxides and in particular magnetite and maghemite. Thanks to their superparamagnetic property, they are

mainly used in biomedical field in MRI or for hyperthermia treatment. Is possible to functionalize their surface to make them more biocompatible and allow the active targeting.

In table 3.1 the main organic and inorganic nanoparticles are summarized with their principal biomedical application.

Table 3. 1 Summary of main organic and inorganic NPs with principal application

NANOPARTICLES	
Organic	Inorganic
• Liposomes → Carriers • Dendrimers → Drug derlivery sytem; Imaging techniques • Carbon Nanotube → Drug carriers; Biosensors; Tissue-repairs scaffolds.	• Quantum dot → Bioimaging; Label for bioassays. • Metallic NPs → Coniugate ligants; Imaging techniques • Magnetic NPs → Drug carriers; Bioimaging; Hyperthermia; Targeting.

3.1 Magnetic Nanoparticles

In recent years, magnetic nanoparticles have significantly attracted the interest of the scientific community for their ability to be used in different fields of research such as technology and medicine. A reason of great interest is the possibility to use them in different biomedical applications, such as contrast agents for resonance, heat sources for hyperthermia and vectors for drugs delivery, especially in cancer therapy. The most widely used magnetic NPs are based on magnetic iron oxides and in particular magnetite and maghemite. These materials are preferred thanks to their low toxicity, high biocompatibility and stability.

Magnetite (Fe_3O_4) differs from most other iron oxides because it contains both divalent and trivalent iron ions. It presents an inverse spinel structure in which the O2-anions form a closed, cubic face-centered packing and the bi- and trivalent iron ions occupy the interstitial and octahedral tetrahedral sites. In particular, the Fe3 + ferric ions are distributed on all the tetrahedral sites and half of the octahedral sites, while the Fe2 + ferrous ions occupy the rest of the octahedral sites.

Maghemite (γ-Fe_2O_3) is composed by a cubic structure. Oxygen anions give rise to a cubic close-packed array in which ferric ions are distributed over

tetrahedral sites (eight Fe ions per unit cell) and octahedral sites (the remaining Fe ions and vacancies). The maghemite can be considered as fully oxidized magnetite (Figure 3.1).

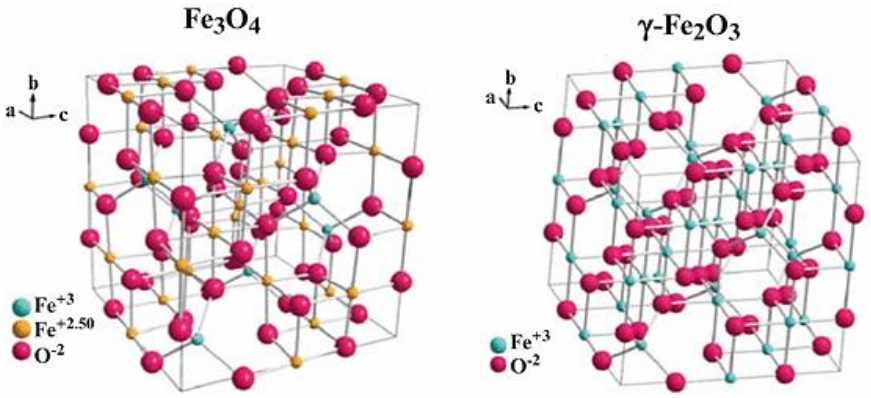

Figure 3. 1 Magnetite(Fe_3O_4) and Maghemite(γ-Fe_2O_3) structure[5]

3.1.1 Properties

3.1.1.1 Magnetic Properties

Iron oxide nanoparticles can be classified according to their response to external magnetic field. In particular, the description of the orientation of the magnetic moment in a particle helps to identify the different types of magnetism observed in nature. The magnetic properties of the particles can be described depending on the magnetic induction (M) with respect to the applied magnetic field (H).

In many materials the relation between M and H is linear:

$$M = \mu H$$

where μ is the magnetic permeability of the particles. The iron oxide particles show paramagnetism if μ> 1, diamagnetism if μ <1. In the vacuum μ = 1. Alternatively, magnetic susceptibility (χ) is used as an estimate of the efficiency of the magnetization response (M) of the material to an external magnetic field (H). It can be defined as

$\chi = \delta M / \delta H$ or as $\chi = \mu - 1$

and is a dimensionless quantity. Paramagnetic particles have χ> 0, diamagnetic particles χ <0 and in a vacuum χ = 1.

Particles with unpaired electronic spins, align spontaneously so that the material can exhibit magnetization without the application of an external magnetic field and are called ferromagnetic particles. In the study of the magnetic properties, much importance is given to the M vs. H diagrams representing the magnetic hysteresis curves (Figure 3.2).

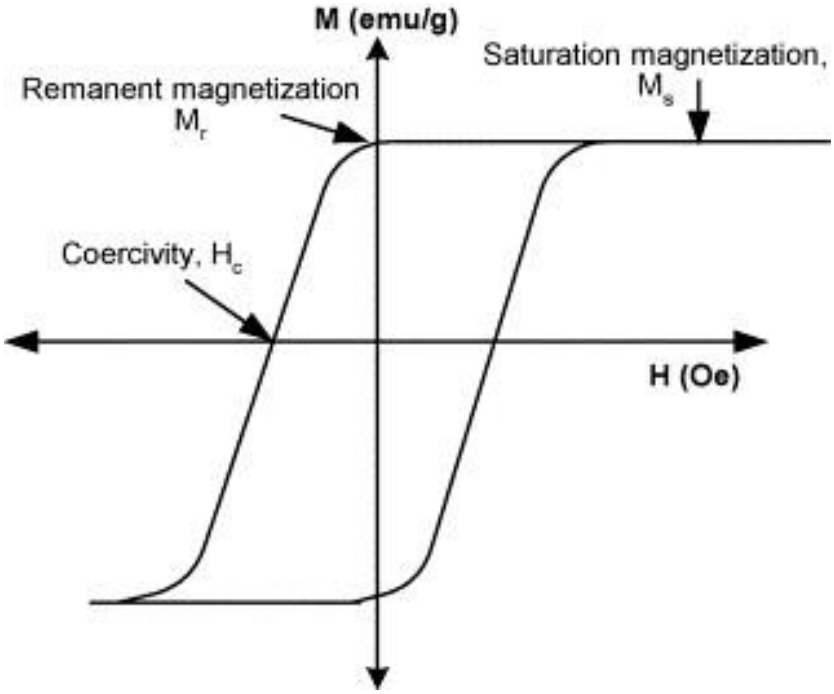

Figure 3. 2 Hysteresis cycle of a multidomain material, where h is the magnetic field amplitude and m the magnetization of the material[6]

An irreversible behavior in magnetization is indicated by the fact that a residual magnetization Mr remains in the sample for a certain time, even when the external magnetic field (H) is removed. This phenomenon depends on the decay speed of the magnetization which is specific for each material. The area within the curve represents the energy needed to reverse the magnetization. Ms is the saturation magnetization that is obtained when all the spins are aligned with respect to the external field; Hc is the coercivity, that is the field intensity that must be applied to bring the residual magnetization of the sample to zero.

If we talk about nanoparticles, we must consider that these materials have different chemical-physical characteristics compared to the starting bulk material[7]; in fact, the small dimensions and the high surface area of the magnetic particles lead to a radical change in the magnetic properties: being single magnetic domains they

exhibit phenomena of superparamagnetism[8]. Coercitivity results to be particularly interesting because when the size of the ferromagnetic material decreases to a value corresponding to the critical diameter, the H_c reaches a maximum which allow to change from a multi-domain structure to a single domain configuration. For even smaller sizes, coercivity becomes zero and the particle exhibits superparamagnetic characteristics.

Domains are groups of spins oriented in the same direction which act cooperatively. They are separated by domain walls, which have the characteristic width and energy related to their formation and existence. The coercivity is dependent on the particle size, in particular, the Hc increase with the decrease of the grain size (D), so is proportional to 1/D. While the magnetic domain moves closer to the grain size, the multidomain material change into a single domain material, and the H_c increase because of the impossibility to change the magnetization only by shifting the domain walls.

In superparamagnetic systems (when nanoparticles have a diameter below a threshold value of 20 nm) the particles are considered single domain ferromagnets without domain walls. NPs lose the ability to store magnetization and so the application of an external magnetic field determines a strong magnetization, but with the removal of this field, no residual magnetic force remains between the particles[9]. The superparamagnetic nanoparticles, called SPIONs (Super Paramagnetic Iron Oxide Nanoparticles), show a high saturation magnetization, and no coercivity and residual magnetization, as reported in their typical hysteresis cycle[10] (figure 3.3).

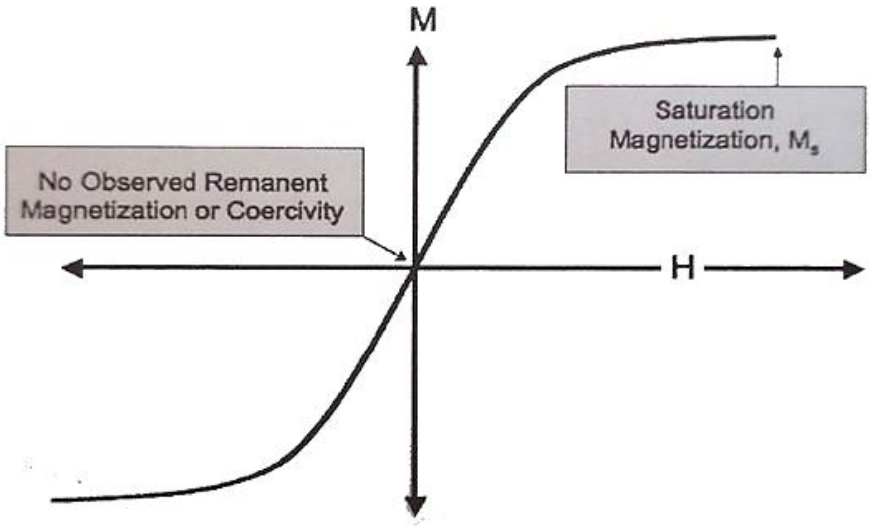

Figure 3. 3 Hysteresis loop for superparamagnetic materia

As said, when the external field is removed, no residual magnetization is left in the nanoparticles: this loss tends to occur with a typical relaxation mechanism. Basically, when such external magnetic field is applied, the particle's magnetic moment needs to overcome an energy barrier in order to rotate and align with the field itself. For magnetic single domain nanoparticles, the energy barrier K*V decreases with decreasing particle volume V and the time needed to establish the thermal equilibrium is given by the Neel relaxation time:

$$\tau_N = \tau_0 \, e^{\frac{KV}{kT}}$$

Where τ_0 is about10^{-9} s and represent a characteristic flipping time (expression of the anisotropy energy), K is the magnetic anisotropy, KV is the anisotropy energy and kT the thermal energy (where k is the Boltzmann constant and T is the temperature). However, exist another relaxation mechanism which may occur due to the ability of particles to rotate freely in fluid magnetic particle suspension, which commonly is termed Brownian relaxation. With this rotation the comparatively high magnetic anisotropy barrier may be avoided when the external field changes direction. The relaxation time of that rotation may be approximated by

$$\tau_B = \tau_0 \, \frac{3\eta V_h}{kT}$$

Where η is the viscosity of the carrier liquid and V_h is the effective hydrodynamic volume of nanoparticles.

It is notable how τ_N is influenced by parameters related only to particles, while τ_B is linked to the system in which the NPs are dispersed, or rather to its viscosity and its ability to influence the hydrodynamic volume of the NPs. Both sources of friction generated due to the delay in the rotation of the magnetic moments with respect to the applied magnetic field (figure 3.4), lead to a dissipation of energy in the form of heat.

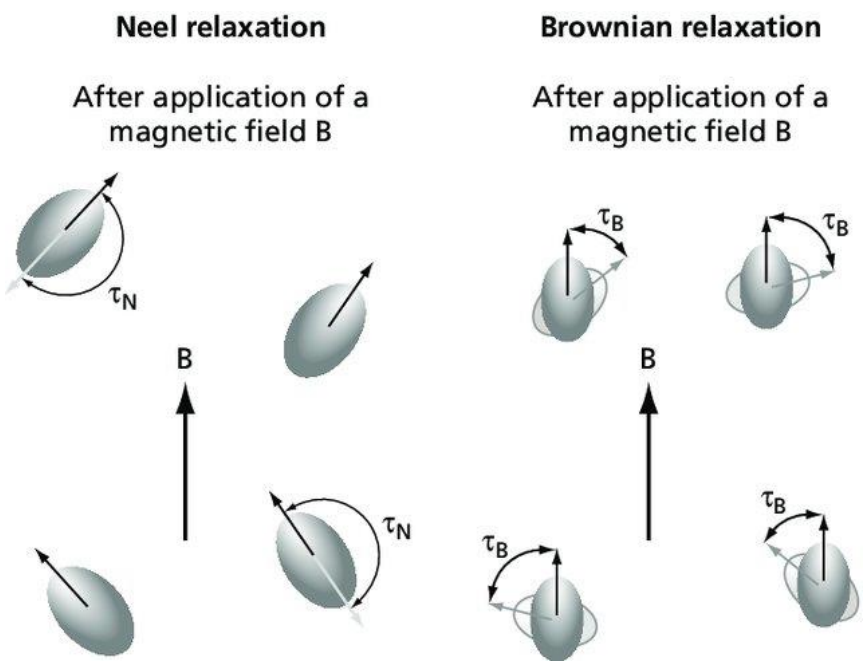

Figure 3. 4 Relaxation processes that influence the heating properties of magnetic nanoparticles[12]

Particles choose the simplest route to reach reversal of magnetization with respect to the external magnetic field, in fact, they follow the process with the smallest relaxation time constant.

The overall relaxation can be defined with the following equation, where the faster relaxation mechanism is dominant.

$$\tau_{eff} = \frac{\tau_B \tau_N}{\tau_B + \tau_N}$$

The heat dissipation value is calculated using both the harmonic mean of the relaxations and their relative contributions depending on the particle diameter such as:

$$P\,(f,H) = \mu_0 \pi f H^2 \chi'' \qquad [\mathrm{W/m^3}]$$

Where P is the heat dissipated, μ_0 is the permeability of the free space (magnetic field constant), f and H^2 respectively the frequency and strength of the applied magnetic field and χ'' is the susceptibility of the magnetic field (imaginary part), dependent on the frequency.

Thanks to this equation it is possible to calculate the energy produced by a NPs in suspension in a viscous fluid in terms of specific absorption speed (SAR) which is also a function of the particle diameter. SAR could be defined as Specific loss power (SPL) or in some cases Specific power absorption (SPA) and has the following equation:

$$SAR = 4.1868\,\frac{P}{\mathrm{m_e}} = \mathrm{C_e}\frac{dT}{\mathrm{dt}}$$

where P is the power absorbed by the sample under examination (dissipated by the nanoparticles), $\mathrm{m_e}$ is the mass of the magnetic nanoparticles and Ce is the specific heat capacity of the sample.

Therefore, with SAR calculation, is possible to evaluate the ability of the material under study to transform magnetic energy into heat; hence determine at which rate electromagnetic energy is absorbed by a unit of mass of a biological material and so to calculate the main parameter determining the heating of the tissues.

3.1.1.2 Colloidal properties

A colloid[13] is a solution that has particles between 1 nm and 1 μm in diameter, able to remain uniformly distributed throughout the solution. A simple colloidal dispersion is therefore a two-phase system that includes the dispersed phase characterized by the small particles and the dispersing phase that surrounds them. The colloidal solution shows different physico-chemical properties from those of

the atoms or molecules that constitute it, which change according to the size of the particles that compose the solution.

In particular, the liquid layer with the ions surrounding the particle is composed by two regions: an internal one (stationary layer, or Stern) with the ions strongly bound to the charged particle, and an external one (diffuse layer, or Gouy- Chapman), where interactions are weaker. The two zones constitute a double electric layer around each particle.

Inside the diffuse layer (of a much greater thickness than the Stern layer) the ions form metastable structures: when the particle moves in the liquid, the ions move with it; in particular, those beyond the shear plane replace and are continually replaced by free ions present in the liquid so that the dimensions of the double layer remain constant.

Figure 3.5 shows, for a generic charged particle, the variation of the electric potential as a function of the distance from its surface: we can see how decreases rapidly inside the stationary layer, more slowly inside the diffuse layer and then even more slowly until it vanishes.

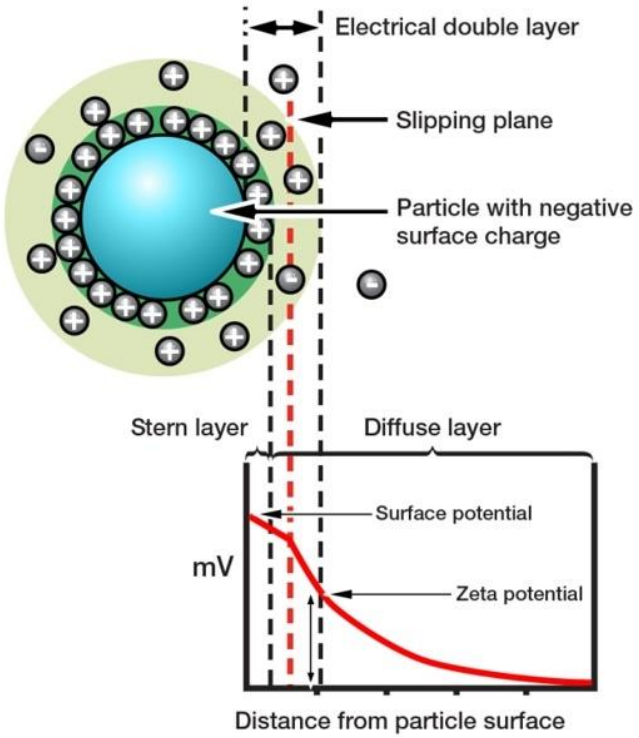

Figure 3. 5 Zeta potential influences whether particles will repel or attract when held in suspension[14]

The main characteristics of colloidal systems can be attributed to the interface between dispersed phase and dispersing medium. In fact, each particle has a well-defined surface that presents the typical interfacial properties: adsorption, electrical state, coalescence. Therefore, the surface-volume ratio of the dispersed particles has a very notable influence in determining the behavior of colloidal systems.

In particular, since the intrinsic charge on the surface of the particle is shielded by the stationary layer charges, the interactions between particles will be regulated precisely by the surface potential present at this layer. Moving away from the particles surface along the potential curve in figure 3.5, the cutting plane is reached: the potential in this point is called zeta potential (ζ) and defines the behavior of the dispersed systems, in particular of the suspensions. The zeta potential change with the pH of the solution in which the particles are dispersed (figure 3.6), so it is possible to modify its value by adding electrolytes, so that their ions are adsorbed on the particles surface themselves.

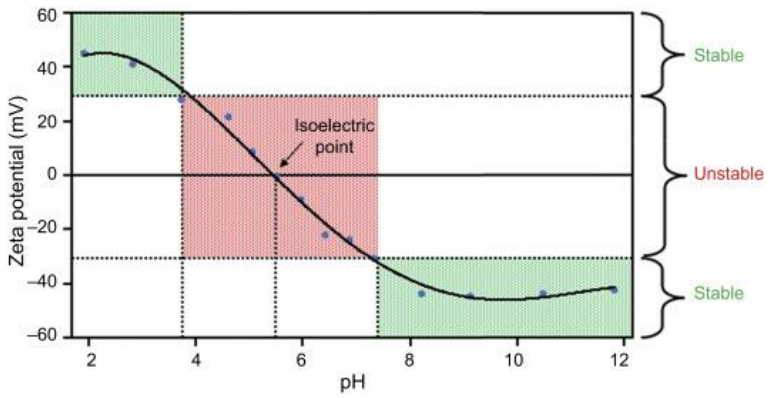

Figure 3. 6 Z potential by varying pH[15].

When two particles are so close together that their double layers' overlap, they repel each other with an electrostatic force whose intensity depends on the zeta potential: if it is too low (typically less than ± 25 mV), the repulsive force will not be strong enough to overcome the van der Waals attraction between the particles, and these will begin to agglomerate. When this happens the suspension is unstable.

A high ζ potential prevents the agglomeration of the particles and keeps the dispersion uniform and free to flow. Therefore, for the preparation of most formulations, the goal is to maximize the zeta potential.

The ζ potential depends on the density of the surface charge and on the double layer thickness; the density of the surface charge, in turn, depends on the concentration of the potential produced by the ions in ionic solvents. In many systems the H + ion determines the potential, so the ζ potential depends on the pH.

The ζ potential is positive for low pH values and negative for high values. The pH for which the ζ potential is zero defines the isoelectric point (IEP) of the dispersed system, so the pH value for which there are no surface charges. The IEP is a property of the particle surface and is the value around which there is poor stability since the van der Waals forces are more evident.

In biomedical field, colloidal suspensions of iron oxide particles, find many applications, this because they have a unique combination of fluidity and interaction with an external magnetic field. However, in aqueous solution these particles have each iron atom of the surface which acts as a Lewis acid and is easily dissociating by donating a pair of electrons and leaving the surface functionalized with hydroxyl groups, which, being amphoteric, can react with both acids and bases[16].

Therefore, depending on the solution pH, the magnetite surface can be positive or negative and can cause undesired interactions around its isoelectric point, which lead to the formation of clusters or agglomerates. If two large clusters of particles then adhere, each particle in the magnetic field is further magnetized. Finally, the adhesion of the remaining magnetic particles causes a mutual magnetization which leads to a greater increase in the total aggregation.

Then, in order to be able to use them in the biomedical field, is necessary the stability of the colloids which is obtainable by functionalizing the surface of the particles in order to prevent unwanted adhesions[17] by controlling for example the pH, the temperature or the ionic strength.

3.1.2 Biomedical applications

During the last decades, magnetic nanoparticles have been proposed as suitable nanostructures for therapeutic and diagnostic purposes thanks to their well-known chemical-physical properties. Magnetite (Fe_3O_4) is the most promising candidate

due to its high biocompatibility and biodegradability and of course, it need specific requirements in order to be applied in this field:

- Biocompatibility
- Non-Toxicity
- Having sizes smaller or comparable to those of different biological entities
- Having a well-defined morphological and microstructure properties
- Good colloidal and chemical stability
- Good response to the external magnetic field and no remnant magnetization when the field is turned off.

Thanks to this good physical, chemical and magnetic properties, SPIONs can be used for different biomedical applications such as magnetic separation, drug delivery, Magnetic Resonance Imaging (MRI) and Magnetic Fluid Hypertermia[18].

3.1.2.1 Magnetic separation

In biomedical contest it is often necessary, for numerous biological assays and analyses, to separate specific organic entities from their original environment. SPIONs can be used with this aim by acting as magnetic separator. For this purpose, the biological entities need first to be targeted with a magnetic material, this is made possible through an appropriate chemical surface functionalization of the magnetic nanoparticles with specific biocompatible molecules (e.g. Polyvinyl alcohol (PVA), dextran or phospholipids)[19–21]. This functionalization provides the link between the particles and the target site as well as increase the colloidal stability of the magnetic fluid.

After this first step, the magnetically labelled material is then separated from its native solution by passing the fluid mixture through a fluid-based magnetic separation device which recognize and stops the labelled entities[18].

Magnetic separation has been successfully used in many sector of biomedical and biological research. For example, it has been proven to be a very high sensitive technique for the separation of rare tumor cells from the blood[22]. It has been used to perform 'magnetic enzyme linked immunosorbent assays' in combination with optical sensing. In which fluorescent enzymes are used to optically determine the number of labelled cells by the assay enzymes[23,24]. Magnetic separation has been used in polymerase chain reactions as a pre-processing technology in which the sample of DNA is amplified and identified.[25] In another application, magnetic

separation has been used to localize targeted cells at specific locations for cell counting and detection via optical scanning.[26] Thanks to all this applications, magnetic separation using biocompatible nanoparticles, is a versatile technique to achieve different purpose in diagnostic field.

3.1.2.2 Drug delivery

Magnetically targeted drug delivery is another important application of SPIONs that can be used as carriers for anti-cancer drugs. The term drug delivery indicates the mechanism through which substances and drugs are delivered in particular areas of the body affected by diseases or tumors making the treatment more specific and effective, limiting side effects on the healthy tissues and reducing the necessary dosage. The functionalization of the magnetic particles through a superficial chemical processing and the following loading of drugs, allow to make them selective in the detection of the tumor cells. Therefore, the purpose of the use of magnetic nanoparticles for these uses is twofold, on the one hand the systemic distribution of cytotoxic medicine is reduced by reducing the related side effects and on the other hand the dose required for an effective drug effect is reduced.

The process essentially consists in the intravascular injection of magnetic nanoparticles towards points of the body affected by a tumor. Once reached the desired position, the drug can be released through an external magnetic field application or through changes in physiological conditions such as pH, osmolality or temperature. For this type of application, the dimensions, the charge and the surface chemistry of the nanoparticles are particularly important characteristics as they strongly influence the circulation time in the body through the blood vessels. The optimal diameters range for this use is between 10 and 100 nm. The lower limit is based on the fact that too small particles are easily expelled through kidney cleansing. The upper limit otherwise is not well defined but is set according to the type of tumor into which the nanoparticles must penetrate.

In table 3.2, some examples of SPIONs for drug delivery currently under investigation are shown, the table also shows the SPIONs coatings and the drugs tested[27].

Table 3. 2 SPIONs for drug delivery currently under investigation[27]

Coating	Delivery system	Drug tested	Examination route
Carbon	Aqueous media	Carminomycin and rubomycin	In vivo(Rat) Injected into the tail vein
Anhydroglucose	Aqueous media	Epirubicin	In vivo(Human) Intravenous injection
Phosphated starch	Aqueous media	Mitoxantrone	In vivo(Mice) The magnetic NPs were injected either into the femoral artery close to the tumour or intravenously
Poly(lactic-co-glycolic acid)	Microspheres and microcapsules	Dexamethasone acetateIn vitroand	In vivo(intra-articular)
Amphiphilic block copolymers of maleimide-terminated poly(ethyleneglycol)-block-poly(D,L-lactide) and methoxy-terminatedpoly-(ethylene glycol)-block-poly(D,L-lactide)	Multifunctional polymeric micelles	Doxorubicin	In vitro
Albumin	Microspheres	Doxorubicin	In vitro
Polyethylene glycol fumarate	Aqueous media	Tammoxifen	In vitro
Oleic acid	Aqueous media	Doxorubicin and paclitaxel	In vitro
Oleic acid–Pluronic	Aqueous media	Doxorubicin	In vitro
Poly(acrylic acid)	Aqueous media	Taxol	In vitro
None	Porous hollow nps	Cisplatin	In vitro
Chitosan, O-carboxymethylchitosan and(N-succinyl-O-carboxymethylchitosan	Aqueous media	Camptothecin	In vitro
Poly(lactic acid) and poly(lactic-co-glycolic acid)	Microspheres	Interferon alpha-2b	
Silica	Hollow mesoporous sphere	Ibuprofen	In vitro
Cross-linked chitosan	Microspheres	Aspirin	In vitro

3.1.2.3 Magnetic Resonance Imaging (MRI)

Superparamagnetic nanocrystals of iron oxides can be used as contrast agents in MRI, a non-invasive imaging technique used in the medical field to discriminate different tissue on the base of their biochemical composition. MRI is based on the nuclear magnetic resonance of the protons of the water present in the body. The operating principle is based on exposing the patient to a static magnetic field B0

that can go, depending on the analysis to be conducted, from a few tenths of a tesla up to 8 and 9 tesla. This strong magnetic field, makes the proton's magnetic moments line up with it and the tissues to be analyzed acquire a net magnetization M given by the action of the field B0. The alignment of the moments with the field is never complete, rather a precession motion is generated around the direction of the field B0 at a certain frequency ω0 (Larmor frequency) of the order of MHz. By applying an alternating magnetic radiation, perpendicular to the initial field and with a frequency equal to the Larmor frequency, it is possible to further tilt the magnetic moments with respect to the initial direction of an angle called flip angle. By applying the alternating magnetic field at the right frequency, energy is supplied to the system by exploiting the phenomenon of resonance, hence the name of the technique. The radiofrequency magnetic pulse is then switched off and the magnetic moments of the protons present in the various tissues return to their original configuration, resulting in a variation in the magnetic field flow. This phenomenon of relaxation that develops once the alternating magnetic field is turned off, takes place with two distinct time constants; the first one, indicated with T1, represents the return time of the magnetization component along the direction of the field B0 and depends on the protons interaction with the surrounding molecules, while the second one, indicated with T2, represents the return time of the magnetization component transversal to the field B0 and depends on the mutual interaction of neighboring protons[18].

The final image is obtained through a 2D Fourier transform of the spatial signal frequencies. Tumors and diseased cells can be detected due to the different return rate to the original magnetization situation by protons placed in different tissues; this effect is used to create contrast between different types of tissue in the body. If we assume to have the applied field B0 along the z axis, the components of the longitudinal and transverse magnetization will relax according to the formulas:

$$mz = m \cdot (1 - \exp -t/T1) \qquad (2.8)$$

$$mx,y = m \cdot \sin(\omega 0t + \varphi) \exp -t/T2 \qquad (2.9)$$

From these relaxation processes is possible to generate the magnetic resonance images, which contrast strongly depends on T1 and T2. This two values can change a lot depending on the tissue and on the external magnetic field.

However, in many tissues, the intrinsic contrast is not sufficient and external contrast agents are used to improve it. In particular, the use of contrast agents shortens the relaxation times T1 and T2.

In recent years, research has developed around the use of superparamagnetic iron oxides nanoparticles to improve contrast. As can be seen from Figure 3.7, with the addition of magnetic nanoparticles, the resolution of MRI images increases greatly, allowing the identification of diseased or tumoral areas otherwise impossible to see[18,28–30].

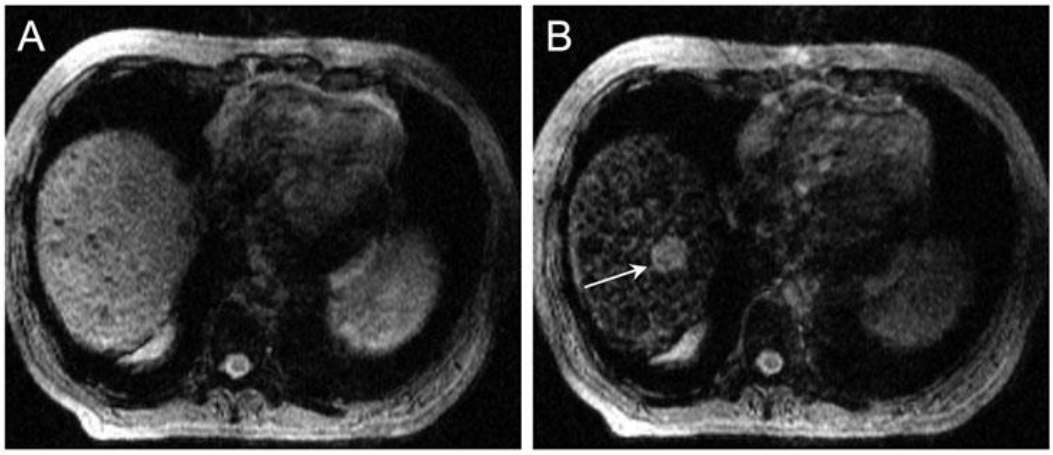

Figure 3. 7 Iron oxide nanoparticles as RES contrast media for MRI. MR images of the hepatic dome before (A) and after injection of iron oxide nanoparticles (Ferumoxide: 1.4 ml) (B). The lesion (arrow) is clearly visible after injection of the iron oxide nanoparticles, but not before. The increase of contrast between the lesion and the liver is due to a darkening of the normal liver. Moreover, please note the heterogeneous aspect of the liver, corresponding to cirrhosis. In this context, the hepatic nodule is highly suspect of a hepatocellular carcinoma.[10]

This is possible because the real transverse relaxation time T * 2 is related to the ideal time T2 from equation 2.10 in which γ is the gyromagnetic factor.

$$1/(T^*2) = 1/(T2) + \gamma(\Delta B0/2) \qquad (2.10)$$

This means that by inserting magnetic nanoparticles within the tissue or even inside the cells, localized dipolar fields are generated which, as described by equation 2.10, reduces the decay time by increasing the contrast in the image.

During the last decades, many advance have been made in the design and preparation on SPIONs as contrast agent[31,32], in table 3.3 are shown some of novel SPIONs used as contrast agent in MRI with specific surface modification and in vitro or in vivo applications.

Table 3. 3 Summary of novel SPION as Contrast Agents in MRI[31]

Name	Magnetic core	Surface	Core diameter (nm)	Overall size (nm)	Zeta Potential (mV)	In vitro	In vivo
Fe2O3-PLL	γ- Fe_2O_3	PLL		6.2	-42	Rat MSCs Human MSCs Human umbilical cord blood MSCs	Rat brain
N-dodecyl-PEI2k/SPIO	Fe_3O_4	N-dodecyl-grafted PEI 2K		54.7	+40	Mouse MSC	Mice subcuta-neous
iron oxide–loaded cationic nanovesicle	Fe_3O_4	(1)PEI-SA (2)PEG-PGA	6	150	+20	Rat MSCs	Rat brain
CMCS-SPIONs	Fe_3O_4	(Carboxymethyl)chitosan	6-10	55.4	21.4	Human MSCs	
ED-Pullulan coating SPIO	Fe_3O_4	Ethylenediamine Pullulan		94	+10	Rat MSCs	
UFH-SPIOs	Fe_3O_4	Unfractionated heparin		50-150		Human MSCs	Nude mice kidney
IONP-6PEG-HA	Fe_3O_4	Amine-functionalizd six-armed PEG covalently linked to hyaluronic acid	10	75	-9.1	Human MSCs	
TMA–SPIONs	Fe_3O_4	Polyacrylic acid modified by 2-aminoethyl-trimethyl ammonium		101	+40	Human MSCs	Mice brain
PDMAAm-coated γ-Fe_2O_3 NPs	γ- Fe_2O_3	PDMAAm		77.8		Human MSCs	
FITC-PLMA-MNPs	Fe_3O_4	FITC-PLMA		100	-34.5	Human MSCs	
Magnetic PLGA MPs	Fe_3O_4	PLGA(carboxyl end-group)	10	0.4-3 µm	40	Mouse MSCs	BALB/C mice back and ears
Citrate SPION	Fe_3O_4	Citrate	6-7	90.13	-27.3	Human MSC	Mice muscle
SPIO@SiO_2-NH_2	Fe_3O_4	SiO_2-NH_2	6	8.5		Rabbit MSCs	Rabbits brain
Mag-Dye@MSNs	Fe_3O_4	SiO_2 and FITC- incorporated mesoporous silica				Human MSCs	Nude mice brain

Hyperthermia

Another important application of iron oxide nanoparticles is their use in hyperthermia treatments. Hyperthermia is the heating of the tumor tissue increasing

the temperature of a localized area, a specific region or the entire body from a physiological value of 37 ° C up to values in the range between 41 and 45 ° C by means of external mediators[33,34]. It is considered as a potential therapy able to fill the gap between the tolerable toxicity and the desirable benefits, due to its low toxicity[34].

Nowadays a lot of trials have been carried out to demonstrate the efficacy of this therapy and the reduction of side effect. In fact, if hyperthermia is used alone, it can destroy cancer cells through antineoplastic and immunological effects, while it makes cancer cells more sensitive to radiation or to chemotherapeutic agents, if it is combined with other strategies[34].

The use hyperthermia as an anticancer therapy is particularly advantageous since the neoplastic environment show a higher heat sensitivity than healthy tissues: this is due to the high acidity resulting from the increase in glycolytic activities inside the diseased cells[35,36]. In particular, typical features of solid tumors is presenting a disordered vasculature with acidic, hypoxic and energy lacking regions[33]. This characteristic allows hyperthermia to be more selective than other treatment by keeping most healthy cells undamaged while bringing cancer cell to apoptosis after a treatment up to 44°C[33,37].

In particular, a specific dose of SPIONs is injected in the tumor region, then an external alternated magnetic field is applied in order to create an adequate field intensity and frequency that allow SPIONs to absorb energy useful to heat the surrounding tissue. The surrounding temperature can be maintained over the therapeutic range of 41-42°C for the required time in order to destroy cancer cells. In many studies, to obtain an effective tumor cells inactivation, numerous in vitro test have been performed with different kind of cancer cell and SPIONs concentration. Different physical properties of SPIONs has been changed in order to optimize the particles absorption into the cells. Through these researches it has been shown that the position of the particles inside the cell (intracellular, interstitial, bound to the membrane) is very important as it affects the efficiency of hyperthermia. In order to the treatment be successful, it is also necessary to optimize the shape and size of the nanoparticles to obtain the greatest heating power possible[38,39].

In hyperthermia treatments, the most used nanoparticles are SPIONs due to their high heating rate, appropriate magnetic properties and excellent biocompatibility.

In table 3.4 are summarized some pre-clinical studies performed using SPIONs as magnetic hyperthermia therapy system. Moreover, despite the promising results obtained in pre-clinical studies, further optimizations are needed to create clinically feasible SPIONs which allow the use of an adequate amount of NPs and not too high magnetic fields and frequencies[40].

Table 3. 4 Sample of pre-clinical study of SPIONs in hyperthermia treatment[40]

Field strength (kA/m)	Frequency (kHz)	Field strength x frequency (A/m•s)	Quantity of Fe delivered	Target	Targeting Mechanism	Summary of Results
38 kA/m	980 kHz	3.724×10^{10}	1700 mg/kg	Squamous Cell Carcinoma	EPR	Durable ablation of tumors in 84% of hyperthermia group compared to 0% for controls
5 kA/m	366 kHz	1.830×10^{9}	13.30 mg/kg*	Melanoma	EPR + Porphyrins	Tumor volume was smaller in the hyperthermia group ($p<0.1$)
56–113 kA/m	153 kHz	1.729×10^{10}	150 mg/kg*	Breast Cancer	EPR + Antibody targeting integral membrane glycoprotein	Tumor doubling/tripling/quadrupling times were increased significantly ($p < 0.05$) except for the group that received the lowest energy

*Assuming 20 g average weight of mice.
EPR, enhanced permeability and retention; kA/m, kiloampere/metre; kHz, kilohertz; A/m•s, ampere/meter•second.

3.1.3 Functionalization

It is essential develop a specific functionalization in order to chemically stabilize bare NPs against their two main problem: aggregation and intrinsic instability. In fact, small NPs tend to aggregate and form large particles by reducing their surface energy and consequently their dispersibility, moreover bare NPs are easily oxidized in air due to their high chemical activity and this leads the NPs to lose their magnetism[41].

By taking into account that most of biological media are similar to aqueous solution, is crucial for biomedical application obtain water dispersible SPIONs. To stabilize SPIONs in water and avoid their major problems[41,42] is possible to use different type of functionalization both with organic and inorganic materials. Moreover, the new material layer can be useful to provide functional terminal groups for additional coating by other materials, or for the attachment of therapeutic and targeting agents.

Silica-coated Iron Oxide NPs are studied in many research activities because of their well-known biocompatibility and stability. Thanks to its intrinsic physical-chemical composition, Silica coating allow to improve stability and dispersibility by overcoming undesirable side reactions and thanks to the abundant silanol group present on its layer, provides functional terminal groups to further functionalize SPIONs surface. For biomedical application, the most studied structure is core-shell, in which each Fe_3O_4 NP is coated by a silica layer and the most conventional routes to prepare Silica-coated SPIONs are Stöber method and microemulsions synthesis.

In Stöber synthesis is typically used Tetratethyl ortho silicate (TEOS) which easily bind the SPIONs surface through OH groups, the resulting silica-coated NPs have diameters ranging from 50 to 2000 nm depending on type of reagents used and on solution pH[43]. Is therefore possible to create silica layer with a specific thickness, by controlling the reaction parameters. With Stöber method, the amount of silane used is crucial to regulate the thickness of silica shell that should be adequate to the final application for which silica-coated NPs has been created[44,45]. With microemulsion synthesis, is possible to have a better regulation of the silica layer thickness if compared with Stober method. Moreover this method prevents the formation of multicore or core-free NPs[46]. Different studies have been performed in which uniform silica shells with controlled thickness can be realized on the nanometer scale[46,47].

Another common way to functionalize SPIONs is to displace hydrophilic ligands on NP surface by using small molecules which allow to change the polarity from hydrophobic to hydrophilic[48]. The main advantage of this method is the retention of a small hydrodynamic radius without losing the original magnetic properties. 3-aminopropyltriethyloxysilane (APTES), is one of the common silane used for anchoring $–NH_2$ group to bare NPs. In fact, APTES coated SPIONs are well-known for their potential in biomedical application thanks to the demonstrated improvement of cytocompatibility and hemocomptibility given by the acetylation of the amine group on the NPs surface[49]. Different other functional group have been studied to produce strong covalent interaction between SPIONs and ligand molecule, such as carboxylic acid as citric acid[50] and DMSA[51]. For example, is possible to synthetize water soluble SPIONs directly using citric acid with co-precipitation method as explained in our previous work[52]. Therefore, a wide variety

of small molecules can be used to successfully functionalize bare SPIONs in order to generate water-dispersible NPs solution usable for post connecting with other metal ions, biomolecules or biological entities.

For biomedical applications, several other approaches are based on polymers functionalization of SPIONs, this because polymerization not only provides colloidal stability and different multifunctional groups[53], but also increase the repulsive force between NPs, their stability and biocompatibility[54]. It is noteworthy that the polymeric material should be selected properly because its presence on SPIONs may influence negatively their magnetic properties.

Another common route to functionalize SPIONs is using metal nanoparticles such as Gold and Silver, which possess a range of attractive properties that in combination with magnetic NPs makes them interesting due to their physicochemical properties[55,56]. Generally, the most used nanostructured SPIONs/metal NPs are core-shell, core-satellites, nanodumbell or nanoflowers which can be synthetized by microemulsion, thermal decomposition or multi-step methods[57,58]. The main studied nanostructure are core-shell NPs in which Au ions are directly reduced on SPIONs surface in order to create specific coating with controllable properties[59]. The hybrid core-shell structure can also be prepared through layer-by-layer self-assembly, which is a method to generate multilayers NPs with an ordinated structure thanks to the molecular interactions and chemistry conjugation[60,61]. Another recent study[62] is focused on preparing hybrid gold nanorods (Au NRs)-SPIONs structure by aqueous based self-assembly approach, in order to maintain the original optical and magnetic properties of gold and magnetic NPs. In this process, in order to allow the attachment between Au NRs and SPIONs, a functionalization with carboxyl group on Au surface has been required. Of course the strain energy between Au and SPIONs is determinant for structure stability and the functional performance. It is necessary to take into account that in all the above mechanism, the introduction of surfactants to the synthesis can influence the properties and the stability of SPIONs.

3.1 Gold Nanoparticles

In recent years, gold nanoparticles (GNPs) have been brought to the forefront of cancer research due to their high stability, ease of synthesis and surface modification and excellent biocompatibility, in fact, even at high concentration, they present very low toxicity[63]. Moreover, GNPs have attracted great interest because no damage on organs is detected after their prolonged exposition, this NPs are generally taken up by many organs mainly by liver and spleen and could be ejected via the hepatobiliary system[64]. One of the most important ability of Au nanospheres is their ability to get different properties by changing their size and modifying their shape, those make them interesting for medical purpose.

GNPs can be synthetized by different methods, the most common, thanks to their simplicity and scalability, are the Turkevich method and the Burst-Schiffrin one. Turkevich method involves the reduction of metal salt in the presence of a capping and a stabilizing agent. In particular, it consists in the reduction of tetrachloroauric acid ($HAuCl_4$) by citrate which chemically bind to the metal core and prevents aggregation. This allow to produce GNPs of about 15nm in diameter[65]. The Burst-Schiffrin method instead, allows to synthesize smaller GNPs by transferring the gold ions from an aqueous solution to an organic phase by means of a phase transfer agent, then the reduction is carried out with borohydride[66].

3.2.1 Properties

Metallic particles of nanometric dimensions are mainly studied for their innovative properties that are not present in massive metal. In fact, they present a unique photo-physical phenomenon, called localized surface plasmon resonance (LSPR), resulting from the interaction with light radiation[67,68].

When a metal nanoparticle is exposed to light, the electric field of the incident wave induces a polarization of the free electrons present within the conduction band. In fact, in the presence of an oscillating electromagnetic field, the conduction electrons of the metal nanoparticle, free to move, are subjected to collective coherent oscillations, known as plasmonic oscillations (figure 3.8). A displacement of the negative charges compared to the positive ones occurs, generating a charge

difference resulting in a dipole formation. The surface area and the distance between negative and positive charges in the dipole, define the resonance wavelength at which SPR occurs.

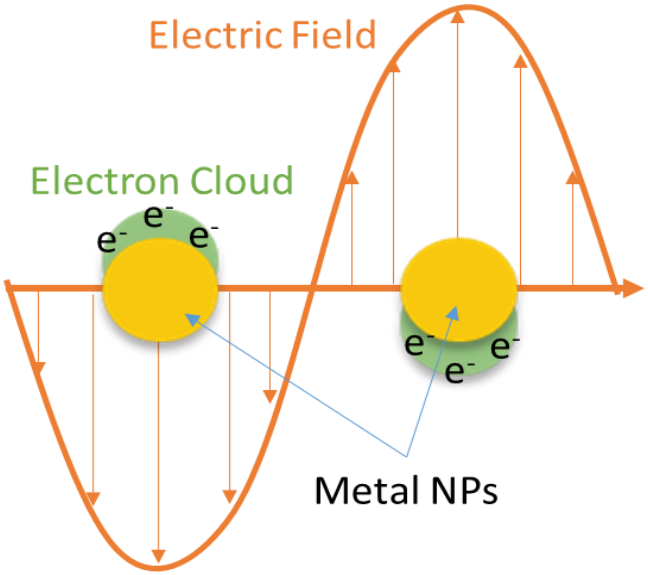

Figure 3. 8 Schematic description of LSPR in gold NPs

One of the most important properties of LSPR derives from the possibility of varying the position of the plasmonic peak by changing size, shape, composition of the nanostructure and dielectric characteristics of the medium in which the nanostructures are dispersed. Since nanoparticles have a high surface area / volume ratio, the plasmonic frequency is very sensitive to the dielectric nature of its interface with the medium. This peculiarity makes them extremely interesting for biomedical applications[68,69].

The optical absorption properties of spherical NPs were demonstrated through the Mie theory[69], which takes into consideration two phenomena: scattering and absorption. Scattering occurs when the electronic oscillations coming from light exposure cause the emission of part of the incident electromagnetic energy in all directions, while the absorption is the phenomenon for which excited elementary charges can transform and dissipate photonic energy in the form of thermal energy. According to this theory, in small plasmonic nanoparticles the absorption dominates the light radiation extinction process, but with increasing size also scattering appears. For example, as shown in figure 3.9 GNPs approximately around 20 nm

in size exhibit a plasmonic peak at 520 nm. The size increase of nanospheres or their aggregation, involves the coupling of the surface plasmons with a consequent shift of the plasmonic frequencies, accompanied by a widening of the peak.

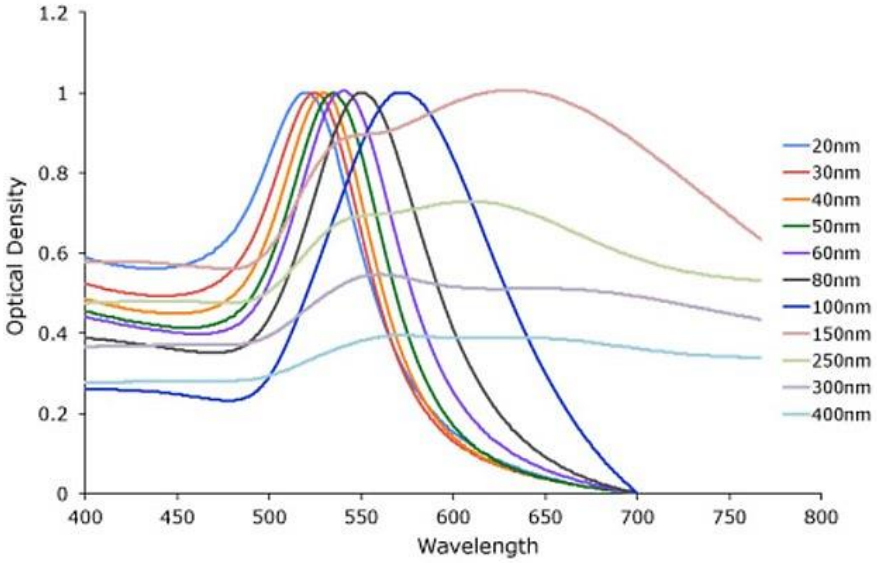

Figure 3. 9 Gold nanoparticle size dependant surface plasmon resonance.[70]

Is noteworthy how the SPR peak of nanometric spheres are included in a wavelength between 520 nm and 650 nm, so limited to the visible region. In many biological applications, especially in in vivo studies, it is preferable to work in the spectral region of the near IR (NIR), 650-900nm. As shown in figure 3.10B, this area is characterized by a high transmission in soft tissues given by a low absorption of deoxygenated and oxygenated hemoglobin (<650nm) and water (>900nm) in the blood and tissue scattering, for this reason light can penetrate deeply in the tissues without interfering with tissues and organs[71]. LSPR peaks in the NIR region can only be obtained from non-spherical GNPs such as Gold nanorods (GNRs)[72]. In this case, two plasmonic bands are observed (Figure 3.10 A), resulting from electronic oscillations along the two axes. The "transverse" plasmonic band, at about 520nm, corresponds to the oscillation along the shortest axis of the particle, the "longitudinal" one, in the NIR region, is defined by the length/width ratio[69,73].

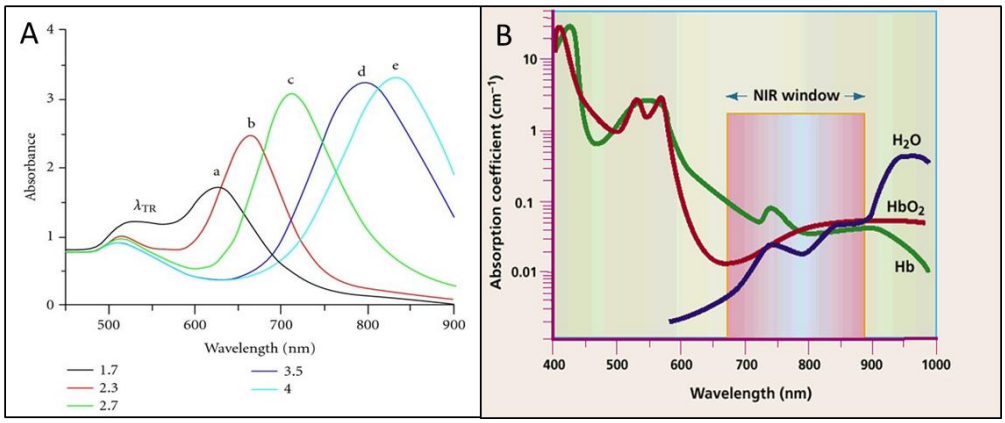

Figure 3. 10 A: Optical absorption spectra of AuNRs with different aspect ratios (a-e).[74] B: absorbance of water, deoxygenated haemoglobin (Hb) and oxygenated haemoglobin (HbO_2)[71]

GNPs possess other important properties such as their simple chemistry which allow functionalization of their surface with the required ligands. In fact, they can be easily conjugated with polymers, small molecules useful for molecular targeting or with recognition binders for high specificity in biological recognition molecules. Moreover, they are photostable and do not undergo photobleaching, allowing the use of higher excitation energies and longer irradiation times;

Specific control of nanoparticle size distribution and shape/diameter, high biocompatibility and large available surface area that can be easily functionalized with a very dense layer of ligands, make GNPs a very promising nanomaterial for applications in the fields of drug delivery, diagnostics, and therapy[75].

3.2.2 Biomedical Applications

Thanks to the peculiar properties of GNPs they found different applications in biological fields, in fact, they are used as systems for specific targeting, agents for photothermal therapies, as carrier for drug delivery or contrast agent for molecular imaging[76].

In table 3.5 are summarized the main GNPs application listed by type of nanoparticles[77].

Table 3. 5 GNPs main application[77]

Type of Gold	Size	Photothermal Conversion Efficacy	Laser	Treatment	Application	Brief Mechanism
Gold nanorods	17 × 56 nm	22%	0.4 W/cm^2, 808 nm	PTT	In vitro cell eradication	Specific targeted, NIR wavelength
	10 × 38 nm	95%	CW laser, 809 nm		In vivo cancer treatment	Nontargeted, NIR wavelength
	13 × 44 nm	55%	815 nm		In vivo cancer treatment	Specific targeted GNRs laden macrophages, NIR wavelength
	7 × 26 nm	50%	2 W/cm^2, 808 nm	PDT	In vitro Cell eradication PS delivery	Single light wavelength both for PTT and PDT, Specific targeted
					In vitro and in vivo PS delivery cancer treatment	Double light wavelength for PTT and PDT, PS coated GNRs, nontargeted
Gold nanocages	45 nm edge length, 5 nm wall thickness	64%	0.4 W/cm^2, 808 nm	PTT	In vitro cells eradication	Specific targeted, NIR wavelength
					In vivo cancer treatment	PEG coated nanocage specific targeted, NIR wavelength
				PDT	In vitro and in vivo PS delivery, cancer treatment	Double light wavelength for PTT and PDT, PS coated nanocages, nontargeted
Gold sphere	20 nm	97–103%	0.28 W, CW laser, 532 nm	PTT	In vitro cell eradication	Specific targeted, NIR fs wavelength
					In vitro cell eradication	Targeted cells with two specific antibodies to form nanocluster Visible and NIR wavelength
					In vitro cell eradication	Specific targeted, visible wavelength
Gold nanoshell	50 nm	59%	815 nm	PTT	In vivo cancer treatment	PEG coated, nontargeted, NIR wavelength
	145 nm	25%	2 W/cm^2, 808 nm		In vitro cell eradication	PEG coated, specific targeted, NIR wavelength
	154 nm	30%	815 nm		In vitro core of solid tumors treatment	Au-laden monocytes/macrophages, NIR wavelength
	152 nm	39%	CW laser, 2 W/cm^2, 810 nm	PDT	In vitro, PS delivery, cells eradication	A two-photon femtosecond pulsed laser for both PTT and PDT, PS coated GNRs, nontargeted
					In vitro cells eradication	Double light wavelength for PTT and PDT, specific targeted
Gold nanoflower	145 × 123 × 10 nm	74%	1 W/cm^2, 808 nm	PTT	In vitro and in vivo cancer treatment	Nontargeted, NIR wavelength
Gold nanoring	400 nm	56%	CW laser, 0.1 W/mm^2, 700–900 nm	PTT	In vitro cell eradication	Specific targeted, NIR wavelength

3.2.2.1 Photothermal Therapy (PTT)

PTT is a treatment which consists in exploiting light radiation in the visible (Vis) or near infrared (NIR) to produce heat in a specific target region of the body in order to kill cancer cells by inducing their apoptosis. In fact, thanks to the SPR effect of GNPs, when nanoparticles are irradiated with a laser light in a specific wavelength, they can transform the radiation into thermal energy by producing heat which bring cancer cells into apoptosis[78–80]. They can also kill bacterial cells with same mechanism as reported in other studies[81,82].

GNPs show a million times higher absorption capacity than conventional dye molecules, are photostable, biocompatible and have a high conversion efficiency of the light absorbed into heat, this allow to overcome the most common problem of the conventional organic dyes as for example the low absorption efficiency and the photobleaching phenomenon at which they are subjected, which leads them to lose their fluorescence ability over time.

The main advantage of using PTT is using light as external stimulus because it is easy to regulate, focus, and remotely controlled by a pulsed or continued wave laser. This ease of control enables better targeted treatments that lead to less damage to healthy tissues, in fact, it is known that cancer cells have more high heat sensitivity if compared with normal ones[83]. In order to better select cancer cells, GNPs can also be functionalised with specific target ligand which recognise the tumour cells to treat.

Due to the heat produced, that should rise the temperature in a range between 43°C and 46°C[84,85], the nanostructures alter cellular functions causing their destruction, this follow the same mechanism of SPIONs hyperthermia explained above, for which cancer cells goes in apoptosis due to their sensibility to high temperature if compared with healthy ones. The mechanisms of cell death are based on protein denaturation, on cavitation damage induced by the thermal expansion of the nanoparticles, on the breakdown of the cellular structure and, finally, on the evaporation of the cytosol.

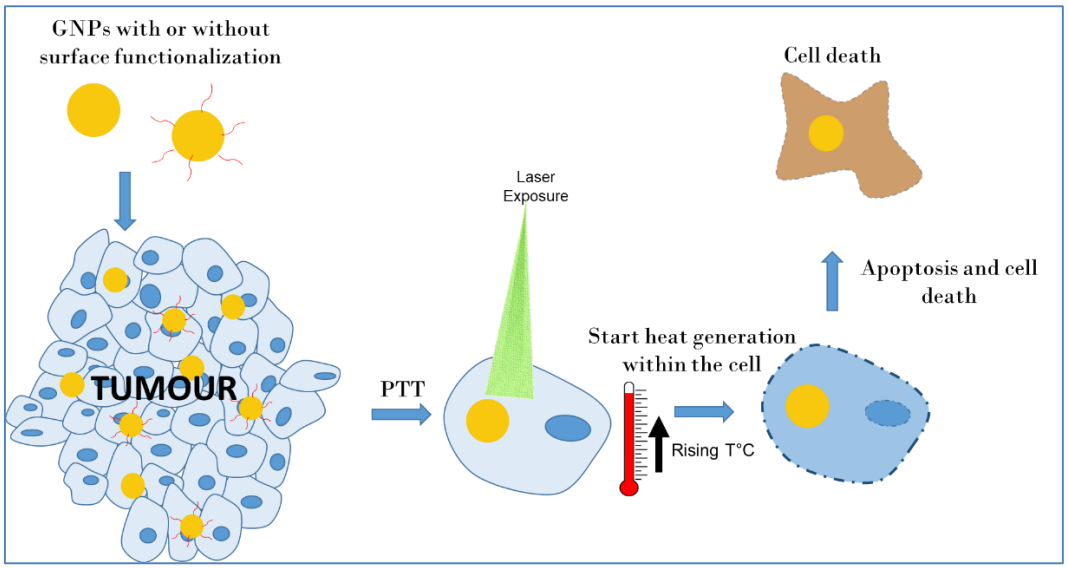

Figure 3. 11 Schematic representation of PTT with GNPs

PTT using radiation in the visible is limited to in vitro studies or to superficial tumour (as skin tumours or buccal mucosa tumours) due to their poor penetration capacity into biological tissues. In order to penetrate more deeply in tissues, near infrared light must be used, as these radiations undergo minimal absorption by hemoglobin and water molecules.

Finally, to ensure the maximal GNPs absorption of irradiation, it is important that there is an overlap between the frequency of the incident wave and the absorption band (LSPR spectrum) of the particles. Usually, as shown in figure 3.9, for GNPs this band falls in the visible light region, but can be moved towards higher wavelengths using nanostructures that have larger dimensions or a different morphology. Moreover, it is possible to obtain a resonance peak at higher wavelengths by mixing cationic dyes (such as toluidine blue) with GNPs suspension[86]: the strong interaction between dyes and NPs trigger the aggregation of nanoparticles into large clusters followed by a new peak developing with higher wavelength on the spectra.

3.2.2.2 Molecular imaging

Thanks to the high scattering and the high photostability if compared with other dyes, GNPs have emerged as extremely promising for cellular imaging and monitoring. This is possible thanks to the scattering properties typical of GNPs that depends on their size and shape. In different studies is shown how GNPs with a size range between 20 and 100 nm are suitable for this purpose, their strong emission power makes them easily detected by using a commercial microscope under dark-field illumination. This make GNPs a promising tool for cancer cell imaging.

3.2.2.3 Drug delivery and Targeting

As mentioned for SPIONs, also GNPs are widely studied for they ability to be functionalised with different targeting molecule and to act as drug delivery system in order to deliver drugs and release them to destroy specific cells. This means that the delivery of free drug molecules takes place with better solubility, protection from the biological environment and better distribution in the biological system.

As already highlighted, therapeutic delivery can take place by functionalising GNPs surface with high affinity ligands that selectively detect cells, organs or tissues. These target GNPs could accumulate in diseased tissues by reducing unwanted absorption into healthy tissue, thus limiting undesirable side effect. Targeting can also help to achieve greater efficiency by reducing the drug dose administered.

The advantage of using GNPs as drug carrier is given by their simple synthesis techniques that involve the presence of particular chemical species on GNPs surface. These molecules form a shell that covers and stabilizes the particles and at the same time provides binding sites (such as free –SH groups) to which various other molecules of interest can be easily attached.

3.1 Silver Nanoparticles

Silver Nanoparticles (AgNPs) have obtained great attention thanks to their interesting and promising characteristic suitable for many biomedical applications. In particular, AgNPs have great potential not only in the development of novel antimicrobial and antibacterial agents (for which they gained impressive attention worldwide)[87,88], but also for a broad range of other applications as drug-delivery carriers, wound dressing, biomaterial and medical device coatings, detection and diagnostic platforms, since they possess good physical and optical properties and biochemical features that can be tailored by changing the size and shape of AgNPs[89]. This NPs in a size range between 1nm to 100nm possess better chemical, physical and biological characteristics if compared with their bulk forms, and this is mainly due to, in addition to their size, also to their shape, crystallinity, composition and structure[90,91].

AgNPs can be synthetize by facile and safe process which offer reproducibility and repeatability, represented by the chemical reduction of silver salt by sodium borohydrate or sodium citrate[92,93]. The use of AgNPs has been limited due to their instability in bacteria-rich environments, which generate a diminution of their anti-pathogenic activity and thus the limitation of their antimicrobial effect. For this reason, in order to improve the stability of NPs, new synthesis methods have been studied with many organic and inorganic, natural and synthetic materials as capping agent[94–97]. Moreover, a green chemistry method to synthetize AgNP which uses biological entities has been proposed as a valuable alternative to other synthesis routes in order to limit their toxicity by reducing metal ions[98,99].

3.3.1 Properties

As already anticipated for GNPs, metallic NPs are mainly studied for their unique properties given by their small size. Thus, also AgNPs possess the exceptional ability to scatter visible light thanks to the LSPR effect which is produced by the collective oscillation of the electron present on their surface. Also for AgNPs, the optical properties can vary by changing the size, shape and composition of nanomaterial which affect the vibration of the free electron of the metallic surface and thus their absorption wavelength. For AgNPs of around 10-20

nm in size, the peak falls in the visible region at 410nm, as shown in figure 3.12 while larger spheres exhibit increased scattering and show peaks that shift towards longer wavelengths.

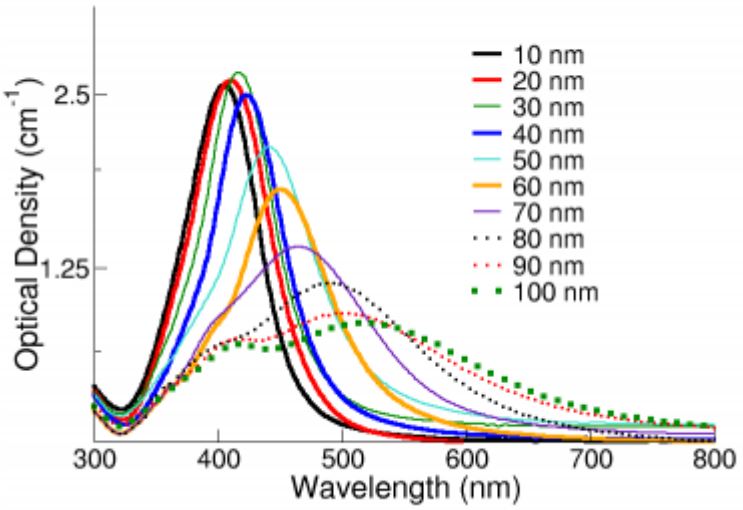

Figure 3. 12 Extinction spectra of AgNPs[100]

Thanks to their tunable optical response, AgNPs can be utilize in different applications as thermal absorbers or as highly bright reporter molecules, but of course the main properties of AgNPs which make them particularly interesting in nanomedicine is their antimicrobial property. In fact, the use of AgNPs have received much attention thanks their chemical cytotoxic property which make them potential anticancer and antibacterial agent. The precise anti-pathogenic mechanism has not been defined clearly, but from current literature it is postulate that the antimicrobial effect exerted from nanosilver can be summarised by different phenomena[101–103] (schematically shown in the picture 3.13): 1) adhesion of AgNPs on the microbial membrane which cause the damage of cell surface and resulting functional and structural alterations; 2) the internalization of NPs inside the cells and the nucleus; 3) the release of Ag+ ions can generate ROS (reactive oxygen species) which implies the sub-cellular structure damage modulating the microbial signal-transduction pathways; 4) genotoxicity by modifying the intracellular signal transduction pathways. Despite various hypothesis, the most remarkable mechanism for which AgNPs exploit the antimicrobial effect is the ROS and free-

radical production[104] given by the releasing rate of silver ions which is strongly influenced by numerous features including size, shape, concentration, colloidal stability, oxidation state and capping agent of AgNPs[101,105].

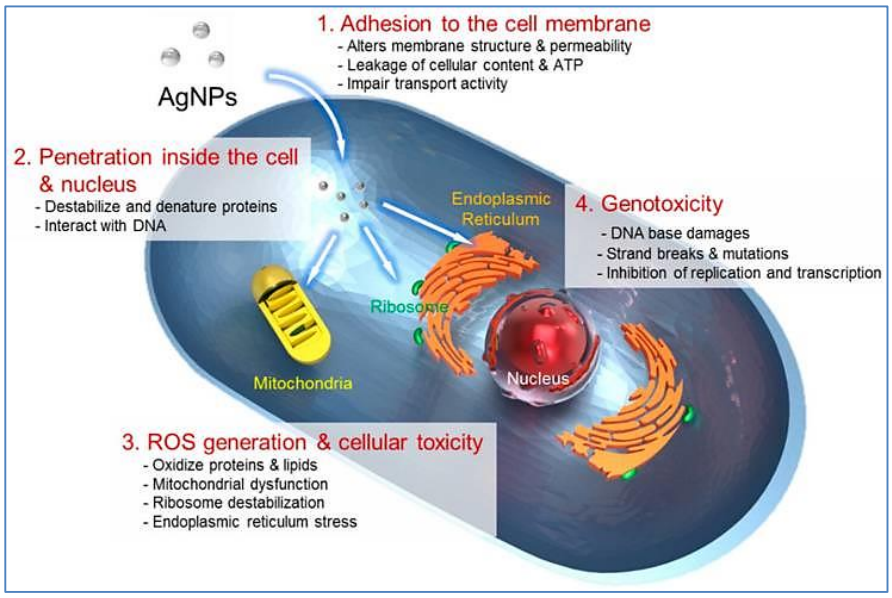

Figure 3. 13 The four main routes of cytotoxic mechanism of AgNPs[106]

Therefore, is necessary to choose correctly the NPs characteristic by considering the antimicrobial treatment and the releasing rate of the silver ions needed for the target application. The potential effect of changing size[107], shape[108] and surface[109] of AgNPs should be take into account, in fact, there is a significant dependence on the size of the particle: if the particle diameter decreases the total surface area increase, and increase also the ion release rate. If the available surface area decreases due to particles destabilization or cluster formation, the ion release rate will decrease. Also the shape has to be considered, because a non-spherical NPs have different crystal facets that dissolve at different rates, resulting in shape-specific ion release rates. The same happen if some molecules are absorbed on the NPs surface which can modulate the dissolution rate.

3.3.2 Biomedical Applications

Thanks to their distinctive physiochemical properties and anti-inflammatory, anti-angiogenesis, antiviral, antifungal, and antibacterial functional features, AgNPs play an important role in the development of novel biomedical applications. In table 3.6 are reported some example of AgNPs emerging application[110].

Table 3. 6 Example of emerging AgNPs application[110].

Medical domains	Examples
Anesthesiology	Coating of breathing mask and endotracheal tube for mechanical ventilatory support
Dentistry	Silver-loaded SiO_2 nanocomposite resin filler as aadditive in polymerizable dental materials
Diagnostics	Nanosilver pyramids for enhanced biodetection Ultrasensitive and ultrafast platform for clinical assays for diagnosis of myocardial infarction Fluorescence-based RNA sensing Magnetic core/shell Fe3O4/Au/Ag nanoparticles with turnable plasmonic properties
Drug delivery	Remote laser light-induced opening of microcapsules
Eye care	Coating of contact lens
Imaging	Silver dendrimer nanocomposite for cell labeling Fluorescent core-shell $Ag@SiO_2$ nanoballs for cellular imaging Molecular imaging of cancer cells
Neurosurgery	Coating of catheter for cerebrospinal fluid drainage
Orthopedics	Additive in bone cement Implantable material using clay-layers with starch-stabilized silver nanoparticles Coating of intramedullary nail for long bone fractures Coating of implant for joint replacement Orthopedic stockings
Patient care	Superabsorbent hydrogel for incontinence material
Pharmaceutics	Treatment of dermatitis Inhibition of HIV-1 replication Treatment of ulcerative colitis Treatment of acne

3.3.2.1 Antimicrobial Application

Among the multiple application of AgNPs, impressive attention is directed toward their bactericidal effect which makes them suitable for unconventional

antimicrobial application in wound dressing, tissue scaffold and biomaterials coating. AgNPs have been broadly used as antibacterial and anticancer agents thanks to their intrinsic cytotoxicity given by their high degree of toxicity against cells. Essential aspect has to be maintained in order to exploit their cytotoxic ability which include maintaining the correct size of AgNPs, improving their stability and their dispersion by avoiding aggregation[111]. In fact, the degree of toxicity against cell is given by the surface area (thus the size and the dispersion) of nanoparticles. In many studies is shown how the positive surface charge of NPs makes them more appropriate to remain for longer time on the tissue surface or on the blood vessel side, this represent the best route for administrating anticancer agent[112]. AgNPs have been applied to different cancer cell lines[113–115] and it has been demonstrated that the smallest sized NPs were more efficient in ROS production than the biggest NPs[116]. Moreover, AgNPs shown also the anti-angiogenic and anti-proliferative activity on cells by damaging DNA and producing genomic instability which induces apoptosis, cells disfunction and causes cytoskeletal injury[117]. This promote the anti-proliferative activity of cancer cells by blocking the cell cycle and division.

Currently, much attention is devoted to use AgNPs in design and develop wound and burn dressing, thanks to the intrinsic anti-inflammatory and antibacterial effect of metallic NPs. Other application in which the cytotoxic effect of AgNPs has been extensively used are textile, pharmaceutics industry and medical device coating[118]. In fact, the specific toxicity against bacteria, has led to the incorporation of AgNPs in a wide variety of products such as antifouling surface coatings, various pharmaceutical formulations as burn ointments, wound dressings and bandages. AgNP-coated bandage is one of the most innovative application in which silver can kill harmful microbes while contemporaneously allowing better healing at the injured tissue. In addition, AgNPs have also been utilized as antimicrobial agent in dental resin[119] and in food packaging so that foods can last for longer without contamination.

3.3.2.2 Other Applications

Thanks to the attractive physico-chemical properties, AgNPs are also plasmonic structure which are able to absorb light and scatter to a specific wavelength, this makes them a suitable approach for cancer theranosctic[120]. In fact,

they can be selective attached to a specific cancerous cell and, after being irradiated, the scattered light can be used for imaging purpose or for selective hyperthermia[121]. Moreover, the broad spectrum bioactivity of this NPs, makes them promising agent in critical tumours and multi-drug resistance approaches. AgNPs can also be utilized as highly sensitive probes for imaging and targeting small molecules, proteins, cells tissue, DNA and tumor[122,123].

Another potential application of AgNPs is for cardiovascular disease. Many researchers are studying the effect of AgNPs on different types of cell present in the complex vascular system, and the data shown potential benefit of metal nanoparticles in phatological and physiological stages of the cardiovascular system. This can be useful for the development of novel specific molecular therapy[124]. For example, the first cardiovascular medical device coated with silver was a prosthetic silicone heart valve, developed to reduce the inflammation response and to avoid the bacterial infection[125].

Another emerging application of AgNPs is related to human eye infectious. Nanosilver-based materials shown promising potential toward the development of therapy of eye-related infectious conditions: AgNPs coated with calcium indicators result to be less harmful than retinal cells[126,127]. As the human eye is a complex organ that can be easily exposed to microbial[128,129], the use of silver-containing nanomaterials could be a promising technique for their treatment and more in-depth studies are needed to evaluate the use of AgNPs as a bactericidal agent in ocular applications.

1. Conde J, Doria G, Baptista P. Noble metal nanoparticles applications in cancer. *J Drug Deliv*. 2012;2012:751075. doi:10.1155/2012/751075
2. Ma X, Zhao Y, Liang X-J. Theranostic nanoparticles engineered for clinic and pharmaceutics. *Acc Chem Res*. 2011;44(10):1114-1122. doi:10.1021/ar2000056
3. Minelli C, Lowe SB, Stevens MM. Engineering nanocomposite materials for cancer therapy. *Small*. 2010;6(21):2336-2357. doi:10.1002/smll.201000523
4. Baptista PV. Cancer Nanotechnology - Prospects for Cancer Diagnostics and Therapy. *Curr Cancer Ther Rev*. 2009;5(2):80-88. doi:http://dx.doi.org/10.2174/157339409788166733
5. Reichel V, Faivre D. Magnetite Nucleation and Growth. In: *New Perspectives on Mineral Nucleation and Growth*. ; 2017:275-291. doi:10.1007/978-3-319-45669-0_14
6. Mathew DS, Juang R-S. An overview of the structure and magnetism of spinel ferrite nanoparticles and their synthesis in microemulsions. *Chem Eng J*. 2007;129(1):51-65. doi:https://doi.org/10.1016/j.cej.2006.11.001
7. Babes L, Denizot B, Tanguy G, Le Jeune JJ, Jallet P. Synthesis of iron oxide nanoparticles used as MRI contrast agents: a parametric study. *J Colloid Interface Sci*. 1999;212(2):474-482.
8. Goya GF, Berquo TS, Fonseca FC, Morales MP. Static and dynamic magnetic properties of spherical magnetite nanoparticles. *J Appl Phys*. 2003;94(5):3520-3528.
9. Gupta AK, Gupta M. Synthesis and surface engineering of iron oxide nanoparticles for biomedical applications. *Biomaterials*. 2005;26(18):3995-4021.
10. Hofmann-Amtenbrink M, Hofmann H, Montet X. Superparamagnetic nanoparticles–a tool for early diagnostics. *Swiss Med Wkly*. 2010;140(ARTICLE).
11. Aktas S. Gas phase preparation of magnetic nanoparticle hydrosols. October 2014.
12. Fu C, Ravindra N. Magnetic iron oxide nanoparticles: Synthesis and applications. *Bioinspired, Biomim Nanobiomaterials*. 2012;1:229-244. doi:10.1680/bbn.12.00014
13. Schramm LL. *Emulsions, Foams, and Suspensions: Fundamentals and*

Applications. John Wiley & Sons; 2006.

14. Malvern Panalytical. Investigating the Impact of Particle Characteristics on Suspension Rheology.
15. Pate K, Safier P. Chemical metrology methods for CMP quality. In: *Advances in Chemical Mechanical Planarization (CMP)*. ; 2016:299-325. doi:10.1016/B978-0-08-100165-3.00012-7
16. Laurent S, Forge D, Port M, et al. Magnetic iron oxide nanoparticles: synthesis, stabilization, vectorization, physicochemical characterizations, and biological applications. *Chem Rev*. 2008;108(6):2064-2110.
17. Choi Y-W, Lee H, Song Y, Sohn D. Colloidal stability of iron oxide nanoparticles with multivalent polymer surfactants. *J Colloid Interface Sci*. 2015;443:8-12.
18. Pankhurst QA, Connolly J, Jones SK, Dobson J. Applications of magnetic nanoparticles in biomedicine. *J Phys D Appl Phys*. 2003;36(13):R167-R181. doi:10.1088/0022-3727/36/13/201
19. Pardoe H, Chua-Anusorn W, Pierre TGS, Dobson J. Structural and magnetic properties of nanoscale iron oxide particles synthesized in the presence of dextran or polyvinyl alcohol. *J Magn Magn Mater*. 2001;225(1-2):41-46.
20. Sangregorio C, Wiemann JK, O'Connor CJ, Rosenzweig Z. A new method for the synthesis of magnetoliposomes. *J Appl Phys*. 1999;85(8):5699-5701.
21. Molday RS, Mackenzie D. Immunospecific ferromagnetic iron-dextran reagents for the labeling and magnetic separation of cells. *J Immunol Methods*. 1982;52(3):353-367.
22. Liberti PA, Rao CG, Terstappen LWMM. Optimization of ferrofluids and protocols for the enrichment of breast tumor cells in blood. *J Magn Magn Mater*. 2001;225(1-2):301-307.
23. Yazdankhah SP, Hellemann A-L, Rønningen K, Olsen E. Rapid and sensitive detection of Staphylococcus species in milk by ELISA based on monodisperse magnetic particles. *Vet Microbiol*. 1998;62(1):17-26.
24. Kala M, Bajaj K, Sinha S. Magnetic bead enzyme-linked immunosorbent assay (ELISA) detects antigen-specific binding by phage-displayed scFv antibodies that are not detected with conventional ELISA. *Anal Biochem*.

1997;254(2):263-266.

25. Hofmann W-K, de Vos S, Komor M, Hoelzer D, Wachsman W, Koeffler HP. Characterization of gene expression of CD34+ cells from normal and myelodysplastic bone marrow. *Blood*. 2002;100(10):3553-3560.
26. Tibbe AGJ, de Grooth BG, Greve J, Liberti PA, Dolan GJ, Terstappen LWMM. Optical tracking and detection of immunomagnetically selected and aligned cells. *Nat Biotechnol*. 1999;17(12):1210.
27. Mahmoudi M, Sant S, Wang B, Laurent S, Sen T. Superparamagnetic iron oxide nanoparticles (SPIONs): Development , surface modi fi cation and applications in chemotherapy. *Adv Drug Deliv Rev*. 2011;63(1-2):24-46. doi:10.1016/j.addr.2010.05.006
28. Yoo D, Lee J-H, Shin T-H, Cheon J. Theranostic magnetic nanoparticles. *Acc Chem Res*. 2011;44(10):863-874. doi:10.1021/ar200085c
29. McNamara K, Tofail SAM. Nanosystems: the use of nanoalloys, metallic, bimetallic, and magnetic nanoparticles in biomedical applications. *Phys Chem Chem Phys*. 2015;17(42):27981-27995. doi:10.1039/c5cp00831j
30. Krishnan KM. Biomedical Nanomagnetics: A Spin Through Possibilities in Imaging, Diagnostics, and Therapy. *IEEE Trans Magn*. 2010;46(7):2523-2558. doi:10.1109/TMAG.2010.2046907
31. Li L, Jiang W, Luo K, et al. Superparamagnetic Iron Oxide Nanoparticles as MRI contrast agents for Non-invasive Stem Cell Labeling and Tracking. *Theranostics*. 2013;3:595-615. doi:10.7150/thno.5366
32. Lodhia J, Mandarano G, Ferris N, Eu P, Cowell S. Development and use of iron oxide nanoparticles (Part 1): Synthesis of iron oxide nanoparticles for MRI. *Biomed Imaging Interv J*. 2010;6:e12. doi:10.2349/biij.6.2.e12
33. van der Zee J. Heating the patient: a promising approach? *Ann Oncol Off J Eur Soc Med Oncol*. 2002;13(8):1173-1184. doi:10.1093/annonc/mdf280
34. Baronzio G, Hager E. *Hyperthermia in Cancer Treatment: A Primer.* New York: Springer. Available from: http://scholar. google. com/scholar; 2006.
35. Roti Roti JL. Cellular responses to hyperthermia (40-46 degrees C): cell killing and molecular events. *Int J Hyperth Off J Eur Soc Hyperthermic Oncol North Am Hyperth Gr*. 2008;24(1):3-15. doi:10.1080/02656730701769841
36. Cavaliere R, Ciocatto EC, Giovanella BC, et al. Selective heat sensitivity of

cancer cells. Biochemical and clinical studies. *Cancer*. 1967;20(9):1351-1381. doi:10.1002/1097-0142(196709)20:9<1351::aid-cncr2820200902>3.0.co;2-#

37. Fajardo LF. Pathological effects of hyperthermia in normal tissues. *Cancer Res*. 1984;44(10 Suppl):4826s-4835s.

38. Gonzales-Weimuller M, Zeisberger M, Krishnan KM. Size-dependant heating rates of iron oxide nanoparticles for magnetic fluid hyperthermia. *J Magn Magn Mater*. 2009;321(13):1947-1950. doi:10.1016/j.jmmm.2008.12.017

39. Fortin J-P, Wilhelm C, Servais J, Ménager C, Bacri J-C, Gazeau F. Size-Sorted Anionic Iron Oxide Nanomagnets as Colloidal Mediators for Magnetic Hyperthermia. *J Am Chem Soc*. 2007;129(9):2628-2635. doi:10.1021/ja067457e

40. Chang D, Lim M, Goos JACM, et al. Biologically Targeted Magnetic Hyperthermia: Potential and Limitations. *Front Pharmacol*. 2018;9:831. doi:10.3389/fphar.2018.00831

41. Wu W, Wu Z, Yu T, Jiang C. Recent progress on magnetic iron oxide nanoparticles : synthesis , surface functional strategies and biomedical applications. *Sci Technol Adv Mater*. 2015;16. doi:10.1088/1468-6996/16/2/023501

42. Conde J, Dias JT, Grazú V, Moros M, Baptista P V. Revisiting 30 years of biofunctionalization and surface chemistry of inorganic nanoparticles for nanomedicine. *Front Chem*. 2014;2(48):1-27. doi:10.3389/fchem.2014.00048

43. Stöber W, Fink A, Bohn E. Controlled growth of monodisperse silica spheres in the micron size range. *J Colloid Interface Sci*. 1968;26(1):62-69. doi:https://doi.org/10.1016/0021-9797(68)90272-5

44. Pinho SLC, Laurent S, Rocha J, et al. Relaxometric Studies of γ-Fe2O3@SiO2 Core Shell Nanoparticles: When the Coating Matters. *J Phys Chem C*. 2012;116(3):2285-2291. doi:10.1021/jp2086413

45. Pinho SLC, Pereira GA, Voisin P, et al. Fine tuning of the relaxometry of gamma-Fe2O3@SiO2 nanoparticles by tweaking the silica coating

thickness. *ACS Nano*. 2010;4(9):5339-5349. doi:10.1021/nn101129r

46. Ding HL, Zhang YX, Wang S, Xu JM, Xu SC, Li GH. Fe3O4@SiO2 Core/Shell Nanoparticles: The Silica Coating Regulations with a Single Core for Different Core Sizes and Shell Thicknesses. *Chem Mater*. 2012;24(23):4572-4580. doi:10.1021/cm302828d
47. Park J-N, Zhang P, Hu Y-S, McFarland EW. Synthesis and characterization of sintering-resistant silica-encapsulated Fe3O4magnetic nanoparticles active for oxidation and chemical looping combustion. *Nanotechnology*. 2010;21(22):225708. doi:10.1088/0957-4484/21/22/225708
48. Liu Y, Li Y, Li X-M, He T. Kinetics of (3-Aminopropyl)triethoxylsilane (APTES) Silanization of Superparamagnetic Iron Oxide Nanoparticles. *Langmuir*. 2013;29(49):15275-15282. doi:10.1021/la403269u
49. Shen M, Cai H, Wang X, et al. Facile one-pot preparation, surface functionalization, and toxicity assay of APTS-coated iron oxide nanoparticles. *Nanotechnology*. 2012;23(10):105601. doi:10.1088/0957-4484/23/10/105601
50. Răcuciu M, Creanga D, Airinei A. Citric-acid-coated magnetite nanoparticles for biological applications. *Eur Phys J E Soft Matter*. 2006;21:117-121. doi:10.1140/epje/i2006-10051-y
51. Jun Y, Huh Y-M, Choi J, et al. Nanoscale Size Effect of Magnetic Nanocrystals and Their Utilization for Cancer Diagnosis via Magnetic Resonance Imaging. *J Am Chem Soc*. 2005;127(16):5732-5733. doi:10.1021/ja0422155
52. Miola M, Ferraris S, Pirani F, et al. Reductant-free synthesis of magnetoplasmonic iron oxide-gold nanoparticles. 2017;43(March):15258-15265. doi:10.1016/j.ceramint.2017.08.063
53. Yang X, Grailer JJ, Rowland IJ, et al. Multifunctional SPIO/DOX-loaded wormlike polymer vesicles for cancer therapy and MR imaging. *Biomaterials*. 2010;31(34):9065-9073. doi:10.1016/j.biomaterials.2010.08.039
54. Dias AMGC, Hussain A, Marcos AS, Roque ACA. A biotechnological perspective on the application of iron oxide magnetic colloids modified with polysaccharides. *Biotechnol Adv*. 2011;29(1):142-155. doi:10.1016/j.biotechadv.2010.10.003

55. Barnett CM, Gueorguieva M, Lees MR, McGarvey DJ, Darton RJ, Hoskins C. Effect of the hybrid composition on the physicochemical properties and morphology of iron oxide–gold nanoparticles. *J Nanoparticle Res*. 2012;14(10):1170.
56. Mahmoudi M, Serpooshan V, Laurent S. Engineered nanoparticles for biomolecular imaging. *Nanoscale*. 2011;3(8):3007-3026. doi:10.1039/C1NR10326A
57. Kirui DK, Rey DA, Batt CA. Gold hybrid nanoparticles for targeted phototherapy and cancer imaging. *Nanotechnology*. 2010;21(10):105105.
58. Guo S, Dong S, Wang E. A general route to construct diverse multifunctional Fe3O4/metal hybrid nanostructures. *Chem Eur J*. 2009;15(10):2416-2424.
59. Wang L, Luo J, Maye MM, et al. Iron oxide–gold core–shell nanoparticles and thin film assembly. *J Mater Chem*. 2005;15(18):1821-1832.
60. Chiang I-C, Chen D-H. Structural characterization and self-assembly into superlattices of iron oxide–gold core–shell nanoparticles synthesized via a high-temperature organometallic route. *Nanotechnology*. 2008;20(1):15602. doi:10.1088/0957-4484/20/1/015602
61. Grzelczak M, Vermant J, Furst EM, Liz-Marzán LM. Directed Self-Assembly of Nanoparticles. *ACS Nano*. 2010;4(7):3591-3605. doi:10.1021/nn100869j
62. Truby RL, Emelianov SY, Homan KA. Ligand-Mediated Self-Assembly of Hybrid Plasmonic and Superparamagnetic Nanostructures. *Langmuir*. 2013;29(8):2465-2470. doi:10.1021/la3037549
63. Maier S, Atwater H. Plasmonics: Localization and guiding of electromagnetic energy in metal/dielectric structures. *J Appl Phys*. 2005;98. doi:10.1063/1.1951057
64. Lasagna-Reeves C, Gonzalez-Romero D, Barria MA, et al. Bioaccumulation and toxicity of gold nanoparticles after repeated administration in mice. *Biochem Biophys Res Commun*. 2010;393(4):649-655. doi:10.1016/j.bbrc.2010.02.046
65. Malik P, Mukherjee TK. Recent advances in gold and silver nanoparticle based therapies for lung and breast cancers. *Int J Pharm*. 2018;553(1):483-

509. doi:https://doi.org/10.1016/j.ijpharm.2018.10.048

66. Zhao P, Li N, Astruc D. State of the art in gold nanoparticle synthesis. *Coord Chem Rev*. 2013;257(3):638-665. doi:https://doi.org/10.1016/j.ccr.2012.09.002

67. Murphy CJ, Sau TK, Gole AM, et al. Anisotropic metal nanoparticles: Synthesis, assembly, and optical applications. *J Phys Chem B*. 2005;109(29):13857-13870. doi:10.1021/jp0516846

68. Jain PK, Huang X, El-Sayed IH, El-Sayed MA. Noble metals on the nanoscale: optical and photothermal properties and some applications in imaging, sensing, biology, and medicine. *Acc Chem Res*. 2008;41(12):1578-1586. doi:10.1021/ar7002804

69. Link S, El-Sayed MA. Shape and size dependence of radiative, non-radiative and photothermal properties of gold nanocrystals. *Int Rev Phys Chem*. 2000;19(3):409-453. doi:10.1080/01442350050034180

70. Dattila F. Applications of carbon nanostructures to dye-sensitized solar cells. October 2017.

71. Weissleder R. A clearer vision for in vivo imaging. *Nat Biotechnol*. 2001;19(4):316-317. doi:10.1038/86684

72. Alkilany AM, Murphy CJ. Toxicity and cellular uptake of gold nanoparticles: what we have learned so far? *J Nanopart Res*. 2010;12(7):2313-2333. doi:10.1007/s11051-010-9911-8

73. Niidome T, Yamagata M, Okamoto Y, et al. PEG-modified gold nanorods with a stealth character for in vivo applications. *J Control Release*. 2006;114(3):343-347. doi:10.1016/j.jconrel.2006.06.017

74. Kumar A, Boruah B, Liang X-J. Gold Nanoparticles: Promising Nanomaterials for the Diagnosis of Cancer and HIV/AIDS. *Hindawi Publ Corp J Nanomater*. 2011;17. doi:10.1155/2011/202187

75. Dykman LA, Khlebtsov NG. Gold nanoparticles in biology and medicine: recent advances and prospects. *Acta Naturae*. 2011;3(2):34-55.

76. Shilpi S, Khatri K. Gold Nanoparticles as Carrier(s) for Drug Targeting and Imaging. *Pharm Nanotechnol*. 2015;04:1. doi:10.2174/2211738504666151127192830

77. Kim HS, Lee DY. Near-Infrared-Responsive Cancer Photothermal and Photodynamic Therapy Using Gold Nanoparticles. *Polym* . 2018;10(9).

doi:10.3390/polym10090961

78. Sau TK, Rogach AL, Jäckel F, Klar TA, Feldmann J. Properties and Applications of Colloidal Nonspherical Noble Metal Nanoparticles. *Adv Mater*. 2010;22(16):1805-1825. doi:10.1002/adma.200902557

79. Huang X, El-Sayed IH, Qian W, El-Sayed MA. Cancer Cell Imaging and Photothermal Therapy in the Near-Infrared Region by Using Gold Nanorods. *J Am Chem Soc*. 2006;128(6):2115-2120. doi:10.1021/ja057254a

80. Ma L, Li F, Fang T, Zhang J, Wang Q. Controlled Self-Assembly of Proteins into Discrete Nanoarchitectures Templated by Gold Nanoparticles via Monovalent Interfacial Engineering. *ACS Appl Mater Interfaces*. 2015;7(20):11024-11031. doi:10.1021/acsami.5b02823

81. Mitra P, Chakraborty PK, Saha P, Ray P, Basu S. Antibacterial efficacy of acridine derivatives conjugated with gold nanoparticles. *Int J Pharm*. 2014;473(1-2):636-643. doi:10.1016/j.ijpharm.2014.07.051

82. Jarvis RM, Law N, Shadi IT, O'Brien P, Lloyd JR, Goodacre R. Surface-Enhanced Raman Scattering from Intracellular and Extracellular Bacterial Locations. *Anal Chem*. 2008;80(17):6741-6746. doi:10.1021/ac800838v

83. Vinod M, Jayasree RS, Gopchandran KG. Synthesis of pure and biocompatible gold nanoparticles using laser ablation method for SERS and photothermal applications. *Curr Appl Phys*. 2017;17(11):1430-1438. doi:https://doi.org/10.1016/j.cap.2017.08.004

84. Terentyuk GS, Maslyakova GN, Suleymanova L V, et al. Laser-induced tissue hyperthermia mediated by gold nanoparticles: toward cancer phototherapy. *J Biomed Opt*. 2009;14(2):1-9. https://doi.org/10.1117/1.3122371.

85. Zhang Y, Zhan X, Xiong J, et al. Temperature-dependent cell death patterns induced by functionalized gold nanoparticle photothermal therapy in melanoma cells. *Sci Rep*. 2018;8(1):8720. doi:10.1038/s41598-018-26978-1

86. Kitching H, Kenyon AJ, Parkin IP. The interaction of gold and silver nanoparticles with a range of anionic and cationic dyes. *Phys Chem Chem Phys*. 2014;44(0):6050-6059. doi:10.1039/c3cp55366c

87. Geraldo DA, Needham P, Chandia N, Arratia-Perez R, Mora GC, Villagra

NA. Green synthesis of polysaccharides-based gold and silver nanoparticles and their promissory biological activity. *Biointerface Res Appl Chem*. 2016;6:1263–1271.

88. Alexander JW. History of the medical use of silver. *Surg Infect (Larchmt)*. 2009;10(3):289-292. doi:10.1089/sur.2008.9941
89. Nedelcu I-A, Ficai A, Sonmez M, Ficai D, Oprea O, Andronescu E. Silver based materials for biomedical applications. *Curr Org Chem*. 2014;18(2):173-184.
90. Syafiuddin A, Salim MR, Beng Hong Kueh A, Hadibarata T, Nur H. A review of silver nanoparticles: Research trends, global consumption, synthesis, properties, and future challenges. *J Chinese Chem Soc*. 2017;64(7):732-756.
91. Desireddy A, Conn BE, Guo J, et al. Ultrastable silver nanoparticles. *Nature*. 2013;501(7467):399.
92. Muhammad H, Juluri RR, Fojan P, Popok V. Polymer films with size-selected silver nanoparticles as plasmon resonance-based transducers for protein sensing. *Biointerface Res Appl Chem*. 2016;6(5):1564-1568.
93. Mahmoud KH, Abbo M. Synthesis, characterization and optical properties of gelatin doped with silver nanoparticles. *Spectrochim Acta Part A Mol Biomol Spectrosc*. 2013;116:610-615.
94. Panzarini E, Mariano S, Vergallo C, et al. Glucose capped silver nanoparticles induce cell cycle arrest in HeLa cells. *Toxicol Vitr*. 2017;41:64-74.
95. Lau CP, Abdul-Wahab MF, Jaafar J, Chan GF, Rashid NAA. Toxic effect of high concentration of sonochemically synthesized polyvinylpyrrolidone-coated silver nanoparticles on Citrobacter sp. A1 and Enterococcus sp. C1. *J Microbiol Immunol Infect*. 2017;50(4):427-434.
96. Muhammad Z, Raza A, Ghafoor S, et al. PEG capped methotrexate silver nanoparticles for efficient anticancer activity and biocompatibility. *Eur J Pharm Sci*. 2016;91:251-255.
97. Chien C-S, Lin C-J, Ko C-J, Tseng S-P, Shih C-J. Antibacterial activity of silver nanoparticles (AgNP) confined to mesostructured silica against methicillin-resistant Staphylococcus aureus (MRSA). *J Alloys Compd*. 2018;747:1-7.

98. Ahmed S, Ikram S. Silver nanoparticles: one pot green synthesis using Terminalia arjuna extract for biological application. *J Nanomed Nanotechnol*. 2015;6(4):309.
99. Fayaz AM, Balaji K, Girilal M, Yadav R, Kalaichelvan PT, Venketesan R. Biogenic synthesis of silver nanoparticles and their synergistic effect with antibiotics: a study against gram-positive and gram-negative bacteria. *Nanomedicine Nanotechnology, Biol Med*. 2010;6(1):103-109.
100. Nanocomposix. https://nanocomposix.com/pages/silver-nanoparticles-optical-properties.
101. Durán N, Durán M, De Jesus MB, Seabra AB, Fávaro WJ, Nakazato G. Silver nanoparticles: A new view on mechanistic aspects on antimicrobial activity. *Nanomedicine Nanotechnology, Biol Med*. 2016;12(3):789-799.
102. Zheng K, Setyawati MI, Leong DT, Xie J. Antimicrobial silver nanomaterials. *Coord Chem Rev*. 2018;357:1-17.
103. Akter M, Sikder MT, Rahman MM, et al. A systematic review on silver nanoparticles-induced cytotoxicity: Physicochemical properties and perspectives. *J Adv Res*. 2018;9:1-16.
104. Thomas R, Soumya KR, Mathew J, Radhakrishnan EK. Inhibitory effect of silver nanoparticle fabricated urinary catheter on colonization efficiency of Coagulase Negative Staphylococci. *J Photochem Photobiol B Biol*. 2015;149:68-77.
105. Koduru JR, Kailasa SK, Bhamore JR, Kim K-H, Dutta T, Vellingiri K. Phytochemical-assisted synthetic approaches for silver nanoparticles antimicrobial applications: A review. *Adv Colloid Interface Sci*. 2018;256:326-339.
106. Lee SH, Jun B-H. Silver Nanoparticles: Synthesis and Application for Nanomedicine. *Int J Mol Sci*. 2019;20(4):865. doi:10.3390/ijms20040865
107. Lee J-H, Lim J-M, Velmurugan P, et al. Photobiologic-mediated fabrication of silver nanoparticles with antibacterial activity. *J Photochem Photobiol B Biol*. 2016;162:93-99.
108. Ghiuță I, Cristea D, Croitoru C, et al. Characterization and antimicrobial activity of silver nanoparticles, biosynthesized using Bacillus species. *Appl*

Surf Sci. 2018;438:66-73.

109. Zhou Y, Hu K, Guo Z, et al. PLLA microcapsules combined with silver nanoparticles and chlorhexidine acetate showing improved antibacterial effect. *Mater Sci Eng C*. 2017;78:349-353.
110. Rawat M. A REVIEW ON GREEN SYNTHESIS AND CHARACTERIZATION OF SILVER NANOPARTICLES AND THEIR APPLICATIONS: A GREEN NANOWORLD. *World J Pharm Pharm Sci*. 2016:730-762.
111. Suresh AK, Pelletier DA, Wang W, Morrell-Falvey JL, Gu B, Doktycz MJ. Cytotoxicity induced by engineered silver nanocrystallites is dependent on surface coatings and cell types. *Langmuir*. 2012;28(5):2727-2735.
112. Schlinkert P, Casals E, Boyles M, et al. The oxidative potential of differently charged silver and gold nanoparticles on three human lung epithelial cell types. *J Nanobiotechnology*. 2015;13(1):1.
113. Jeyaraj M, Sathishkumar G, Sivanandhan G, et al. Biogenic silver nanoparticles for cancer treatment: an experimental report. *Colloids surfaces B Biointerfaces*. 2013;106:86-92.
114. Foldbjerg R, Dang DA, Autrup H. Cytotoxicity and genotoxicity of silver nanoparticles in the human lung cancer cell line, A549. *Arch Toxicol*. 2011;85(7):743-750.
115. Kawata K, Osawa M, Okabe S. In vitro toxicity of silver nanoparticles at noncytotoxic doses to HepG2 human hepatoma cells. *Environ Sci Technol*. 2009;43(15):6046-6051.
116. Carlson C, Hussain SM, Schrand AM, et al. Unique cellular interaction of silver nanoparticles: size-dependent generation of reactive oxygen species. *J Phys Chem B*. 2008;112(43):13608-13619.
117. Zhang W-S, Cao J-T, Dong Y-X, Wang H, Ma S-H, Liu Y-M. Enhanced chemiluminescence by Au-Ag core-shell nanoparticles: A general and practical biosensing platform for tumor marker detection. *J Lumin*. 2018;201:163-169.
118. Sharma VK, Yngard RA, Lin Y. Silver nanoparticles: green synthesis and their antimicrobial activities. *Adv Colloid Interface Sci*. 2009;145(1-2):83-96.
119. Sondi I, Salopek-Sondi B. Silver nanoparticles as antimicrobial agent: a case

study on E. coli as a model for Gram-negative bacteria. *J Colloid Interface Sci*. 2004;275(1):177-182.

120. Vedelago J, Gomez CG, Valente M, Mattea F. Green synthesis of silver nanoparticles aimed at improving theranostics. *Radiat Phys Chem*. 2018;146:55-67.
121. Sharma H, Mishra PK, Talegaonkar S, Vaidya B. Metal nanoparticles: a theranostic nanotool against cancer. *Drug Discov Today*. 2015;20(9):1143-1151.
122. Poudel BK, Soe ZC, Ruttala HB, et al. In situ fabrication of mesoporous silica-coated silver-gold hollow nanoshell for remotely controllable chemo-photothermal therapy via phase-change molecule as gatekeepers. *Int J Pharm*. 2018;548(1):92-103.
123. Ding Q, Liu D, Guo D, et al. Shape-controlled fabrication of magnetite silver hybrid nanoparticles with high performance magnetic hyperthermia. *Biomaterials*. 2017;124:35-46.
124. Gonzalez C, Rosas-Hernandez H, Ramirez-Lee MA, Salazar-García S, Ali SF. Role of silver nanoparticles (AgNPs) on the cardiovascular system. *Arch Toxicol*. 2016;90(3):493-511.
125. Ge L, Li Q, Wang M, Ouyang J, Li X, Xing MMQ. Nanosilver particles in medical applications: synthesis, performance, and toxicity. *Int J Nanomedicine*. 2014;9:2399.
126. Yee W, Selvaduray G, Hawkins B. Characterization of silver nanoparticle-infused tissue adhesive for ophthalmic use. *J Mech Behav Biomed Mater*. 2016;55:67-74.
127. Weng Y, Liu J, Jin S, Guo W, Liang X, Hu Z. Nanotechnology-based strategies for treatment of ocular disease. *Acta Pharm Sin B*. 2017;7(3):281-291.
128. Söderstjerna E, Bauer P, Cedervall T, Abdshill H, Johansson F, Johansson UE. Silver and gold nanoparticles exposure to in vitro cultured retina–studies on nanoparticle internalization, apoptosis, oxidative stress, glial-and microglial activity. *PLoS One*. 2014;9(8).
129. Sung A, Kim T-H. Physical properties of ophthalmic hydrogel polymer

containing zinc oxide nanoparticles. *J Chosun Nat Sci*. 2013;6(2):76-81.

Chapter 4

Biodistribution, Biodegradation and Toxicity

Given the great improvements of nanotechnology in medical field, in the pharmacological sector, for therapy, diagnosis and for their use as biocompatible materials for prosthesis and implant, also human exposure to nanostructured particulate matter is subject of increasing attention. Many studies have revealed that the unique innovative properties that make nanostructures so interesting for industry and biomedicine, such as their small size, large surface area, chemical composition, solubility and geometry, can contribute to their potential toxicological profile towards biological systems, the human body and the environment[1]. Therefore, while on the one hand nanotechnologies are developing extraordinarily in the perspective of expected benefits, on the other the problem of their safety arises with greater insistence.

The nanotoxicology is defined as the safety assessment of nanostructured materials and nanodevices. It has been found that nanoparticles are biologically active, this means that, in terms of toxicity, these biological activities can lead to

potential inflammation and pro-oxidant activities, but also to antioxidant activities[2]. The basic parameters of conventional toxicology are concentration and time, these factors can be easily measured for each chemical products and, after establishing the nature of the dose response of a certain substance, threshold levels can be determined, according to which, a chemical compound can be considered "safe" or " dangerous"[3]. The realization of materials of ever-smaller dimensions leads to variations in the surface chemistry of these structures, increasing their reactivity. For this reason, a lot of research[4–6] has started aimed at studying the toxicological potential of nanomaterials and the effect of the increase of their reactive surfaces due to the increase of the surface-volume ratio.

In addition to the atomic composition, it is very important to evaluate whether the nanoparticles are located inside or on the surface of a solid material or if they are inside a volume of a liquid or a gas, free and able to move in the environment and inside the body. The latter are the particles to be paid more attention to. Thus, in order to evaluate the NPs toxicity is necessary to consider different factors:

- Size, shape and surface charge of nanoparticles: It is only through knowledge of the nanoparticle's properties that their toxicological evaluation is possible. This is important for both industrial and environmental particles and for nanoparticles used in nanomedicine.
- Maximum dose of NPs: It is important to draw meaningful conclusions from in vitro and in vivo experiments in order to calculate the realistic dose for assessing public health risk. This means that it is necessary to test the toxicity of the nanoparticles on real doses rather than high and unrealistic doses, in order to obtain a real biological response. When dealing with high doses it is easier to detect the danger limit and to implement precautions and protections[7]. However, the main public health problems are due to chronic low-dose exposures over time, which can lead to an increase in degenerative diseases[8].
- NPs surface: Smaller is the diameter of a spherical particle, more the surface-volume ratio increases, an increase in the surface implies an increase in chemical reactivity[9]. Therefore, special attention must be paid to the nanoparticle's surface material. Several studies have shown that it is not the nanomaterial itself, but its surface layer that mainly defines the

properties of the compound[10]. This feature can be used to design particles with specific surface properties in order to establish some paths within biological systems. However, this result to be very complicated because, in a biological context, the NPs come into contact with heterogeneous, liquid or gaseous environments, and smaller structures such as atoms, clusters of atoms or macromolecules can attach to them. So it is important to understand not only the type of nanomaterial, but also the environment in which the nanoparticles move.

- The environment: several times it has been said that the nanoparticles released into the environment interact with water, air etc. This involves a variation in surface charge or other surface properties. It is therefore necessary to observe also the behavior of the nanoparticles with the surrounding environment[11].

4.1 Nanoparticles-cells interaction

The interaction mechanisms between NPs and cells are not yet fully understood. The problem comes from the ability of the particles to bind and interact with biological matter and to change their surface characteristics, depending on the environment in which they operate. Scientific knowledge on nanoparticle-cell interaction mechanisms indicates that cells absorb nanoparticles through active or passive mechanisms. Even particles of the same material can exhibit completely different behavior due to small differences in surface coating, charge or size. This makes the categorization of the nanoparticles behavior very difficult when in contact with biological systems. When dealing with nanoparticles smaller than 50nm, the spreading mechanisms are the same used by viruses[12,13]. Therefore, in all nanotoxicology studies, the particle dose should be carefully considered and high attention should be paid not only to the initial concentration with which the cells are exposed to the nanoparticles, but also to the actual quantity of nanoparticles taken by a single cell. The mechanisms that occur on the nanoparticle/cell interface can be both of chemical or physical nature[9].

Chemical mechanisms include[14–18]:

-Production of ROS (reactive oxygen species) (which is one of the main factors involved in inflammatory processes and can involve secondary processes that can cause cell damage and also cell death);

-Release of toxic ions;

-Disorders of electron/ion transport activity of the cell membrane;

-Lipid peroxidation.

-Oxidative damage through catalysis;

The physical mechanisms at the interface are primarily the result of the NPs size and surface properties which leads to the interruption of membrane activity, transport processes, conformation and aggregation of proteins[19–21].

Both chemical and physical interactions lead to a series of processes in the cell that define the biological response. The cell membrane divides the cell from its external environment and permits the selective transport of molecules, ions and nanoparticles. NPs can influence the membrane stability, possibly causing cell death, both directly through physical damage and indirectly through, for example oxidation. The interactions of NPs with membranes mostly depend on their surface properties, this is the reason why surface modifications are essential to design drug delivery systems able to improve the NPs uptake in cells[22].

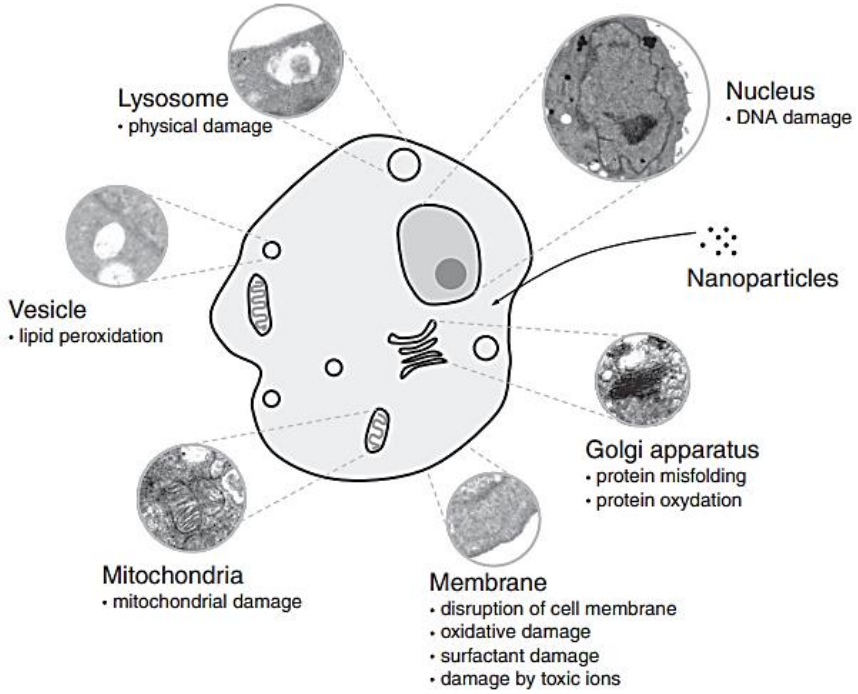

Figure 4. 1 interaction of nanoparticles with cells[23]

In figure 4.1 are shown nanotoxicological mechanisms of the interaction of nanoparticles with cells. Some research confirm how different material can damage cells by different process, compromising the stability and the integrity of cell membrane[24,25]. Is shown how both the nanomaterial itself and the concentration used, are responsible in membrane damage, as well as physical-chemical properties of NPs can make changes in stability and morphology of membrane. Moreover, other studies have shown how specific NPs can influence the mitochondrial function by bringing cell to apoptosis, or how many particles end up inside the lysosomes, the place where the cell tries to digest or expel them[26,27]. In addition, the smaller NPs can also spread within the pores of the nuclear membrane, thus managing to enter the nucleus. In this case, also the DNA damage have to be considered, this can occur both from chemical or physical interaction with NPs (if they are internalized in the nucleus) or through ROS reaction of NPs (if they have not reached the nucleus) which can induce genotoxicity[28,29]. Obviously the size and

shape of the NPs influence their ability to enter or accumulate within the cell or in the intra-nuclear area.

4.2 In vivo nanotoxicology

In order to assess the NPs toxicity, in vitro models are not sufficient to predict possible risks for humans, in vivo studies are therefore needed to clarify the mechanisms and pathways of nanoparticles into a complex multicellular organism[30]. This is especially necessary for nanomaterials used in nanomedicine which are voluntarily administrate inside the body. Iron oxide and gold NPs, are the most used for nanotherapeutic applications thanks to their exceptional bio-conjugation properties, research shows that their coating and surface are of fundamental importance for predicting toxicological effects. However, it is still unclear until what point the body is able to expel them and if the residual NPs tend to accumulate in particular organs, eventually blocking and compromising the body's excretion systems[31,32]. In addition, it is necessary to consider that while at first the NPs biodistribution is regulated by parameters aimed at eluding, as far as possible, the clearance mechanisms and increasing their targeting effectiveness, later, once NPs performed their function, other factors come into play, such as the mechanisms of metabolic regulation. In fact, as soon as the nanoparticles are introduced into the body, the immune system performs a series of physiological mechanisms aimed at recognizing these foreign substances, directing them towards the main excretion pathways[6,8]. Therefore, a sort of "competition" is established between the desired distribution of nanoparticles in specific organs or tissues and their recognition and elimination rate. It is, therefore, extremely important to know the parameters governing these two aspects, in order to improve the NPs expected functionality, increase their therapeutic efficacy and biosafety, while minimizing their toxic effects.

Depending on the application they are intended for, NPs can be administered in different ways, but intravenous injection represents the most commonly used approach. Regardless of the administration method, the human body responds quickly to their presence, trying to eliminate them through two different mechanisms of clearance: the reticuloendothelial system (RES) and renal

clearance[33,34]. It should be underlined that surface modifications aimed at ensuring greater effectiveness of intracellular administration or a better evasion of the RES clearance mechanisms, usually tend to increase their potential toxicity.

Several studies aimed at evaluating the toxicity of magnetic NPs, have observed that after the NPs intracellular degradation processes, there is an excess of iron in the organs that must be regulated, since the accumulation of free iron can increase oxidative stress and cause toxicity[35,36]. As already mentioned, the way in which the body metabolizes the NPs, depends on their chemical composition and especially on the type of coating or ligands present on their surface, but the iron oxide core usually enters the normal body iron reserve and follow the same excretion paths of the endogenous compounds.

Therefore, on the one hand, nanotechnology aims to reap the benefits of nanomaterials with extraordinary performance and on the other, its development must address the problem of their safety, connected to the potential dangers and risks for human beings. It is therefore necessary that the advantages brought by the use of nanotechnology are greater than the potential risks. In recent years, the use of nanoparticles for medical purposes has increased significantly. As regards the nanoparticles for theranostics (in particular SPIONs), many researches have been started on their toxic effects, since they are particularly versatile in in-vivo applications, hence it is necessary to seriously consider their long-term toxicity, and carry out more studies on nanotoxicology in order to make these nanomaterials more and more safe and usable in many field of nanomedicine.

1. Santos-Martinez, M., Radomska, A., Corrigan, O. & Radomski, M. Nanoparticles: Pharmacological and toxicological significance. *Br. J. Pharmacol.* **150,** 552–558 (2007).
2. Singh, S. & Nalwa, H. S. Nanotechnology and Health Safety – Toxicity and Risk Assessments of Nanostructured Materials on Human Health. *J. Nanosci. Nanotechnol.* **7,** 3048–3070 (2007).
3. Sayes, C. M. & Warheit, D. B. Characterization of nanomaterials for toxicity assessment. *Wiley Interdiscip. Rev. Nanomed. Nanobiotechnol.* **1,** 660–670 (2009).
4. Buzea, C., Pacheco, I. I. & Robbie, K. Nanomaterials and nanoparticles: Sources and toxicity. *Biointerphases* **2,** MR17-MR71 (2007).
5. Oberdörster, G. Safety assessment for nanotechnology and nanomedicine: concepts of nanotoxicology. *J. Intern. Med.* **267,** 89–105 (2010).
6. Sahu, S. C. & Hayes, A. W. Toxicity of nanomaterials found in human environment: A literature review. *Toxicol. Res. Appl.* **1,** 2397847317726352 (2017).
7. Song, Y., Li, X. & Du, X. Exposure to nanoparticles is related to pleural effusion, pulmonary fibrosis and granuloma. *Eur. Respir. J.* **34,** 559–567 (2009).
8. Oberdürster, G. Toxicology of ultrafine particles: in vivo studies. *Philos. Trans. R. Soc. London. Ser. A Math. Phys. Eng. Sci.* **358,** 2719–2740 (2000).
9. Nel, A. E. *et al.* Understanding biophysicochemical interactions at the nano–bio interface. *Nat. Mater.* **8,** 543–557 (2009).
10. Navarro, E. *et al.* Environmental behavior and ecotoxicity of engineered nanoparticles to algae, plants, and fungi. *Ecotoxicology* **17,** 372–386 (2008).
11. Nowack, B. The behaviour and effects of nanoparticles in the environment. *Environ. Pollut.* **157,** 1063–1185 (2009).
12. Garnett, M. C. & Kallinteri, P. Nanomedicines and nanotoxicology: some physiological principles. *Occup. Med. (Chic. Ill).* **56,** 307–311 (2006).
13. Yacobi, N. R. *et al.* Mechanisms of alveolar epithelial translocation of a defined population of nanoparticles. *Am. J. Respir. Cell Mol. Biol.* **42,** 604–614 (2010).
14. Kamat, J. P., Devasagayam, T. P. A., Priyadarsini, K. I. & Mohan, H. Reactive oxygen species mediated membrane damage induced by fullerene

derivatives and its possible biological implications. *Toxicology* **155,** 55–61 (2000).

15. Foley, S. *et al.* Cellular localisation of a water-soluble fullerene derivative. *Biochem. Biophys. Res. Commun.* **294,** 116–119 (2002).
16. Auffan, M. *et al.* Relation between the redox state of iron-based nanoparticles and their cytotoxicity toward Escherichia coli. *Environ. Sci. Technol.* **42,** 6730–6735 (2008).
17. Xia, T. *et al.* Comparison of the mechanism of toxicity of zinc oxide and cerium oxide nanoparticles based on dissolution and oxidative stress properties. *ACS Nano* **2,** 2121–2134 (2008).
18. Nel, A., Xia, T., Mädler, L. & Li, N. Toxic potential of materials at the nanolevel. *Science (80-.).* **311,** 622–627 (2006).
19. Hauck, T. S., Ghazani, A. A. & Chan, W. C. W. Assessing the effect of surface chemistry on gold nanorod uptake, toxicity, and gene expression in mammalian cells. *Small* **4,** 153–159 (2008).
20. Leroueil, P. R. *et al.* Wide varieties of cationic nanoparticles induce defects in supported lipid bilayers. *Nano Lett.* **8,** 420–424 (2008).
21. Walczyk, D., Bombelli, F. B., Monopoli, M. P., Lynch, I. & Dawson, K. A. What the cell 'sees' in bionanoscience. *J. Am. Chem. Soc.* **132,** 5761–5768 (2010).
22. Vasir, J. K. & Labhasetwar, V. Quantification of the force of nanoparticle-cell membrane interactions and its influence on intracellular trafficking of nanoparticles. *Biomaterials* **29,** 4244–4252 (2008).
23. Elsaesser, A. & Howard, C. V. Toxicology of nanoparticles. *Adv. Drug Deliv. Rev.* **64,** 129–137 (2012).
24. Rodea-Palomares, I. *et al.* Physicochemical characterization and ecotoxicological assessment of CeO2 nanoparticles using two aquatic microorganisms. *Toxicol. Sci.* **119,** 135–145 (2011).
25. Ginzburg, V. V & Balijepalli, S. Modeling the thermodynamics of the interaction of nanoparticles with cell membranes. *Nano Lett.* **7,** 3716–3722 (2007).
26. Al-Rawi, M., Diabaté, S. & Weiss, C. Uptake and intracellular localization

of submicron and nano-sized SiO 2 particles in HeLa cells. *Arch. Toxicol.* **85,** 813–826 (2011).

27. Xia, T. *et al.* Comparison of the abilities of ambient and manufactured nanoparticles to induce cellular toxicity according to an oxidative stress paradigm. *Nano Lett.* **6,** 1794–1807 (2006).
28. Myllynen, P. Damaging DNA from a distance. *Nat. Nanotechnol.* **4,** 795–796 (2009).
29. Mehrabi, M. & Wilson, R. Intercalating gold nanoparticles as universal labels for DNA detection. *Small* **3,** 1491–1495 (2007).
30. Rivera Gil, P., Oberdörster, G., Elder, A., Puntes, V. & Parak, W. J. Correlating physico-chemical with toxicological properties of nanoparticles: the present and the future. *ACS Nano* **4,** 5527–5531 (2010).
31. Borm, P. J. A. *et al.* The potential risks of nanomaterials: a review carried out for ECETOC. *Part. Fibre Toxicol.* **3,** 11 (2006).
32. Nigavekar, S. S. *et al.* 3 H dendrimer nanoparticle organ/tumor distribution. *Pharm. Res.* **21,** 476–483 (2004).
33. Longmire, M., Choyke, P. L. & Kobayashi, H. Clearance properties of nano-sized particles and molecules as imaging agents: considerations and caveats. *Nanomedicine (Lond).* **3,** 703–717 (2008).
34. Liu, J., Yu, M., Zhou, C. & Zheng, J. Renal clearable inorganic nanoparticles: a new frontier of bionanotechnology. *Mater. Today* **16,** 477–486 (2013).
35. Yarjanli, Z., Ghaedi, K., Esmaeili, A., Rahgozar, S. & Zarrabi, A. Iron oxide nanoparticles may damage to the neural tissue through iron accumulation, oxidative stress, and protein aggregation. *BMC Neurosci.* **18,** 51 (2017).
36. Feng, Q. *et al.* Uptake, distribution, clearance, and toxicity of iron oxide nanoparticles with different sizes and coatings. *Sci. Rep.* **8,** 2082 (2018).

Chapter 5

Materials and methods

The aim of this work project was to develop novel nanoplatforms which can exert different therapeutic and diagnostic properties to meet the needs of nanomedicine in order to overcome the limitations of the traditional treatments, as widely described in previous chapters. This chapter is focused on materials and methods used to synthetize the nanoplatforms and on their characterization. Moreover, the innovative use of Tannic Acid as reducing and stabilizing agent is presented as a new eco-friendly material able to synthetize the nanoparticles through a green synthesis method.

In detail, in paragraph 5.1.1, 5.1.2 and 5.1.3 the synthesis procedures adopted to obtain the magneto-plasmonic nanoplatforms are described, followed by the description concerning the compositional, morphological and structural characterization techniques together with the magnetic and the optical properties of NPs (paragraph 5.2), then the paragraph 5.3 is dedicated to the in vitro cytotoxicity and biological tests carried out through the collaboration with different research groups.

Part of the work described in this chapter has been published during the PhD period in different journal articles and thesis[1–4].

5.1 Synthesis routes

In order to create magneto-plasmonic nanoparticles with specific properties, different synthesis routes were tried and optimized to generate two kinds of nanoplatforms: superparamagnetic iron oxide nanoparticles decorated with gold nanoparticles (MPNPs-Au) and superparamagnetic iron oxide nanoparticles decorated with silver nanoparticles (MPNPs-Ag). One of the main challenge is to prepare MPNPs-Au/Ag through a facile synthesis in which metal NPs are reduced directly on the surface of SPIONs through the innovative use of tannic acid as a reducing agent. Tannic acid was selected since it is an ecofriendly agent with reducing ability and for its natural antioxidant, antimicrobial and antitumoural properties, as described in next section.

Hence, a green synthesis strategy was performed by using TA as both reducing and stabilizing agent without using any other chemicals, minimizing the number of reagents used and consequently reducing production costs. This represent one of the major challenge because, to the author best knowledge, during the last years many studies were devoted to the use of TA as reducing agent with presence of additional stabilizers[5] or as reducing and stabilizing agent[6,7], but this is the first study focused on the ability of TA to act within few minutes as reducing agent for Au or Ag NP and simultaneously stabilize the MPNPs-Au and MPNPs-Ag nanoplatforms dispersion without using any additional reagents.

In particular, in order to produce MPNPs-Au and MPNPs-Ag, two different methods have been adopted in which stabilization and functionalization of NPs were changed and optimized to obtain a NPs dispersion with better physio-chemical and magneto-optical properties. Finally, the best nanoplatform generated, was then optimized by adding the Toluidine Blue to enhance the photo-thermal effect. In figure 5.1 are schematically represented the synthesis routes process.

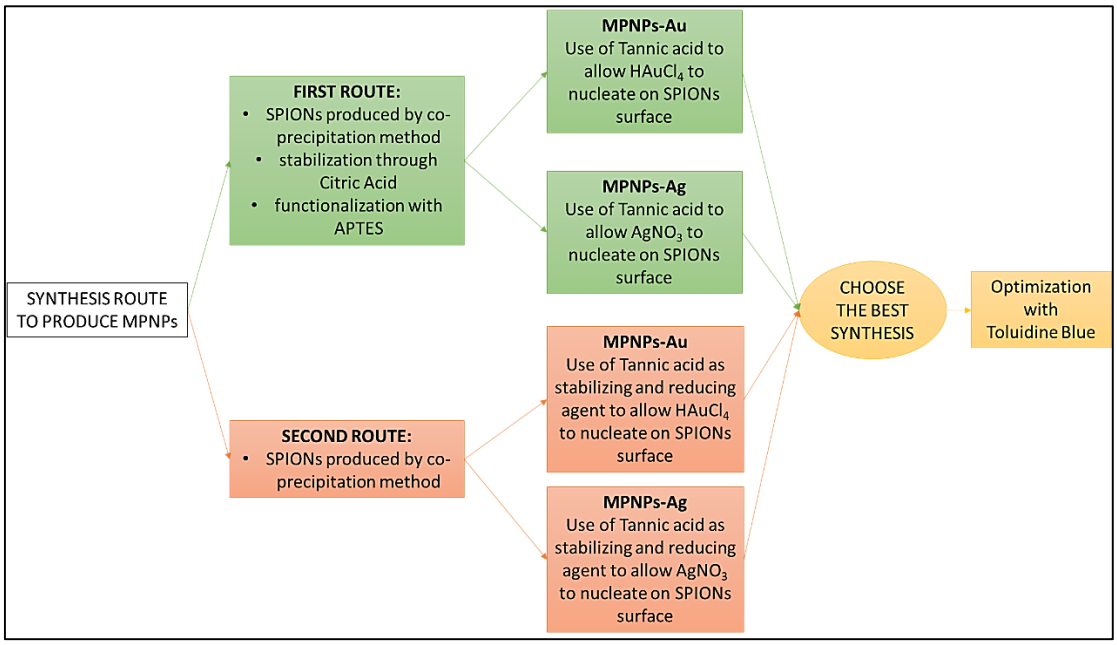

Figure 5. 1 Flow chart of the synthesis routes

For the synthesis, the reagents were all purchased from Sigma-Aldrich, unless otherwise specified in the text.

5.1.1 First route

Synthesis of SPIONs

Superparamagnetic Iron Oxide nanoparticles (Fe_3O_4) were synthesized by the co-precipitation in aqueous medium of Fe^{2+} and Fe^{3+} salts in alkaline environment for ammonium hydroxide NH_4OH (Merck, 25% aqueous solution). According to the literature, solutions of ferrous chloride $FeCl_2 \cdot 4\ H_2O$ (0.1 M) and ferric chloride $FeCl_3 \cdot 6H_2O$ (0.1 M) were used. In order to obtain 0.1 M solutions, 1.02 g of $FeCl_2 \cdot 4H_2O$ and 1.3 g of $FeCl_3 \cdot 6H_2O$ have been dissolved in 50 ml of bi-distilled water each and the two suspension have been magnetically stirred in separate beakers to reach the complete dissolution of the salts. When the salts were completely dissolved, 37.5 ml of the 0.1 M $FeCl_2 \cdot 4H_2O$ were mixed in 50 ml of 0.1 M $FeCl_3 \cdot 6H_2O$ reaching a pH value around 1.9. In order to induce the magnetite formation, NH_4OH was added drop by drop to the obtained solution, under

continuous mechanical stirring, until the pH reached the range of 9.5-10: the reaction mixture turned black, indicating the formation of a suspension of iron oxide NPs (SPIONs). The resulted suspension was then sonicated for 20 minutes in ultrasonic bath (SONICA® Ultrasonic Cleaner) and washed several times with a solution of bi-distilled water. Sedimentation of NPs was magnetically induced and three washing steps have been performed in order to remove all the unreacted compounds and the residual ammonia. The as obtained SPIONs have been finally re-suspended in 100 ml of distilled water with a final pH = 8.5.

Stabilization of the SPIONs suspensions with Citric Acid

The stability of SPIONs in water is quite low, due to anisotropic dipolar attraction[8]. This could limit the nucleation of the Au or Ag nanoparticles on their surface[9]. In order to improve the suspension stability, achieving higher repulsive interactions between magnetite nanoparticles and prevent as much as possible both their aggregation and the formation of clusters of uncontrolled dimensions, Citric Acid (CA) was added as stabilizing agent. CA is a well- known surfactant, as reported in literature by several authors[10–12] composed by three carboxyl and one hydroxyl group (figure 5.2). CA was chosen for its well-known ability to stabilize colloids by using a one-step, short and simple route[13].

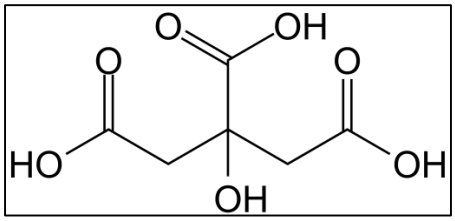

Figure 5. 2 Citric Acid Structure

In this synthesis, 50 ml of SPIONs dispersion was separated by sedimentation from the water using a magnet, then 60 ml of 0.05 M CA solution were added (the concentration of the diluted CA solution was chosen according to literature[14,15] in order to reach an optimal stability with the minimal amount of CA. Then the pH was adjusted to 5.2 with concentrated NH_4OH drop by drop, at this pH the

deprotonation of two carboxyl group of CA take place. The suspension was then heated to 80 °C and stirred (150 rpm) for 90 minutes in order to promote the CA adsorption on SPIONs, made possible thanks to the interaction between the hydroxyl groups of the magnetite surface and one or two of the carboxylate functionalities, forming a carboxylate with iron ions at that specific pH[10,11] while minimizing the magnetite decomposition to maghemite. Subsequently, the stabilized NPs have been washed in 4 steps with 50 ml of bidistilled water by means of an ultrafiltration device (Solvent Resistant Stirred Cells - Merck Millipore) and finally suspended in 60 ml of bidistilled water.
The pH of the final suspension was adjusted to 10.2 with ammonia inducing the de-protonation of the last -COOH terminal groups of the CA and providing a high, negative surface charge on the nanoparticles, thus preventing any strong agglomeration.

Functionalization with amino group by APTES

As it is known in literature[16,17] to introduce terminal amino (-NH_2) groups on the particles surface, a functionalization with (3-aminopropyl) triethoxysilane (APTES) is widely used.

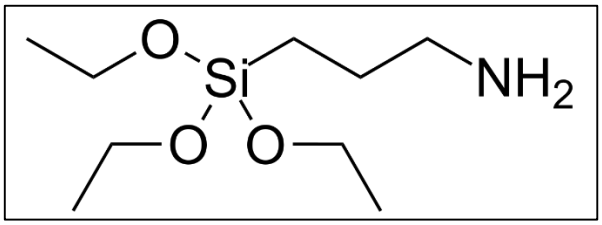

Figure 5. 3 (3-Aminopropyl) triethoxysilane (APTES) Structure

In this synthesis, to enhance the interaction between metal NPs and SPIONs, terminal -NH_2 groups were introduced on the SPIONs surface by the functionalization with APTES (> 98%, Merck). For the functionalization with APTES of CA-coated Fe_3O_4 nanoparticles, 30 ml of SPIONs suspension (at pH = 10.2) were diluted in 450 ml of absolute ethanol (anhydrous, > 99.9%, Carlo Erba

Reagents) and sonicated for 3 minutes. Then, 255 µl of APTES were added to the colloidal suspension and heated at 80 °C under mechanical stirring for three hours at 150 rpm. Subsequently, the mixtures were cooled at room temperature, the nanoparticles were magnetically separated and centrifuged three times at 7500 rpm for 20 minutes to remove all the remnant ethanol and finally resuspended in 30 ml of bi-distilled water. To induce positive charge at the surface of the APTES-coated nanoparticles, a dilute HNO_3 solution (0.05 ml of 6 M HNO_3 with 20 ml of ethanol) was added drop by drop until reaching a pH value ≈ 5–6.

In situ synthesis of metal nanoparticles

In both routes of this project, the SPIONs decoration with gold and silver nanoparticles was obtained by reduction through a simple aqueous method with the innovative use of a green and organic chemical: Tannic Acid (TA). This polyphenolic compound has the great advantage of being useful both as a reducing and a stabilizing agent[18]; moreover, it exhibits excellent antioxidant properties[19]. TA is one of organic compounds characterized by both hydroxyl and phenolic groups, which grant it aggressive reducing power and take part in redox reactions by forming quinones and donating electrons (figure 5.4).

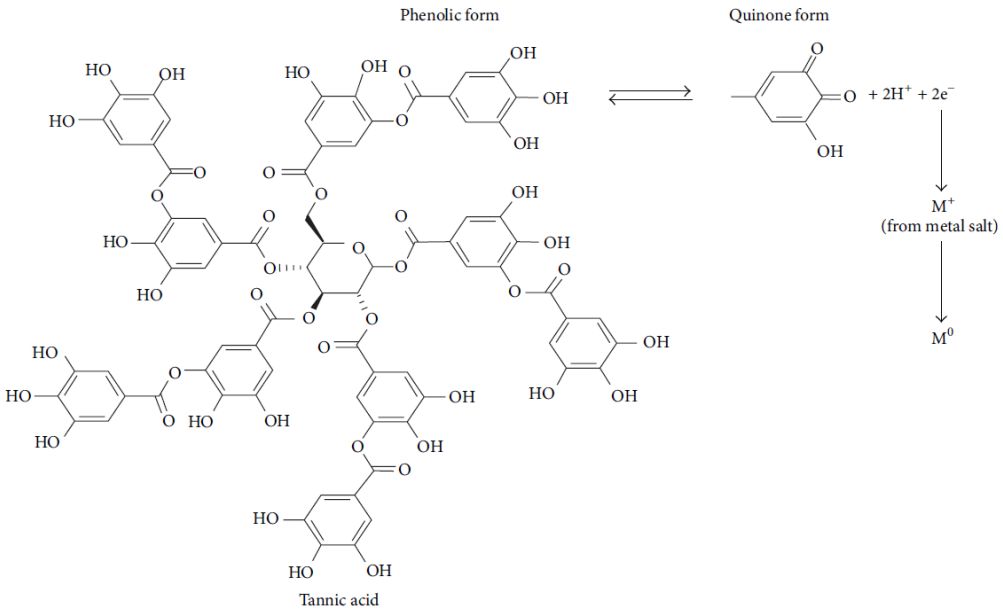

Figure 5. 4 reaction mechanism of tannic acid-based reduction of metal salts. the electrons released from the phenolic groups reduce the metal ions[18].

Noticeable, finally, are TA's antioxidant, antimutagenic antibacterial, antiviral, anti-inflammatory, and anticarcinogenic properties[18–20]. Therefore, in this work TA has been chosen as reducing agent.

A schematic representation of the first synthesis route is reported in figure 5.5.

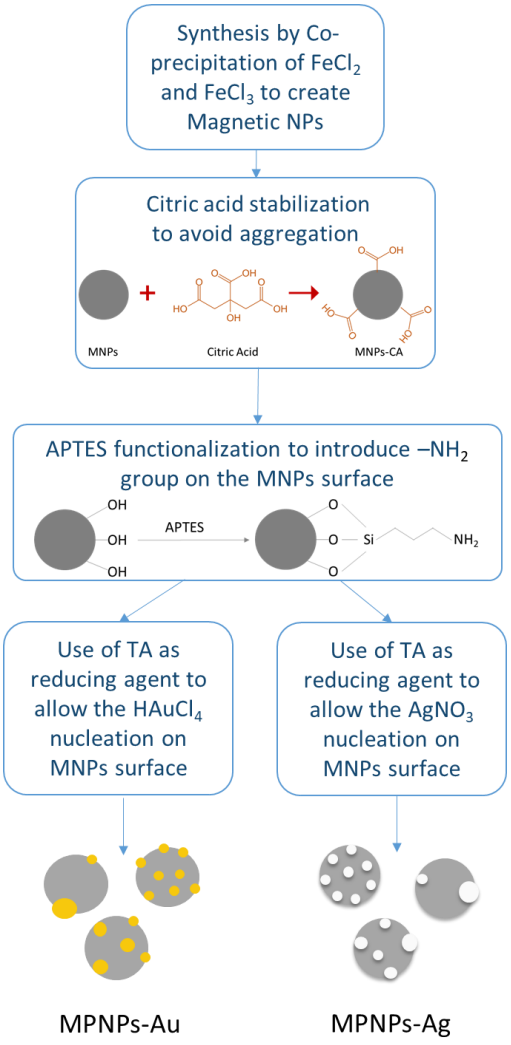

Figure 5. 5 Schematic representation of first synthesis route

MPNPs-Au (first route)

With the aim of testing the best way to reduce Au nanoparticles onto the SPIONs surface and improving the synthesis yield, 3 different methods have been used

(table 5.1): methods A, B and C, which differ one from the other for the sequence adopted to add the reagents to the SPIONs dispersion.

Table 5. 1 Methods adopted to synthetize MPNPs-Au (first route)

METHOD	STEP 1		STEP 2	
A	**CA/APTES-SPIONs + Tannic Acid**	70 °C; 5 min; 150rpm	**+ $HAuCl_4$**	70 °C; 5 min; 150rpm
B	**$HAuCl_4$ + Tannic Acid**	70 °C; 5 min; 150rpm	**+ CA/APTES-SPIONs**	70 °C; 5 min; 150rpm
C	**CA/APTES-SPIONs + $HAuCl_4$**	70 °C; 5 min; 150rpm	**+ Tannic Acid**	70 °C; 5 min; 150rpm

Briefly, TA and $HAuCl_4$ were added to the MNPs dispersion to create the MPNPs-Au. This step was performed by adding, in the order explained through the table 5.1, 1.70 mg of $HAuCl_4$ and 15 mg of TA respectively dissolved in 6.7 ml and 10 ml of bi-distilled water to 10 ml of CA/APTES- SPIONs. By adding the gold salt into a basic environment, $HAuCl_4$ hydrolysis take place and form gold hydroxide ($Au(OH)_3$) suspension. Thus, to reduce the as obtained $Au(OH)_3$ ions on the iron oxide nanoparticles surface, the TA was dissolved in bi-distilled water and buffered with NH_4OH until reaching the pH=8. After each step, the suspension was heated up to 70 °C for 5 minutes in orbital shaker at 150 rpm. Finally, the MPNPs-Au complexes were magnetically separated, thus only Au NPs attached to the CA/APTES-functionalized SPIONs have been collected and all the unreacted elements have been eliminated, and resuspended in 10 ml of bi-distilled water.

MPNPs-Ag (first route)

As reported for MPNPs-Au (first route), also for the Ag grafting the same method described for MPNPs-Ag was adopted, in order to evaluate the best way to reduce silver seeds on SPIONs surface. The table 5.2 report the three methods A, B and C.

Table 5. 2 Methods adopted to synthetize MPNPs-Ag (first route)

METHOD	STEP 1		STEP 2	
A	**CA/APTES-SPIONs + Tannic Acid**	37 °C; 15 min; 150rpm	**+ $AgNO_3$**	37 °C; 15 min; 150rpm
B	**$AgNO_3$ + Tannic Acid**	37 °C; 15 min; 150rpm	**+ CA/APTES-SPIONs**	37 °C; 15 min; 150rpm
C	**CA/APTES-SPIONs + $AgNO_3$**	37 °C; 15 min; 150rpm	**+ Tannic Acid**	37 °C; 15 min; 150rpm

In this case, the precipitation of silver nanoparticles was accomplished in the same way of the Au nanoparticles, but with some variations. 5 mg of $AgNO_3$ were dissolved in 10 ml of water and 2.5 mg of TA were dispersed in 20 ml of bi-distilled water adjusting the pH at 8 in order to increase the reducing power of the acid[18]; then the reagents were added to 10 ml of APTES-coated magnetite nanoparticles following the order shown in table 5.2 for methods A, B and C. In this synthesis, after each step, the dispersion was stirred at 150 rpm for 15 minutes at 37°C by using orbital shaker. Finally, the aqueous suspension was then washed three times with an ultrafiltration device and redispersed in 40 ml of bi-distilled water.

5.1.1 Second route

Synthesis of SPIONs

In the second route, Fe_3O_4 nanoparticles were synthesized by the co-precipitation method in the same way explained for first route in paragraph 5.1.1. Briefly, 1.02 g of $FeCl_2 \cdot 4H_2O$ and 1.3 g of $FeCl_3 \cdot 6H_2O$ have been dissolved in 50 ml of bi-distilled water each and the two suspension have been magnetically stirred until the salt were

completely dissolved. Then, 37.5 ml of the 0.1 M $FeCl_2 \cdot 4H_2O$ were mixed in 50 ml of 0.1 M $FeCl_3 \cdot 6H_2O$ and the pH was adjusted to 9.5-10 with NH_4OH, indicating the formation of a suspension of SPIONs. The resulted suspension was then sonicated for 20 minutes, then washed and finally re-suspended in 100 ml of distilled water.

In situ synthesis of metal nanoparticles and stabilization of NPs

To reduce the process step and simplify the synthesis, in the second route TA were used as stabilizing, capping and reducing agent[21], for this reason all the syntheses were carried out rapidly, in order to avoid the aggregation of SPIONs.
As anticipated in the "first route" description, TA were used to allow silver and gold nanoparticles nucleate on SPIONs surface thanks to its high reducing power. In this route, a green synthesis strategy was performed in which TA was utilized as both a reducing and stabilizing agent without using any other chemicals. In fact, the use of TA alone allows to minimize the number of reagents used and consequently to reduce production costs.

The big advantage to use TA is that under mild acidic/ basic conditions, it can be partially hydrolyze into glucose and gallic acid as shown in figure 5.6. As it is known from the literature[22,23], gallic acid has already been used as an excellent stabilizing and reducing agent also thanks to its antimicrobial, antioxidant and anticancer activities. Nevertheless, at alkaline pH, gallic acid induce formation of metal nanoparticles rapidly at room temperature, but its poor stabilization potential leads to aggregation of the particles in solution. But working under mild acidic/ basic conditions, thanks to the partial hydrolization of the TA, the presence of the glucose guarantee the property of being a good stabilizing agent at alkaline pH.

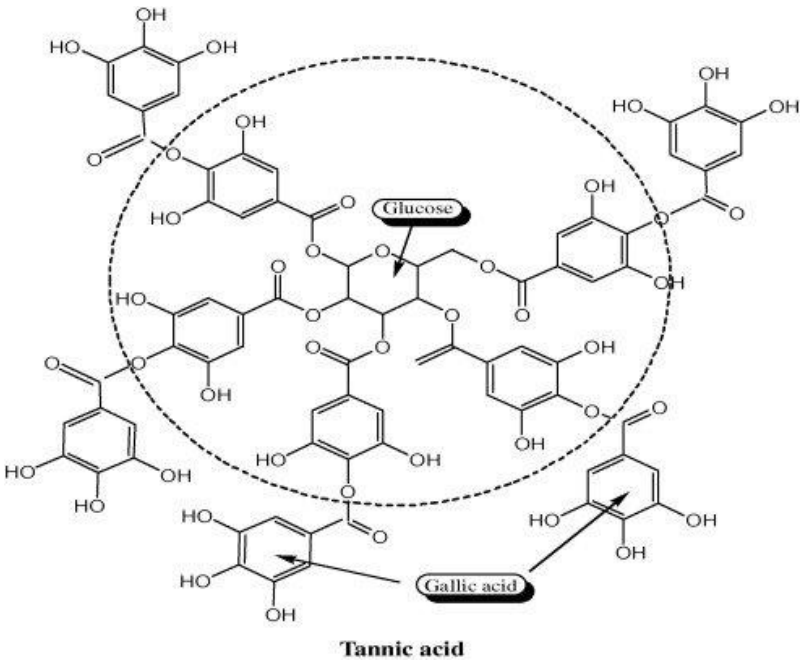

Figure 5. 6 Tannic acid structure[21]

For this reason, in the following synthesis TA is used on bare SPIONs to reduce metal NPs and act as stabilizing agent among nanoparticles.

In the following image (figure 5.7) is reported a schematic representation of second synthesis route.

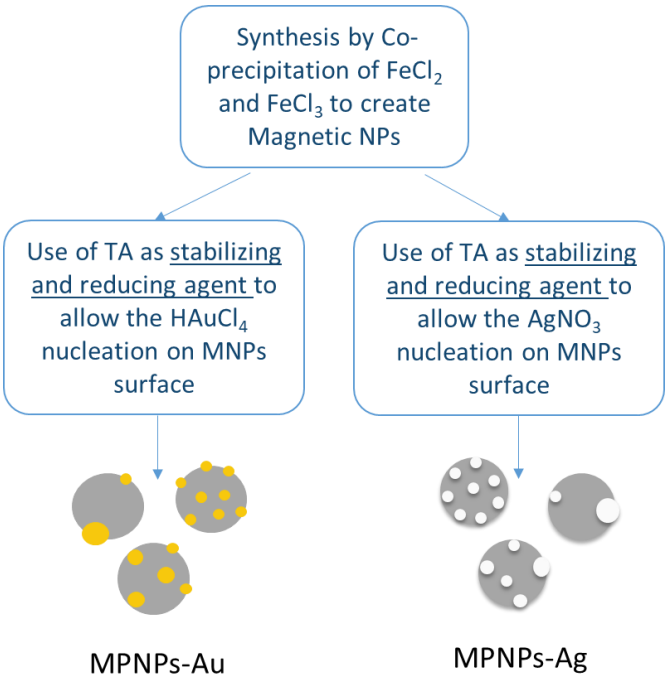

Figure 5. 7 Schematic representation of second synthesis route

MPNPs-Au (second route)

The second route was performed again by using the 3 methods in order to evaluate the best way to reduce Au nanoparticles onto the SPIONs surface (table 5.3)

Table 5. 3 Methods adopted to synthetize MPNPs-Au (second route)

METHOD	STEP 1		STEP 2	
A	**SPIONs + Tannic Acid**	70 °C; 5 min; 150rpm	**+ $HAuCl_4$**	70 °C; 5 min; 150rpm
B	**$HAuCl_4$ + Tannic Acid**	70 °C; 5 min; 150rpm	**+SPIONs**	70 °C; 5 min; 150rpm
C	**SPIONs + $HAuCl_4$**	70 °C; 5 min; 150rpm	**+ Tannic Acid**	70 °C; 5 min; 150rpm

At the beginning, 60 mg of $HAuCl_4$ and 2.55 mg of TA were dissolved respectively in 12 ml and 1.2 ml of water. TA solution was buffered at pH=8 with NH_4OH to improve its reduction power. Then, the solutions were added in the specific order described from table 5.3, to 3.9 ml of the SPIONs dispersion. After each step the dispersion was left in orbital shaker for 5 minutes (70 °C, 150 rpm) in order to promote the Au reduction on SPIONs surface. Finally, the dispersion was washed 3 times through magnetic separation and redispersed in 20 ml of water. To determinate the optimal reaction condition, the pH of $HAuCl_4$ was varied by adding NH_4OH drop by drop to increase the pH from 2 to 8 as will be discussed in results section.

MPNPs-Ag (second route)

The synthesis of MPNPs-Ag was performed again by using the 3 methods (table 5.4) in order to determine the optimal procedure to reduce $AgNO_3$ and stabilize the suspension.

Table 5. 4 Methods adopted to synthetize MPNPs-Ag (second route)

METHOD	STEP 1		STEP 2	
A	**SPIONs + Tannic Acid**	40 °C; 15 min; US	**+ $AgNO_3$**	40 °C; 15 min; US
B	**$AgNO_3$ + Tannic Acid**	40 °C; 15 min; US	**+ SPIONs**	40 °C; 15 min; US
C	**SPIONs + $AgNO_3$**	40 °C; 15 min; US	**+ Tannic Acid**	40 °C; 15 min; US

In this synthesis, 0.6 g of $AgNO_3$ salt were added to 12.5 ml of SPIONs dispersion and sonicated for 15 minutes at 37 °C to prevent aggregation. Then, 0.3 g of TA were dissolved in 10 ml of bi-distilled water and buffered at pH=8 with NH_4OH.

The dispersion was kept in ultrasound device for 15 minutes at 40 °C and then washed with magnetic separation. Finally, the nanoparticles were dissolved in 20 ml of water.

5.1.3 Optimization with Toluidine Blue

Among the big family of dyes, Toluidine Blue (TB) is the most often used as biological stains (figure 5.8); in fact, it is found that TB interact strongly with the gold nanoparticles enhancing the absorption peak on the UV-vis spectra at a longer wavelength, while no interaction is shown with silver nanoparticles[24]. At present, it is not clear how the interaction between Au NPs and the dyes occurs[24,25], one hypothesis is that the dyes interact with the surface of the NPs via the amino group which is weakly aurophilic[26,27], another hypothesis is that TB interact or bind to Au NPs through the sulfur atoms which are known to be extremely aurophilic[28,29].

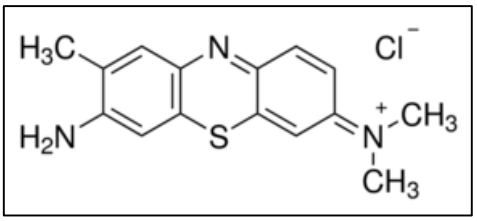

Figure 5. 8 Structure of Toluidine Blue

In this synthesis TB has been used on mangetoplasmonic NPs and the dispersion of MPNPs-Au (second route) was dissolved in 8 ml of bidistilled water in order to obtain a NPs dispersion 5 mM and mixed with 10 µl of a 5 mM dispersion of TB. To assess the effect of TB, a washing step was performed in order to remove all the unreacted compounds, finally, the NPs were redispersed in 8 ml of bidistilled water.

5.2 Nanoparticles Characterization

The analysis of the MPNPs developed through the different synthesis routes was performed in order to study the structural features, the morphology, the

composition and the magneto-optical properties of the as-synthesized samples. The data described in the following sections obtained through the characterization techniques, allowed to attest the sample features and to select the best performing procedures.

5.2.1 Field Emission Scanning Electron Microscopy (FE-SEM) and High-Resolution Transmission Electron Microscopy (TEM)

FE-SEM. In order to investigate the size, the shape and morphological features of nanoparticles, the Field Emission Scanning Electron Microscopy was adopted. This technique is a non-destructive characterization analysis, which consists in an electron gun able to generate a high energy electron beam that passes through a magnetic lens, which deflects and focuses the beam on the specimen surface (Figure 5.9a). The interaction between the electron beam and the sample surface leads to the generation of different signals, which include secondary electrons, backscattered electrons, visible light (cathodoluminescence), photons (characteristic X-rays), diffracted backscattered electrons, and heat (Figure 5.9b).

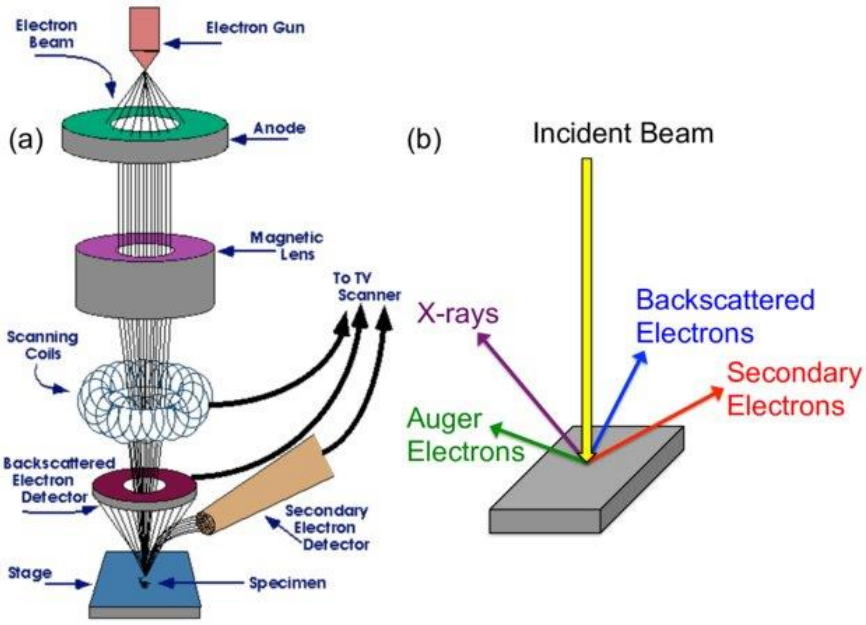

Figure 5. 9: FE-SEM functioning (a) and interaction between the electron beam and the sample (b)[30]

In order to obtain morphological and topographical information, secondary electron and backscattered electrons are exploited among the signal. In particular, the first are low energy electron (energy < 50 eV) generated by inelastic scattering which provide a superficial topographical image; while the second are signals with higher energy (> 50 eV) that comes from deeper region of the sample and provide information closely linked to its chemical composition.

Samples preparation method: for the FE-SEM analysis, 5 μL of the diluted sample dispersion was placed on a Cu grid (300-mesh, S147-3, Agar Scientific, UK) coated with ultrathin amorphous carbon film, then the grid (once dried at room temperature) was located on the appropriate support and analyzed by Zeiss supra 40 GEMINI field emission scanning electron microscope.

TEM is a very preforming technique used to analyze the properties of materials at nanoscale level (*i.e.* morphological, compositional and crystallographic properties). This tool uses the interaction between energetic electrons, which is the source, and the sample; in particular, the working principle consists in an electron beam emitted from a tungsten filament which reaches the sample by passing through a condenser and objective lenses system. Thus, the electron that are transmitted and scattered from the sample, are utilized to create an interference image. The TEM provides information on crystal and internal structures.

Samples preparation method: all the sample analyzed with TEM were detected by means of a holey carbon coated TEM grid (300-mesh, S147-3, Agar Scientific, UK). In particular, after sonication, 5 μL of NPs diluted suspension was dropped on the carbon grid and analyzed once dried.

TEM imaging and related local EDS were performed in part at Italian Institute of Technology, Genova (Italy) by using FEI Tecnai F20 TWIN transmission electron microscope with a Schottky emitter operated at 200 KV; and in part were performed at the Jožef Stefan Institute, Ljubljana (Slovenia) by using a Jeol JEM-2100 TEM, operating at 200 kV and equipped with EDXS (Energy-dispersive X-ray spectroscopy) and SAED (selected area diffraction), performed to analyze the structural characteristics of pure magnetite and MPNPs-Au/Ag.

5.2.2 Energy Dispersive Spectroscopy (EDS)

EDS. The Energy Dispersive Spectroscopy (EDS) allows to detect the elemental composition of the samples through the detection of X –ray spectrum coming from the exposure of the sample to a high-energy electron beam. This X-rays energy depends on the atomic number of the element and is used to obtain information about chemical composition. In detail, when the X-rays reach the detector, cause the ionization and consequently, the generation of an electrical charge which allows to obtain a spectrum reporting the number of counts per channel as a function of the energy of the detected X-rays (keV). The EDS investigation was carried out on all the MPNPs dispersions with the aim to study the chemical composition and correct formation and reduction of metal NPs on SPIONs surface.

Samples preparation method: The EDS investigation was carried out preparing the sample by dropping 5 μL of the NPs dispersion on a Cu grid, then located on the appropriate support for the analysis. The analysis was performed by a Zeiss supra 40 GEMINI x-ray spectroscope equipped with EDS.

5.2.3 Fourier transform infrared spectroscopy (FT-IR)

FT-IR. The structural and elemental analyses on NPs samples were performed by means of Fourier transform infrared spectroscopy in order to provide information on the functional groups present in the molecules. The study of this chemical bonds comes through the formation of signals that can be linked to the presence of specific groups with characteristic frequencies. In particular, the light source of the spectrometer emits IR radiation which can be absorbed by the sample causing the molecules transition from a fundamental state to an excited vibrational state. Each chemical bonds vibrate at a characteristic frequency, depending from their own structure, bond length and angle. So, individual molecules are able to interact with the radiation absorbing it at a specific wavelength. The signal generated from this interaction, is converted by means of Fourier transform, in a traditional IR spectrum (typically between 400 and 4000 cm^{-1}); this spectrum can be associated to an individual chemical bond which identify specific compound in a complex system.

Samples preparation method: To perform FT-IR analyses 1 ml of NPs dispersions were dried at room temperature for 24 h and the as obtained powder was analyzed through a JASCO 4000 Fourier transform infrared spectroscope (FT-IR), which acquired spectra from 4000 to 450 cm^{-1}.

5.2.4 Ultraviolet-visible spectroscopy (UV-Vis)

UV-Vis. UV-Visible Spectroscopy (UV-vis) can be employed to identify the wavelength of compound and their maximum absorbance.

This technique is based on chromophores absorption of monochromatic electromagnetic radiations in the UV (200-350 nm) and visible (350-700 nm) spectral region. In detail, in UV-vis spectrometer is composed by a source (composed by a combination of tungsten/halogen and deuterium lamps), a monochromator, a holder for the sample and a detector (figure 5.10).

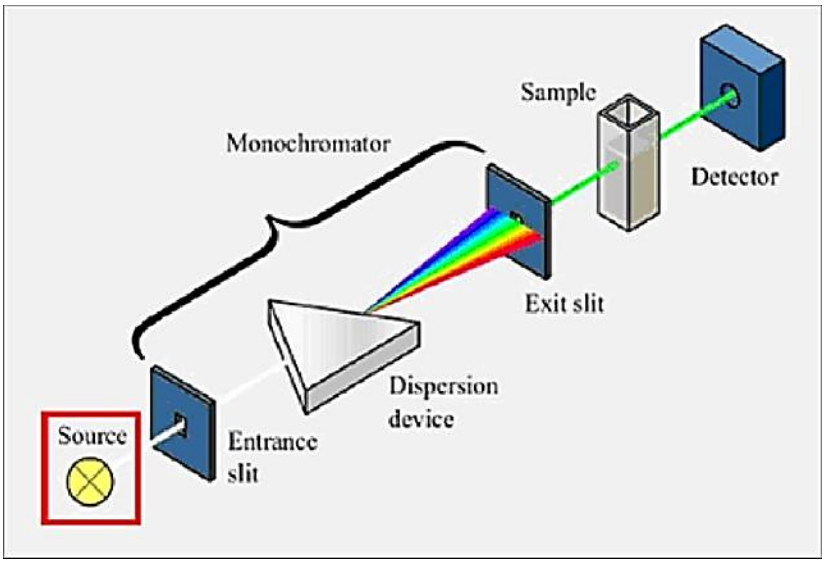

Figure 5. 10 Schematic structure of UV-Vis spectroscopy[31].

Briefly, the light is emitted from source and reaches the monochromator which splits the different wavelengths of light and works as filter so that only light of a single wavelength passes through the sample and reaches the detector. The detector converts the intensity of the light in electric signal which undergoes to amplification and returns a diagram showing the absorbance as a function of the wavelength. In

NPs characterization the UV-Vis analysis is useful to understand at which wavelength a specific compound is able to absorb the maximum light as well as to provide information on the NPs size and aggregation[32–34].

Samples preparation method: In order to analyze sample with UV-Vis spectroscopy and verify the formation of metallic NPs, the baseline was first recorded with bi-distilled water as reference solution (I_0), then the NPs dispersions (I) were diluted in bi-distilled water (1 ml of NPs and 3 ml of bi-distilled water) and placed within a cuvette for the analysis. If $I < I_0$, then the sample absorbed part of the emitted light, this absorbance (A) is correlated to I and I_0 by the equation

$$A = log_{10} \frac{I_0}{I}$$

The absorbance spectra of the samples were recorded with the UV-Vis (UV-2600 SHIMADZU) instrument.

5.2.5 Dynamic Light Scattering (DLS) and ζ potential

DLS. Dynamic Light Scattering (DLS) was used for the determination of particle hydrodynamic radius and particle size distribution. DLS techniques is based on the scattering of light by the particles dispersed in a liquid; these particles, free to move, undergo Brownian motion so they change their position to each other and change the rate at which the intensity of the scattered light fluctuates. On the basis of this fluctuations, is possible to measure the diffusion coefficient. The smaller the particles are, the faster is the Brownian motion and vice versa, larger particles move more slowly. The hydrodynamic radius (particles considered as spheres) can be derived by using the Stokes-Einstein equation.

Samples preparation method: In order to analyze the hydrodynamic radius of NPs, ten measurements of 300 seconds for each sample were processed setting the parameters according to the properties of the solvents and material to be measured. The sample was prepared by diluting SPIONs suspension with bi-distilled water and analyzed by Litesizer™ 500 instrument.

ζ POTENTIAL. In order to investigate the stability of the colloidal suspensions, ζ potential measurements was used. In fact, zeta potential is a key indicator of the stability of colloidal dispersions: in particular, the lower the magnitude of the ζ potential is, the less stable is the colloid and vice versa, a higher magnitude indicates a more stable colloid. The colloids' behavior is related to the z-potential range:

- Rapid coagulation = 0 - ±5
- Incipient instability = ±10 - ±30
- Moderate stability = ±30 - ±40
- Good stability = ±40 - ±60
- Excellent stability = ≥ ±60

Thus, knowledge of ζ potential is important for optimizing processes and for quality control.

Samples preparation method: The sample for ζ potential was prepared by diluting SPIONs suspension with bi-distilled water and the pH ranging from 1 to 12 was analyzed by Litesizer™ 500 instrument, same used for DLS measurement.

5.2.6 Vibrating Samples Magnetometer (VSM)

VMS. The superparamagnetic behaviour and the magnetic saturation of the NPs were evaluated with a Vibrating Samples Magnetometer. VMS is a non-destructive technique useful determine the magnetic properties of a material, as functions of magnetic field, time and temperature. In detail, the sample is placed in a constant magnetic field which magnetize the sample (if the sample is magnetic) by aligning its magnetic domains with the field. Then the magnetic dipole moment of the sample generates a magnetic stray field which change with the sample movement as a function of time. This alternating magnetic field around the sample induces an electric field in the coils that is proportional to the samples 'magnetization. Using specific software, the system provides information on how much the sample is magnetized and how the magnetic field affects its magnetization.

Samples preparation method: To perform this analysis, the NPs suspensions were dried at 37°C to obtain NPs in powder form, then magnetic properties were investigated by means of a DC magnetometer (Lake- Shore 7225) equipped with a cryogen-free magnet system at room temperature in quasi-static condition. Finally obtained magnetization signal was normalized by the mass of the sample.

5.2.7 Laser Irradiation

Laser Irradiation. This kind of analysis has been performed in order to detect ability of MPNPs to increase their temperature exploiting the SPR effect (figure 5.11), useful to evaluate their ability to be used for photothermal treatment in cancer cells. In particular, as described in detail in chapter 3, paragraph 3.2.2, the laser source produces a light with a specific wavelength which hit the sample and allows MPNPs to transform the received radiation into thermal energy by producing heat. Is important to measure the heat produced in order to evaluate the time exposure for each sample and avoid excessive temperature rise.

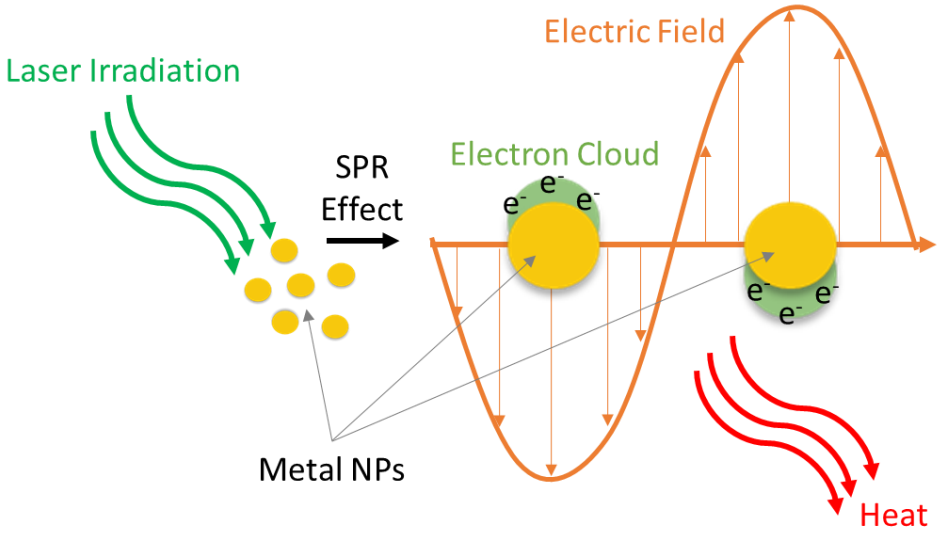

Figure 5. 11 Schematic representation of SPR effect in metal NPs

Samples preparation method: MPNPs dispersion with total volume of 1 mL were irradiated using NIR laser with a wavelength of 808 nm (CNI, model MDL-III-808). Spot size of the laser beam was 1 cm in order to irradiate the entire volume of the vial. Power of the laser was set at 1 W and temperature of the samples was monitored and detected every minutes in real time using a J-type Teflon thermocouple.

5.2.8 Induction heating system

Induction Heating. The induction heating system was used with the aim of evaluating the ability of synthetized NPs to work as therapy system in magnetic hyperthermia application. The analysis consists in the application of an alternated magnetic field with specific power and frequency to the solution samples. In particular, as shown in figure 5.12, the sample is placed in the specific holder inside a coil, then the current produced at the output, flowing inside the coil, generates a magnetic field that interacts with the nanoparticles. This interaction makes NPs generate heating that is dissipated in the surrounding fluid in which they are dispersed. The ability of the nanoparticles to function as magnetic hyperthermia therapy system is assessed by measuring the temperature they produce in a specific period of time.

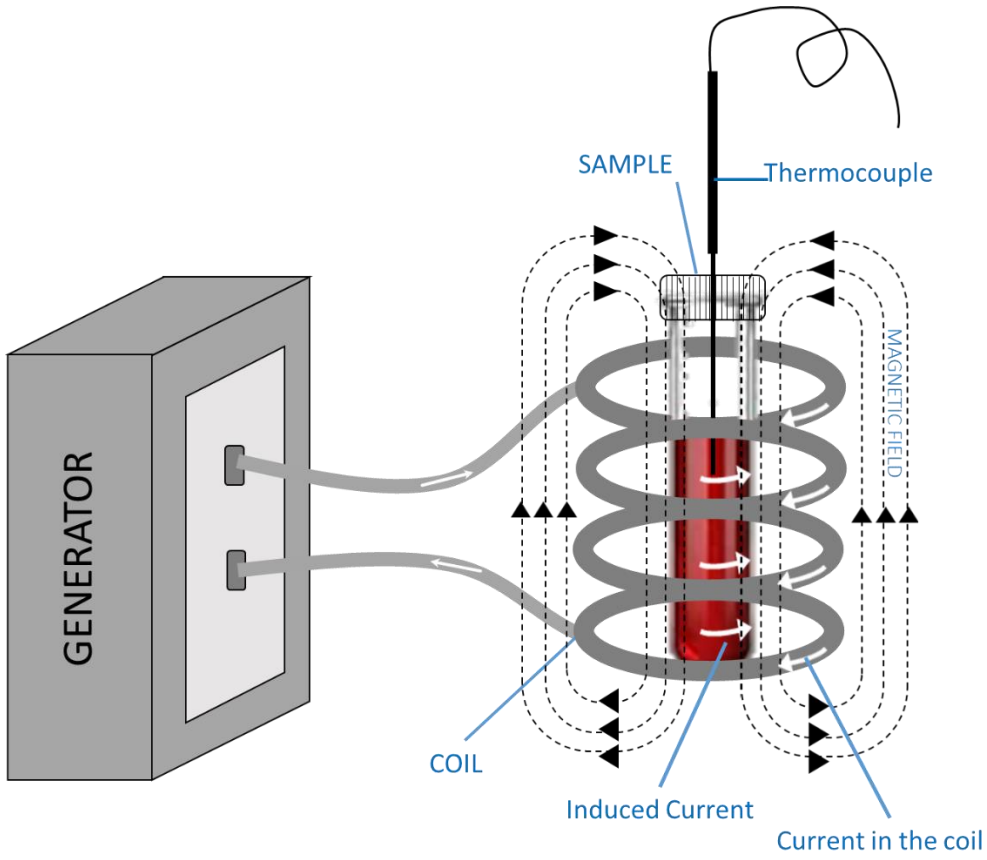

Figure 5. 112: Schematic representation of induction heating system for magnetic hyperthermia therapy applications

Samples preparation method: The samples for the induction heating measurement were prepared by diluting SPIONs suspension with bi-distilled water in order to obtain 1 mg/ml concentration each, then 3 ml of solution has been used for the analysis. The working condition of power and frequency were settled respectively at 3 kW and 220 kHz. Each solution undergoes to magnetic field for 20 minutes and the temperature were detected every 2 minutes with a thermocouple insert inside the NPs dispersion. The induction heating system (FELMI- EGMA 6-10-15 REV.01) was used for this analysis.

5.3 In Vitro Cytotoxicity

Cytotoxicity tests are essential to preliminary asses the biocompatibility of the NPs and to establish the MPNPs concentration that would not damage the healthy cells. For this purpose, in paragraph 5.3.1 and 5.3.2, the biocompatibility tests of MPNPs in contact with different cell lines are described.

Part of the work described in this section has been published during the PhD period in different journal articles and thesis[2–4].

5.3.1 Hemotoxicological Analysis

Hemotoxicological Analysis. The hemotoxicological properties were detected in order to evaluate the toxicological effect of the nanocomposites in contact with red blood cells (RBCs). In particular, with this analysis in possible to evaluate the hemoglobin absorbance using a spectrophotometer which is useful to detect the RBCs hemolysis before and after incubation with nanoparticles.

Samples preparation method: RBCs cells isolated from the fresh whole sheep blood (supplied by Veterinary Faculty- University of Ljubljana, Slovenia) were

washed before use with physiological 0.9% NaCl solution, centrifuged (at 600 rpm for 15 minutes) to remove the supernatant and then resuspended in sterile HBS buffer with 0.9 wt% NaCl to obtain 5 vol.% cell density. 100 μL of RBCs were seeded in each vial and then 100 μL of MPNPs dispersion was added in order to test two different MPNPs concentration: 35 and 100 μg/mL (all the samples were measured in triplicate). The NPs concentration was calculated by drying the NPs dispersion in order to know how many grams of NPs are present in 1 ml of solution, then a specific dilution with water was required to obtain the desired concentrations. The cells exposed to MPNPs were incubated at 37° C for 24 h., then the samples were centrifuged and the number of lysed cells were calculated by measuring the hemoglobin absorbance of the supernatant at 541 nm using a spectrophotometer (BioTek Synergy H4 Hybrid microplate reader). This analysis was completely performed at University of Ljubljana, Slovenia.

5.3.2 Cytocompatibility on healthy and cancer cells

Cytocompatibility: In order to perform this analysis, two different cell lines were used to assess cytotoxicity to simulate skin healthy and tumor conditions. Human primary fibroblast (HGF) were selected as representative for healthy tissue while Human metastatic melanoma cells (A2058) were representative for pathogenic cells.

Samples preparation method:

HGF growth condition

Primary human fibroblasts (HGF) were isolated from normal human gingiva harvested from healthy patient, after informed consent. To isolate cells, the following procedures were used: mucosal epithelia layers were enzymatically divided by dispase that is effective dividing fibronectin and collagen type IV; tissue was submerged into the dispase solution at 4 °C overnight and then digested 30 minutes with a solution of collagenase (1 mg/ml), dispase (0.3 mg/ml) and trypsin (0.25% in phosphate buffer saline -PBS-). Harvested single cells were cultivated in alpha-modified eagle medium (α-MEM, Sigma, Saint Louis, Missouri, U.S.) supplemented with 10% of heat inactivated fetal bovine serum (FBS) and 1% of

antibiotics and antifungal (penicillin, streptomycin and amphotericin) at 37 °C in humidified incubator, 5% CO_2.

A2058 growth condition

A2058 cells were purchased from American Type Culture Collection (ATCC). They were cultivated in RPMI 1640 (Sigma, saint Louis, Missouri, U.S.) supplemented with 10% of heat inactivated fetal bovine serum (FBS) and 1% of antibiotics and antifungal (penicillin, streptomycin and amphotericin) at 37 °C in humidified incubator, 5% CO_2.

Nanoparticles were dispersed using Ultrasonic Bath (30 seconds, room temperature) and then diluted in serum-free media until final concentrations of 25, 50 and 100 µg/ml. To test NPs cytotoxicity, $2x10^4$ cells were seeded onto each well of a 24 multiwell-plate and submerged with 1 ml of fresh medium. Plate was incubated at 37 °C 24 hours to allow complete cell adhesion and spread. Then, Nanoparticles, previously diluted in serum-free media, were dispersed in each well and put in direct contact for 6 and 24 hours. At each time-point, cell viability was evaluated by the Alamar blue assay, a colorimetric metabolic dye based on the use resazurin sodium salt. In presence of metabolic activity, resazurin (a non-fluorescent blue molecule) is metabolized in resafurin (a fluorescent red molecule). Briefly, the ready-to-use alamar solution was added to each well containing cells (200 µl/well) and incubated 3 hours in the dark. Then, 50 µl were collected from each well, transferred to a new black-bottom 96 well plate and the fluorescence evaluated by spectrophotometer (Spark, from Tecan, CH) using a 570 nm wavelength. Cells cultivated with fresh medium were used as control and considered as 100%; test values were normalized towards them and expressed as % over control. Finally, NPs internalization was visually evaluated by optical microscope (EvosFloid, Leica, CH).

5.4 Laser induced phototherapy

This paragraph is dedicated at the cytotoxicity tests performed on healthy and cancer cell lines exposed to different NPs concentrations, in which the laser

irradiation is applied. This will be useful to understand if the NPs are able to be used as tool for photothermal therapy by converting the received light into thermal energy and to establish the MPNPs concentration that would not damage the healthy cells, but could destroy the cancers cells when irradiated. In particular, the cells used to perform the tests were:

• Healthy cell line: human gingivalis fibroblast (HGF), obtained from DS Pharma Biomedical.

• Cancer cell line: squamous carcinoma, buccal mucosa (HO-1-N-1), obtained from JCRB.

Both cells were grown in DMEM (Dulbecco's Modified Eagle Medium) supplemented with 10% of FBS (fetal bovine serum) and seeded in different well plates (MatTek Corporation).

A schematic representation of the procedure adopted for the cytotoxicity test is shown in figure 5.13.

The work described in this paragraph has been performed at Kyoto Institute of Technology (Kyoto, Japan) and has been published during the PhD period[2].

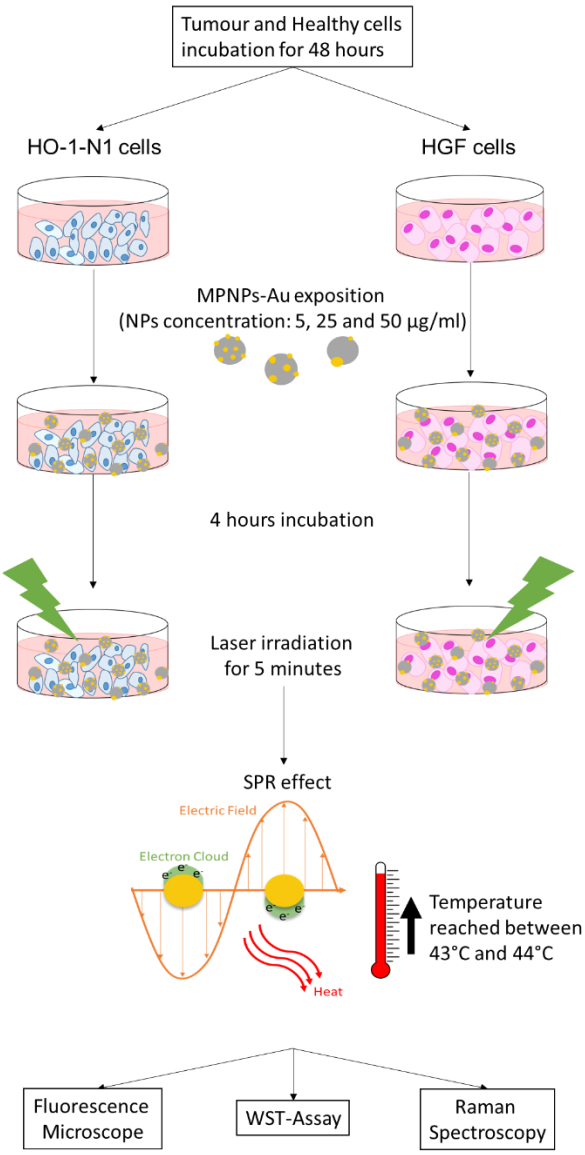

Figure 5. 12 Schematic representation of the procedure adopted for the cytotoxicity test.

5.4.1 Fluorescence microscope (FM)

This biological test is achieved by using the fluorescence microscope in which the resulting images give information about the cellular status. In fact, thanks to the different staining used, it is possible to understand whether cells are damaged or not. To perform FM, HGF and HO-1-N1 cells were seeded in 96 well plates at a density of 2 x 10^4 cells in 200 µl of cells medium. After 48 hours MPNPs were

dispersed in cell culture medium to obtain a final concentration of 5, 25 and 50 μg/ml and were added to the cell cultures in a final volume of 200 μl for each well. 4 hours later the photothermal treatment was performed, applying the irradiation for 5 minutes with a 530 nm continuous wave laser (output: +12 V, 3A; irradiance of 60mWcm−2) until the temperature reached was between 43 °C and 44 °C. Then FM was used to detect the effect of laser irradiation on cell exposed to NPs. The analysis was performed with FM JuLI Stage, AR Brown Co. Cells were stained with: Hoechst 33342® (nuclei, in blue); Annexin (early apoptosis without breaking membrane, in green); PI (cell death with breaking membrane, in red).

5.4.2 WST Assay

WST assay is an analysis which indicates the number of viable cells that can be quantified by measuring the absorbance given from their metabolic activity. HGF and HO-1-N-1 cells were seeded in six well plates at a density of 5 x 10^4 cells/well. After 48 hours MPNPs were dispersed in cell culture medium to obtain a final concentration of 5 and 50 μg/ml and were added to the cell cultures in a final volume of 2 ml for each well. 4 hours later some wells were exposed to a laser irradiation for 5 minutes with a 530 nm continuous wave laser (output: +12 V, 3A; irradiance of 60mWcm−2) until the temperature reached was between 43 °C and 44 °C. The viability of all cell cultures was determined after 4 hours from laser exposure using a standard WST-8 assay (WST-assay-Kit is Dojindo, Cytotoxicity LDH Assay Kit-WST, Lot.KP 870).

5.4.3 Raman spectroscopy

The Raman spectroscopy was performed in order to evaluate the molecules present in the cells, which can be indicators of cellular vitality or cellular stress. In fact, in a Raman shift, when the laser beam hits a cell, chemicals within the cell can absorb and reflect or scatter the light waves. This scattering generates a marker at various wavelengths that can be used to identify specific molecules, which depends on the

molecule type and the chemical bonds present within its structure[35]. Raman spectroscopy was performed on both HGF and HO-1-N1. The cells were seeded in six well plates at a density of 5 x 10^4 cells in 2 ml of cells medium. After 48 hours MPNPs were dispersed in cell culture medium to obtain a final concentration of 50 $\mu g ml^{-1}$ and were added to the cell cultures. 4 hours later the photothermal treatment was performed, applying 530 nm of laser irradiation for 5 minutes until the temperature between 43 °C – 44 °C was reached. Then the Raman spectra were detected 4 hours later with ARAMIS, LabRAM HR800 (Horiba/Jobin Ibon, Kyoto, Japan).

- Laser option: 532 nm, green laser;
- Acquisition time: 10 s;
- Acquisition number: 4;
- Number of spectra acquired: 5 spectra for each sample.

1. Miola M, Ferraris S, Pirani F, et al. Reductant-free synthesis of magnetoplasmonic iron oxide-gold nanoparticles. *Ceram Int*. 2017;43(17):15258-15265. doi:https://doi.org/10.1016/j.ceramint.2017.08.063.
2. Multari C, Miola M, Laviano F, et al. Magnetoplasmonic nanoparticles for photothermal therapy. *Nanotechnology*. 2019;30(25):255705. doi:10.1088/1361-6528/ab08f7.
3. Ormelli C. Magnetoplasmonic nanoparticles for photothermal therapy. 2019. http://webthesis.biblio.polito.it/id/eprint/10653.
4. Li Quadri T. Sintesi e caratterizzazione di nanoparticelle magnetoplasmoniche per applicazioni biomediche= Synthesis and characterization of magnetoplasmonic nanoparticles for biomedical applications. 2019. http://webthesis.biblio.polito.it/id/eprint/11378.
5. Sun L, Zhang ZJ, Wu ZS, Dang HX. Synthesis and characterization of DDP coated Ag nanoparticles. *Mater Sci Eng A*. 2004;379(1-2):378-383.
6. Kadasala NR, Lin L, Gilpin C, Wei A. Eco-friendly (green) synthesis of magnetically active gold nanoclusters. *Sci Technol Adv Mater*. 2017;18(1):210-218.
7. Bulut E, Ozacar M. Rapid, facile synthesis of silver nanostructure using hydrolyzable tannin. *Ind Eng Chem Res*. 2009;48(12):5686-5690.
8. Karimi Z, Karimi L, Shokrollahi H. Nano-magnetic particles used in biomedicine: Core and coating materials. *Mater Sci Eng C*. 2013;33(5):2465-2475. doi:https://doi.org/10.1016/j.msec.2013.01.045.
9. Cozzoli PD, Pellegrino T, Manna L. Synthesis, properties and perspectives of hybrid nanocrystal structures. *Chem Soc Rev*. 2006;35(11):1195-1208. doi:10.1039/B517790C.
10. Cheraghipour E, Javadpour S, Mehdizadeh A. Citrate capped superparamagnetic iron oxide nanoparticles used for hyperthermia therapy. *J Biomed Sci Eng*. 2012;5:715-719. doi:10.4236/jbise.2012.512089.
11. Campelj S, Makovec D, Drofenik M. Preparation and properties of water-based magnetic fluids. *J Phys Condens Matter*. 2008;20(20):204101. doi:10.1088/0953-8984/20/20/204101.
12. Goetze T, Gansau C, Buske N, Roeder M, Görnert P, Bahr M. Biocompatible magnetic core/shell nanoparticles. *J Magn Magn Mater*. 2002;252:399-402.

doi:https://doi.org/10.1016/S0304-8853(02)00624-8.

13. Dheyab MA, Aziz AA, Jameel MS, Noqta OA, Khaniabadi PM, Mehrdel B. Simple rapid stabilization method through citric acid modification for magnetite nanoparticles. *Sci Rep*. 2020;10(1):10793. doi:10.1038/s41598-020-67869-8.
14. Haw CY, Chia CH, Zakaria S, et al. Morphological studies of randomized dispersion magnetite nanoclusters coated with silica. *Ceram Int*. 2011;37(2):451-464. doi:https://doi.org/10.1016/j.ceramint.2010.09.010.
15. Liu Y, Zhong H, Li L, Zhang C. Temperature dependence of magnetic property and photocatalytic activity of Fe3O4/hydroxyapatite nanoparticles. *Mater Res Bull*. 2010;45(12):2036-2039. doi:https://doi.org/10.1016/j.materresbull.2010.09.010.
16. Bini RA, Marques RFC, Santos FJ, Chaker JA, Jafelicci Jr M. Synthesis and functionalization of magnetite nanoparticles with different amino-functional alkoxysilanes. *J Magn Magn Mater*. 2012;324(4):534-539.
17. Yamaura M, Camilo RL, Sampaio LC, Macedo MA, Nakamura M, Toma H. Preparation and Characterization of (3-Aminopropyl)triethoxysilane-Coated Magnetite Nanoparticles. *J Magn Magn Mater*. 2004;279:210-217. doi:10.1016/j.jmmm.2004.01.094.
18. Ahmad T. Reviewing the Tannic Acid Mediated Synthesis of Metal Nanoparticles. Thundat T, ed. *J Nanotechnol*. 2014;2014:954206. doi:10.1155/2014/954206.
19. Dong G, Liu H, Yu X, et al. Antimicrobial and anti-biofilm activity of tannic acid against Staphylococcus aureus. *Nat Prod Res*. 2018;32(18):2225-2228. doi:10.1080/14786419.2017.1366485.
20. Hassanien AS, Khatoon UT. Synthesis and characterization of stable silver nanoparticles, Ag-NPs: Discussion on the applications of Ag-NPs as antimicrobial agents. *Phys B Condens Matter*. 2019;554:21-30.
21. Gülçin İ, Huyut Z, Elmastaş M, Aboul-Enein HY. Radical scavenging and antioxidant activity of tannic acid. *Arab J Chem*. 2010;3(1):43-53.
22. Martínez-Castañon G-A, Nino-Martinez N, Martinez-Gutierrez F, Martinez-Mendoza JR, Ruiz F. Synthesis and antibacterial activity of silver

nanoparticles with different sizes. *J nanoparticle Res*. 2008;10(8):1343-1348.

23. Daduang J, Palasap A, Daduang S, Boonsiri P, Suwannalert P, Limpaiboon T. Gallic acid enhancement of gold nanoparticle anticancer activity in cervical cancer cells. *Asian Pac J Cancer Prev*. 2015;16(1):169-174.
24. Kitching H, Kenyon AJ, Parkin IP. The interaction of gold and silver nanoparticles with a range of anionic and cationic dyes. *Phys Chem Chem Phys*. 2014;44(0):6050-6059. doi:10.1039/c3cp55366c.
25. Narband N, Tubby S, Parkin I, et al. Gold Nanoparticles Enhance the Toluidine Blue-Induced Lethal Photosensitisation of Staphylococcus aureus. *Curr Nanosci - CURR NANOSCI*. 2008;4. doi:10.2174/157341308786306134.
26. Westcott SL, Oldenburg SJ, Lee TR, Halas NJ. Formation and adsorption of clusters of gold nanoparticles onto functionalized silica nanoparticle surfaces. *Langmuir*. 1998;14(19):5396-5401.
27. Leff D V, Brandt L, Heath JR. Synthesis and characterization of hydrophobic, organically-soluble gold nanocrystals functionalized with primary amines. *Langmuir*. 1996;12(20):4723-4730.
28. Gonzalez-Lakunza N, Lorente N, Arnau A. Chemisorption of sulfur and sulfur-based simple molecules on Au (111). *J Phys Chem C*. 2007;111(33):12383-12390.
29. Konno T, Usami M, Toyota A, Hirotsu M, Kawamoto T. Sulfur-bridged Linkage of [Ni (thiolato) 2 (amine) 2]-type Complexes with Linear Gold (I) Ions Assisted by Aurophilic Interaction. *Chem Lett*. 2005;34(8):1146-1147.
30. Walock M. Nanocomposite coatings based on quaternary metal-nitrogen and nanocarbon systems. November 2012.
31. Gohain N. Studies on the structure and function of phenazine modifying enzymes PhzM and PhzS involved in the biosynthesis of pyocyanin. January 2009. doi:10.17877/DE290R-8364.
32. Huang X, El-Sayed MA. Gold nanoparticles: Optical properties and implementations in cancer diagnosis and photothermal therapy. *J Adv Res*. 2010;1(1):13-28. doi:https://doi.org/10.1016/j.jare.2010.02.002.
33. Haiss W, Thanh NTK, Aveyard J, Fernig DG. Determination of Size and Concentration of Gold Nanoparticles from UV−Vis Spectra. *Anal Chem*.

2007;79(11):4215-4221. doi:10.1021/ac0702084.

34. introduction-to-gold-nanoparticle-characterization @ www.cytodiagnostics.com. https://www.cytodiagnostics.com/pages/introduction-to-gold-nanoparticle-characterization.

35. Shen Y, Xu F, Wei L, Hu F, Min W. Live-cell quantitative imaging of proteome degradation by stimulated Raman scattering. *Angew Chem Int Ed Engl*. 2015;53(22):5596-5599. doi:10.1002/anie.201310725.Live-cell.

Chapter 6

Results and discussion

With the final aim to produce new hybrid nanoplatforms (MPNPs) to be used as multifunctional platform in cancer theranostic, several nanoparticles composed of a magnetic core and an external Au NPs or Ag NPs decoration were obtained by different synthesis approaches. One of the major object was to create a facile and reproducible synthesis method able to maintain the peculiar properties of both nanomaterials and to combine the effect of SPIONs and Au/Ag NPs by means of the innovative use of tannic acid.

In particular, to obtain scalable nanostructures and enhance the synthesis yield, several synthesis methods were conducted, and the results related to the structural, morphological and chemical characterization of the obtained systems are presented. With the aim of achieving the best synthesis by exploiting the peculiar characteristics of tannic acid, efforts have been devoted to optimizing a "green" procedure capable of synthesizing the nanocomposites.

Besides the morphological, compositional and structural data, the chapter reports magnetic and optical characterization as well as the results coming from induction heating and laser irradiation, which give information on the NPs ability to produce heat.

Moreover, in paragraph 6.4 the *in vitro* cytotoxicity evaluation of the as-produced MPNPs-Au/Ag nanoparticles is discussed, while in paragraph 6.5 the results concerning the laser induced phototherapy are presented.

Part of the data and images presented in this chapter, with the incorporation of more results and some modification, were already published during the PhD period in different journal articles and thesis[1–4].

It is also important to underline that part of the results presented in this chapter derive from both European and non-European collaborations. In particular, all the results referred to the chemical, morphological, magnetic and optical characterization together with the induction heating and laser irradiation tests were carried out by the author at DISAT (polytechnic of Turin) with the exception of the TEM characterization which was carried out by researchers from the Italian Institute of Technology in Genoa.

The in vitro cytotoxicity tests were carried out in part at the St Joseph Institute of Ljubljana which made the red blood cells available for the NPs haemotoxicity evaluation, and in part at the University of Novara where healthy and cancer cells were compared to evaluate the NPs cytocompatibility.

Finally, all the tests concerning the laser induced phototherapy were carried out by the author during a secondment period at the Kyoto Institute of Technology (Japan).

6.1 First route synthesis characterization

In this paragraph, the morphological, compositional and chemical characterization concerning the first route adopted to synthetize MPNPs-Au and MPNPs-Ag are described. In particular, the paragraph 6.1.1 is dedicated to the characterization of SPIONs stabilized with CA and functionalized with APTES, in order to define if the nanoparticles are suitable to promote the metal NPs reduction on its surface. For this reason, a detailed characterization is performed. Then, in paragraph 6.1.2 and 6.1.3 the preliminary characterization of the different methods used to synthetize MPNPs-Au and MPNPs-Ag are presented in order to select best approaches to generate the NPs suspensions. Therefore, at the end of each

paragraph the best synthesis method is selected for more in-depth characterization that will be presented in paragraph 6.3, together with the best results coming from the second route.

6.1.1 SPIONs stabilized with CA and functionalized with APTES

TEM analysis

Magnetic nanoparticles were firstly characterized by means of TEM analysis in order to assess their size and morphology. In figure 6.1 TEM image of bare iron oxide nanoparticles is shown, in which it is possible to observe the approximately spherical shape of SPIONs, and their dimensional range between 5–20 nm.

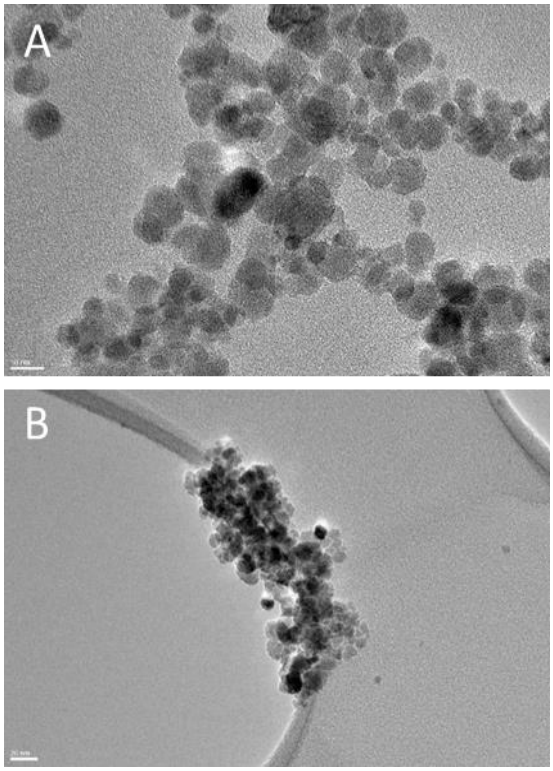

Figure 6. 1: TEM image of Iron Oxide NPs. Scale bar: figure A 10nm; figure B 20nm

The morphology and the size of the sample were not affected by both the addition of CA and APTES as shown in figure 6.2 and figure 6.3 respectively. In fact, it is possible to observe pseudo-spherical well-dispersed nanoparticles with a

size range between 5 and 20 nm in both cases as shown in the graph size distribution (figure 6.2C and 6.3C).

.

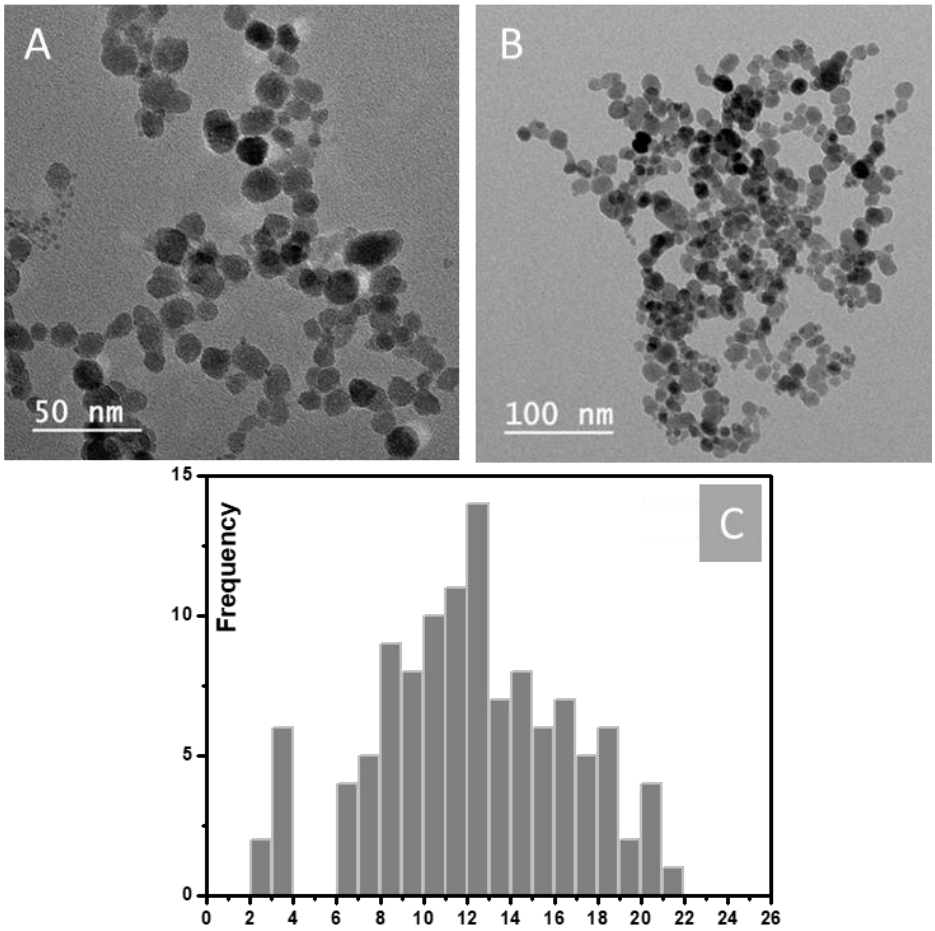

Figure 6. 2: TEM images of SPIONs stabilized with CA and graph size distribution.

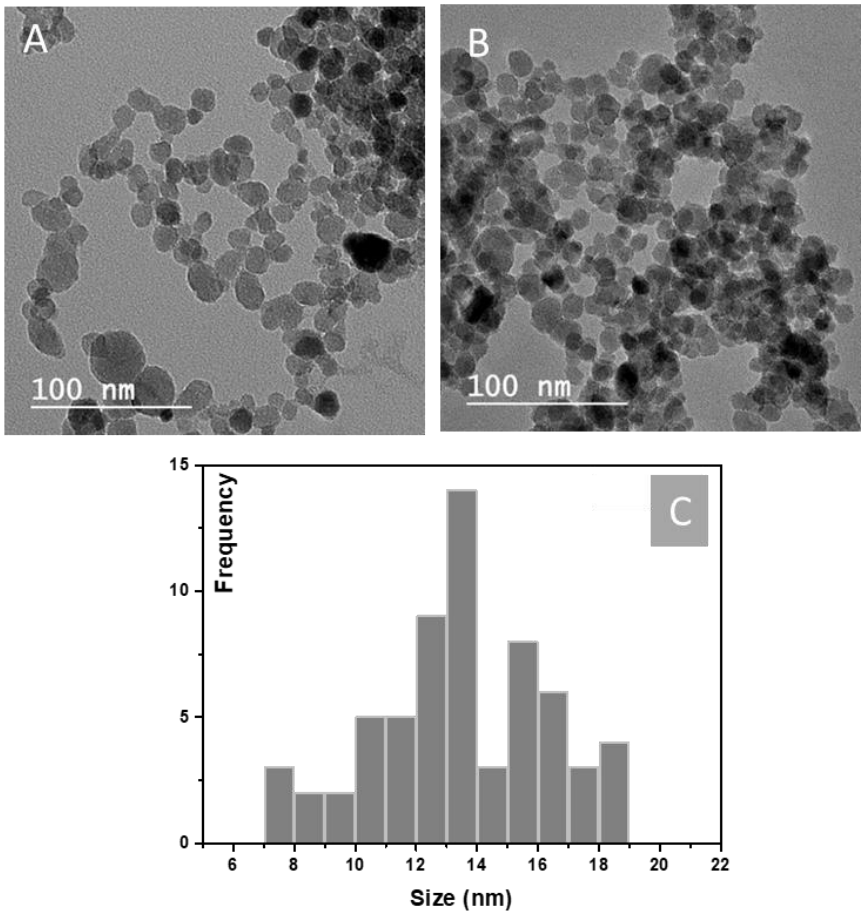

Figure 6. 3: TEM images of SPIONs stabilized with CA and functionalized with APTES and graph size distribution.

FT-IR spectra

To compare the surface properties of SPIONs, CA capped SPIONs and APTES functionalized SPIONs, the FTIR spectra were recorded on each kind of batch. The results are shown in figure 6.4, 6.5 and 6.6 and the main peaks attribution are summarized in table 6.1. In all patterns it is evident the strong vibrational modes of Fe-O bonds of magnetite that are located at 585 cm^{-1} [5,6].

The patterns differ one from each other for the presence, in the case of CA-capped SPIONs, of the main signals of CA. In detail, for the CA-capped SPIONs (figure 6.5), at 1400 cm^{-1} the peak related to the asymmetric stretching of the COO– group of COOH of CA, and around 1600 cm^{-1} the peak ascribable to the vibration of the C–O of the COOH group of CA, can be seen, as a confirmation of a CA radical bound to the magnetite surface. The intense band at about 1600 cm^{-1} in the CA-capped SPIONs spectrum, evidences the binding of a CA radical to the surface

of Fe_3O_4 nanoparticles by chemisorption of carboxylate (citrate) ions[7,8]. This confirms the formation of SPIONs and the effective stabilization with CA, which avoids NPs aggregation.

Regarding the APTES functionalized SPIONs in figure 6.6 the peaks at around 1000 cm^{-1}, which is a characteristic band for the Si-O-Si vibrations in the silane layer, and the Si-OH stretch of APTES at 800 cm^{-1} are evident; this attest the correct functionalization of SPIONs, which can be used for the metal NPs decoration. Thanks to this analysis it is possible to confirm the successful stabilization of SPIONs with CA and functionalization with APTES.

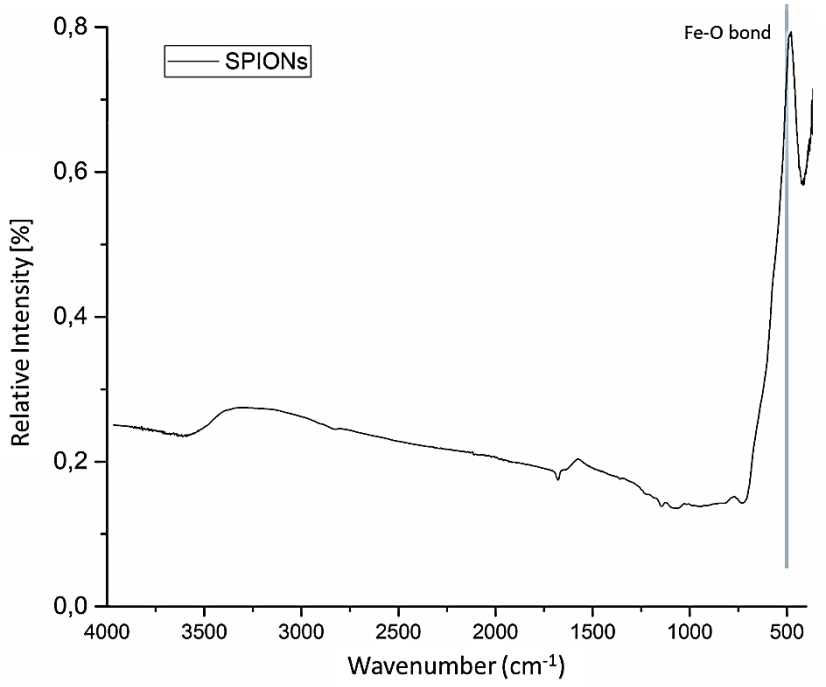

Figure 6. 4: FTIR spectra of SPIONs

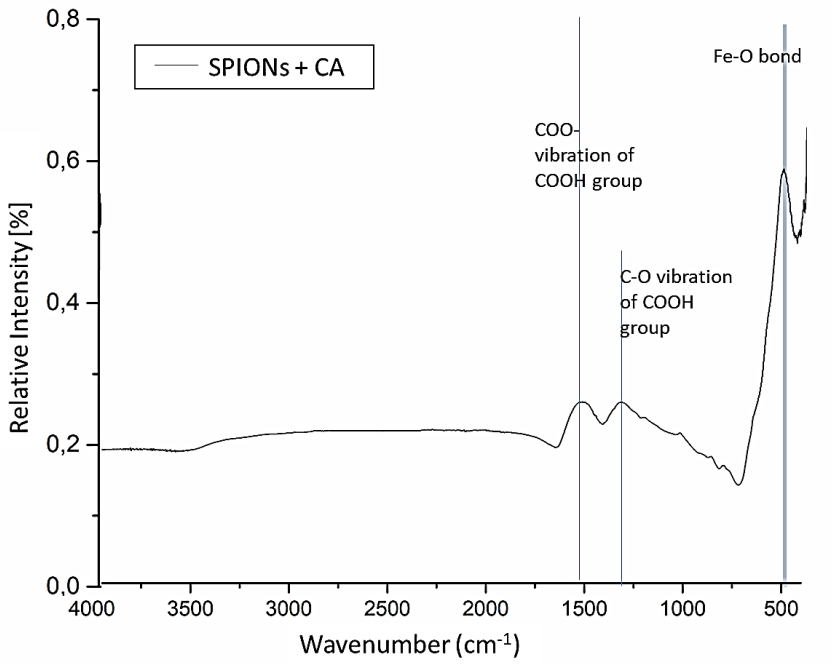

Figure 6. 5: FTIR spectra of CA capped SPIONs

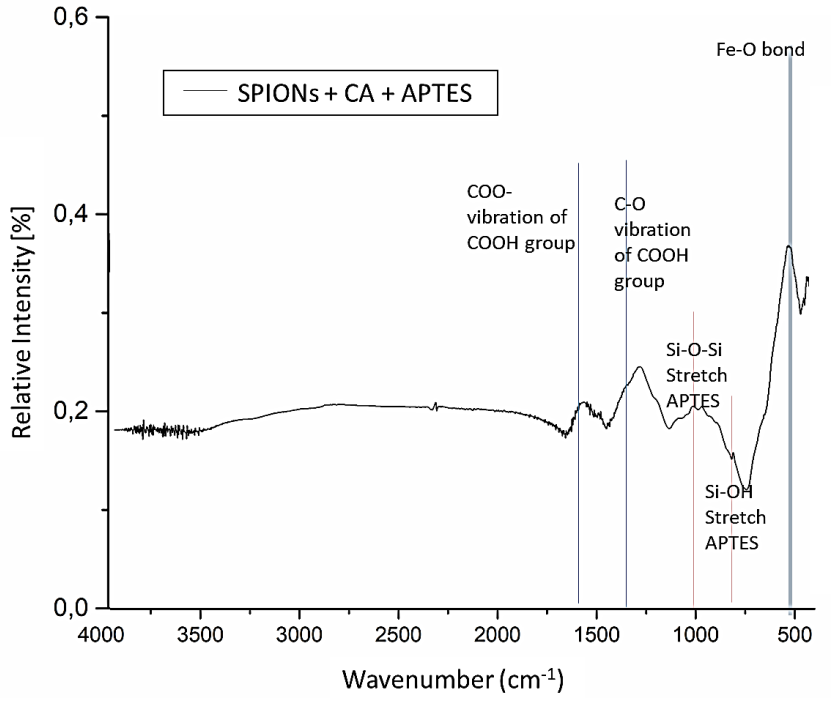

Figure 6. 6: FTIR spectra of CA-capped SPIONs functionalized with APTES

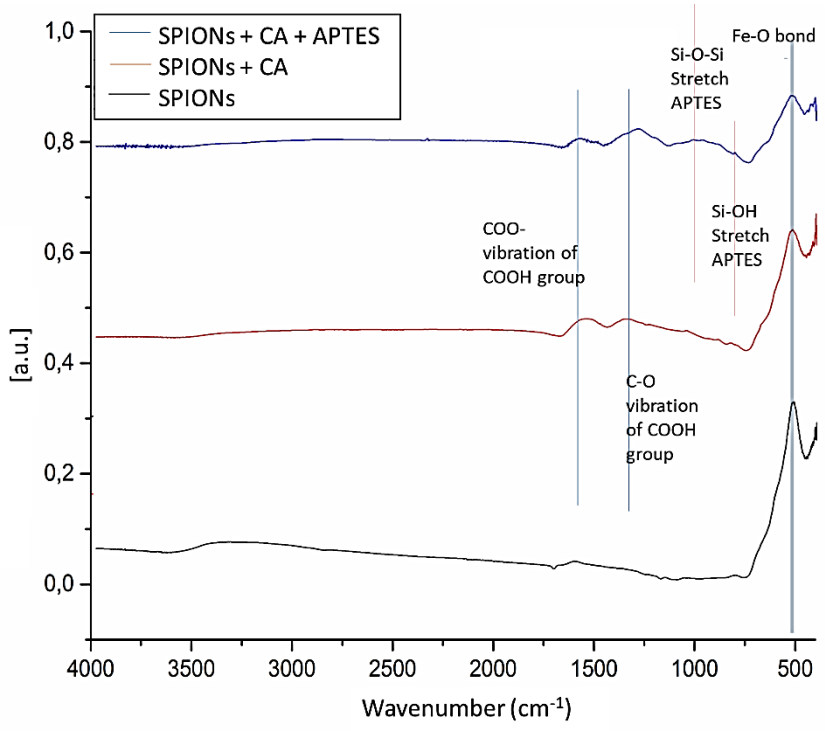

Figure 6. 7: comparison of FTIR spectra with corresponding peaks.

Table 6. 1 FT-IR main peaks assignment

Wavenumber (cm^{-1})	Assignment
585	strong vibrational modes of Fe-O bonds of magnetite
800	Si-OH stretch of APTES
1000	Si-O-Si vibrations in the silane layer
1600	vibration of the C–O of the COOH group of CA
1400	asymmetric stretching of the COO– group of COOH of CA

DLS and Z-potential

The hydrodynamic diameter of NPs was determined by DLS. This analysis shows two important parameters defining the physico-chemical behaviour of NPs in solutions: The Z-average size (hydrodynamic diameter) and the Polydispersity Index (PDI). An average hydrodynamic diameter for Fe_3O_4 NPs of 104.76 nm has been detected, while the PDI, which indicates the breadth of the size distribution,

was 0.21%. This means that the sample is monodisperse and a single particle "species" is present with a hydrodynamic diameter mean of 104,76 nm.

In order to calculate the isoelectric point (IEP) of NPs, the ζ potential measurement has been performed. This is useful to evaluate if the CA adsorption on SPIONs is able to improve the electrostatic repulsion at physiological pH, by inducing a surface charge modification[9,10]. The experimental value of SPIONs IEP is 6.8 as it can be observed in the ζ potential graph in figure 6.8. The CA-capped SPIONs curve shows that the isoelectric point is shifted towards lower pH values and results to be about 2; this confirms the correct absorption of CA on SPIONs surface and its ability to modify the surface charge.

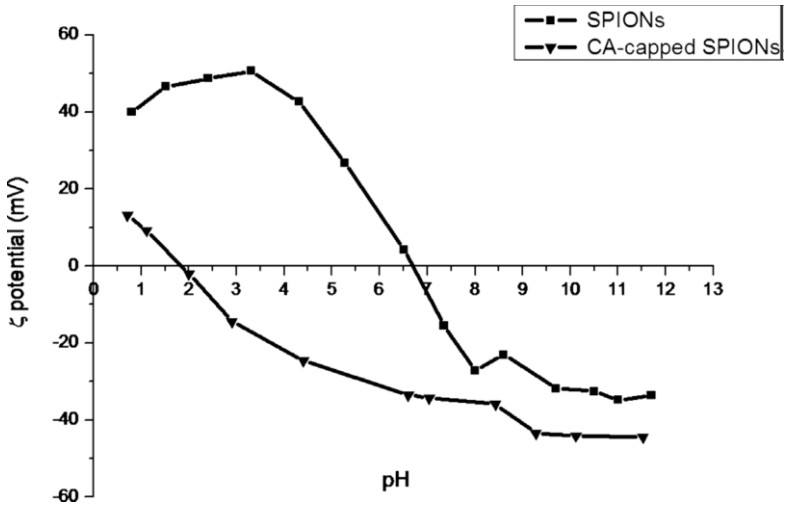

Figure 6. 8: ζ potential measurement of SPIONs and CA-capped SPIONs

6.1.2 MPNPs-Au (first route)

Once defined the correct CA stabilization and APTES functionalization of SPIONs, the analyses on MPNPs-Au have been performed. The three synthesis methods used to create the nanocomposites have been studied by using STEM and UV-Vis analyses; then the synthesis showing the best results has been used as model synthesis for further investigation.

The SEM images reporting the morphological aspect of nanocomposites coming from the method A (figure 6.9) have been acquire in dark field mode, in which high mass materials (such as gold) appear bright[11]. In this method, the tannic

acid was firstly added to CA/APTES-functionalized SPIONs and subsequently the $HAuCl_4$ has been added to allow the Au nucleation directly on SPIONs surface. Analyzing the SEM images, only few bright spots ascribable to Au NPs are visible on SPIONs surface, this indicate that the $HAuCl_4$ reduction did not completely take place or that the Au NPs did not anchor in optimal way on the SPIONs surface. In fact, also from UV-Vis analysis, reported in figure 6.10, any signal is highlighted in the window between 500 nm and 600 nm, band at which the Au NPs should show an absorption peak.

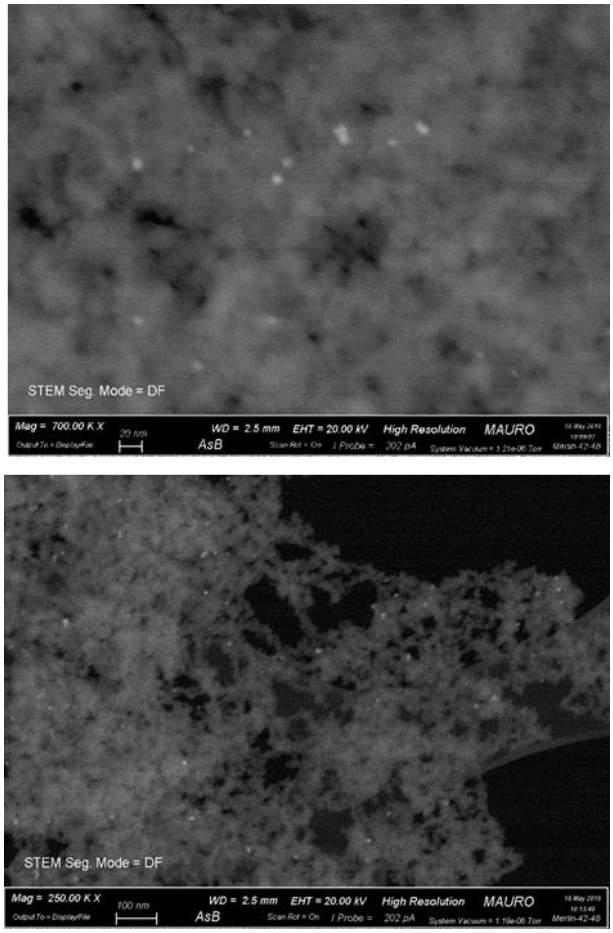

Figure 6. 9: SEM images of MPNPs-Au (first route), method A.

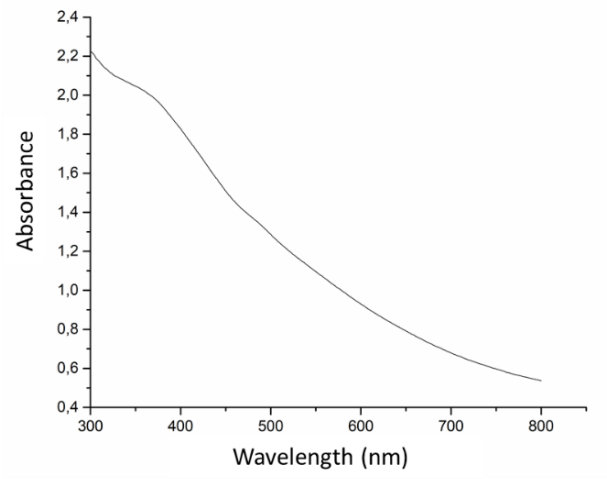

Figure 6. 10: UV-Vis of MPNPs-Au (first route), method A.

In method B, the $HAuCl_4$ were firstly dispersed with tannic acid, in order to reduce the gold salts and generate the Au NPs, and subsequently added to the CA/APTES-functionalized SPIONs solution. Following this method, the Au NPs should attach on SPIONs surface after being reduced by the tannic acid separately. In SEM images reported in figure 6.11, only few spots of Au NPs are still shown, this indicates that the nanoparticles do not stick to the SPIONs surface after being reduced separately from the tannic acid. This is confirmed by the UV-Vis graph in figure 6.12, in which the typical peak of Au NPs is not visible.

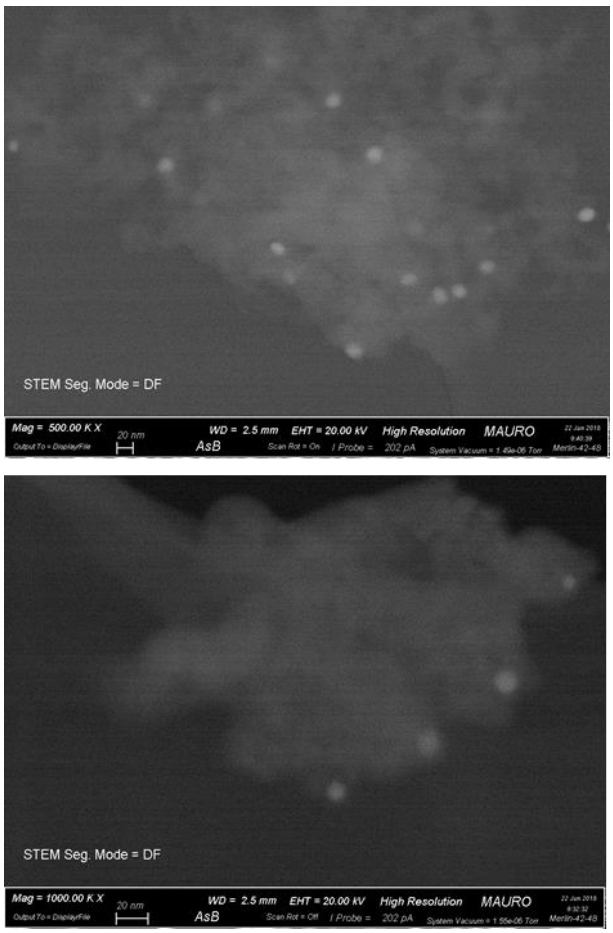

Figure 6. 11: SEM images of MPNPs-Au (first route), method B.

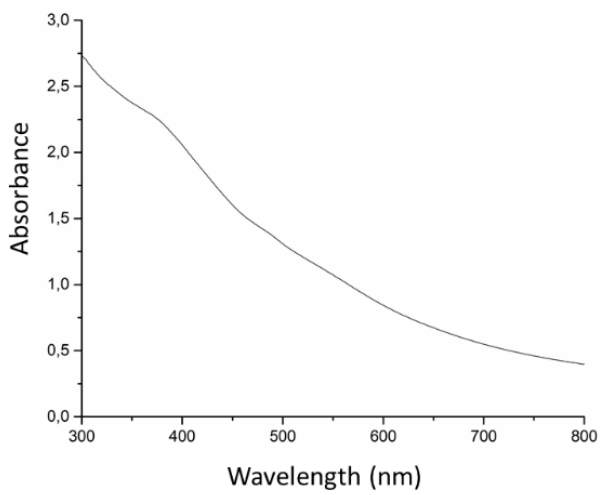

Figure 6. 12: UV-Vis of MPNPs-Au (first route), method B.

In method C, $HAuCl_4$ and CA/APTES-functionalized SPIONs solution were firstly mixed together in order to promote the gold salts adhesion on SPIONs surface and then the tannic acid was added to allow the $HAuCl_4$ reduction. Using this method, the gold nanoparticles are generated only after the SPIONs surface grafting. Analyzing the SEM images (figure 6.13) much more Au NPs are visible if compared with SEM images of methods A (figure 6.9) and B (figure 6.11); this indicates that a lot of Au NPs are attached on the SPIONs surface also after the washing step performed during the synthesis.

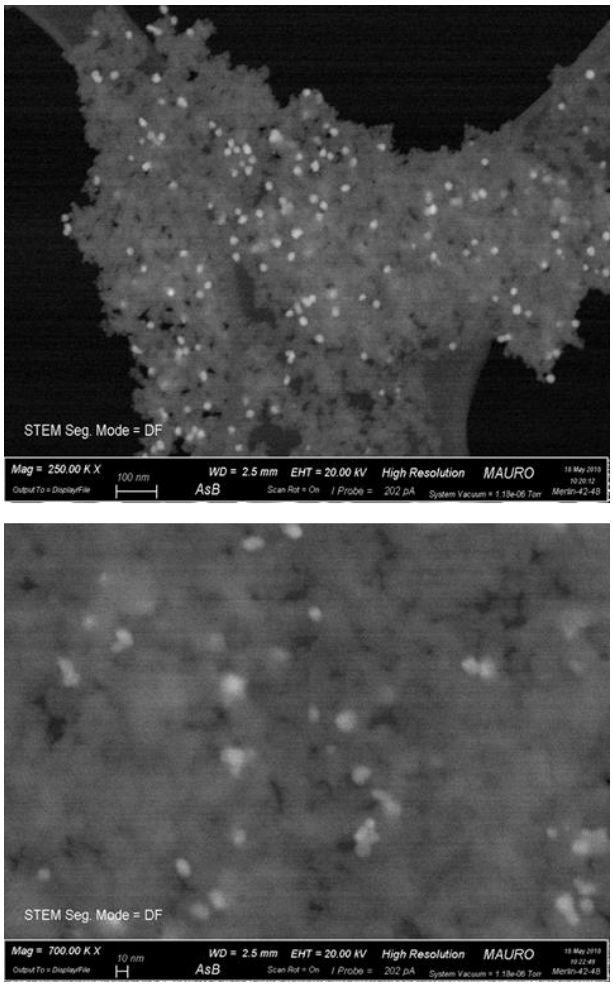

Figure 6. 13: SEM images of MPNPs-Au (first route), method C.

Observing the UV-Vis graph reported in figure 6.14, it is not possible to notice the typical absorbance band of Au NPs, but is only visible a slight curvature

between 500 nm and 600 nm. This may confirm the correct Au NPs grafting on SPIONs surface, but, as suggested from literature[12,13], the Au concentration is probably too low to emit a more intense signal.

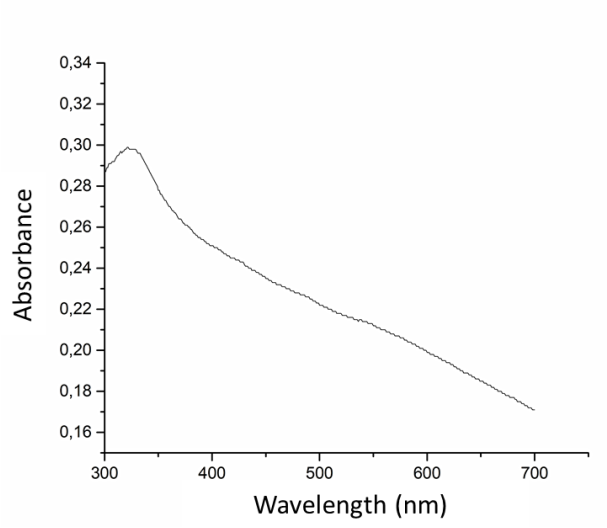

Figure 6. 14: UV-Vis of MPNPs-Au (first route), method C.

Given the poor absorbing peak generated by the MPNPs-Au synthetized with method C, some improvements have been made in order to improve the amount of Au NPs attached to the SPIONs surface. In particular, basing on the fact that $HAuCl_4$ forms several complexes depending on the pH[14,15], which are characterized by different surface charge, the same method has been repeated by changing the $HAuCl_4$ pH before mixing it with the SPIONs solution. Four different pH have been tested, always maintaining the same quantities of reagents: pH= 2; 4; 7; 8. TEM images showing the morphological aspect of gold nanoparticles produced with method C, changing the $HAuCl_4$ pH, are displayed below.

In figure 6.15, the bright field TEM images reporting the MPNPs-Au with $HAuCl_4$ initial pH=2 are visible; it is possible to observe some dark spot ascribable to Au NPs due to their higher mass, which results to have a round shape and a good distribution in the sample, but they are still in poor quantities to show a good absorbing peak.

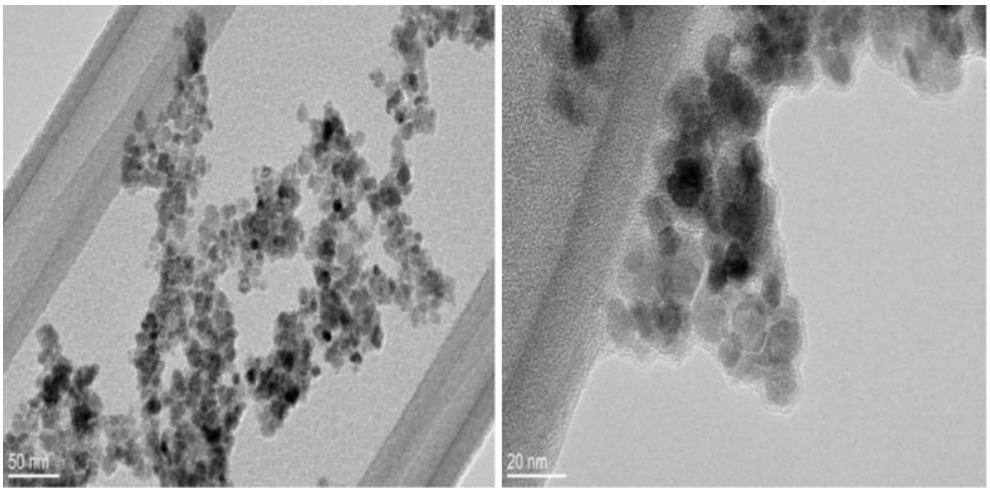

Figure 6. 15: TEM images of MPNPs-Au with $HAuCl_4$ initial pH=2

In the images showed below (figure 6.16) the bright field TEM images coming from the MPNPs-Au with $HAuCl_4$ initial pH=4 are displayed. Here it is noticeable a high degree of aggregation of Au NPs that are attached together in a few areas with a bad distribution in the entire sample.

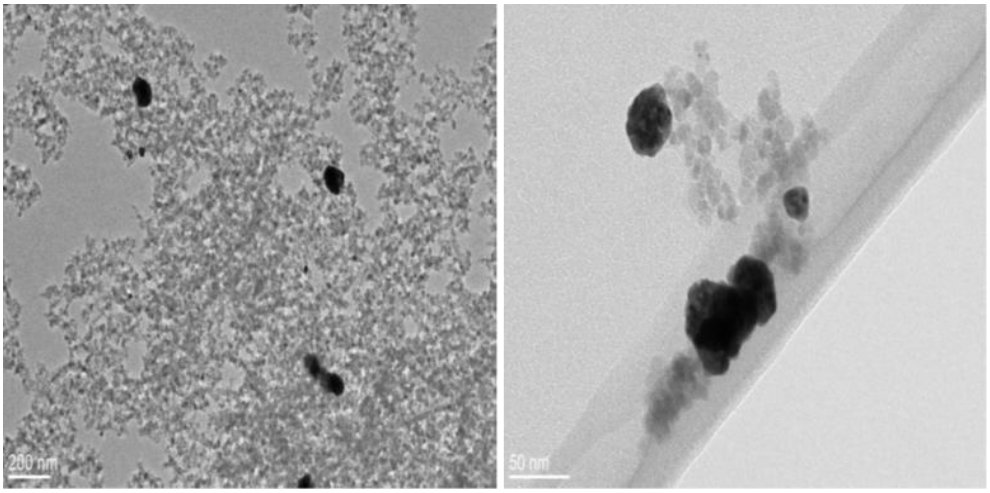

Figure 6. 16: TEM images of MPNPs-Au with $HAuCl_4$ initial pH=4

The syntheses with more basic pH (7/8) were subsequently prepared and the bright field TEM images are shown in the figure 6.17 and in figure 6.18. In both cases it is possible to appreciate well dispersed Au NPs on SPIONs surface with a size range between 10 and 20 nm; moreover, they do not show high levels of

aggregation if compared with the figure 6.15 and figure 6.16 in which the synthesis was performed at a more acidic pH.

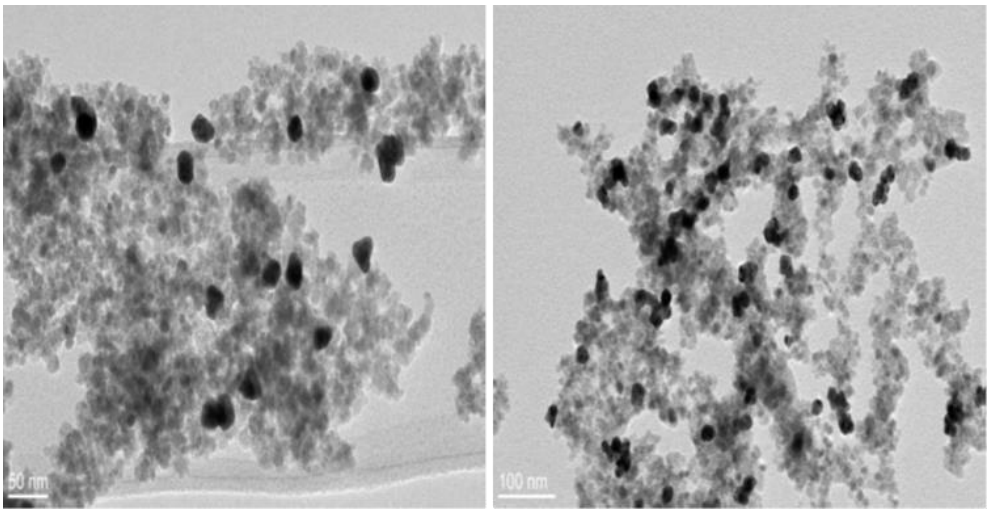

Figure 6. 17: TEM images of MPNPs-Au with $HAuCl_4$ initial pH=7

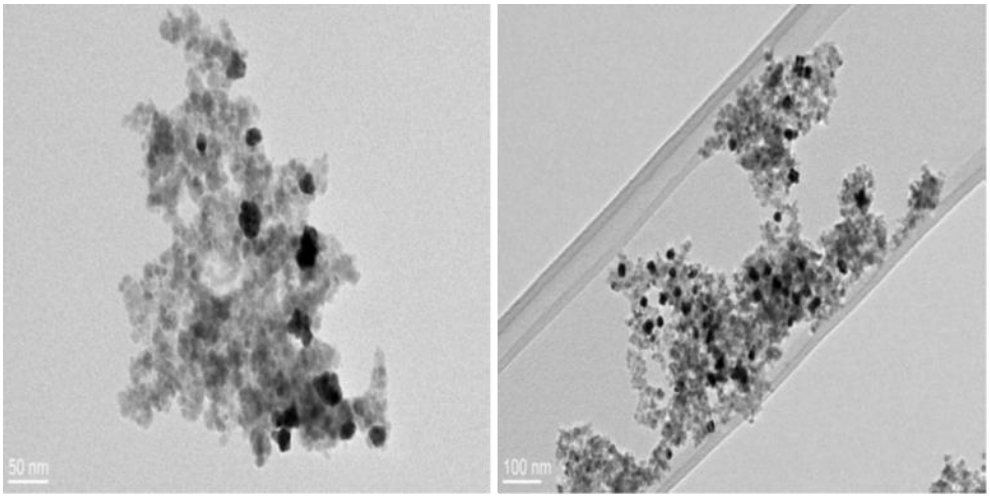

Figure 6. 18: TEM images of MPNPs-Au with $HAuCl_4$ initial pH=8

As shown, the influence of gold solution pH is high; at basic values (7/8) the best results are obtained in terms of NPs dimensions and distributions. Thus, to improve the concentration of Au NPs on the SPIONs surface, a pH=8 has been used.

The UV-Vis analysis was then repeated to verify if there were any improvements in the absorbance curve of the new solution MPNPs-Au that shows a slight increase of the gold peak around 560 nm (figure 6.19).

Therefore, given the improvement in size and dispersion as well as in the presence of the absorption peak, the MPNPs-Au (first route) synthetized following the method C, using an initial $HAuCl_4$ pH=8 has been used as model synthesis for further studies presented in paragraph 6.3.

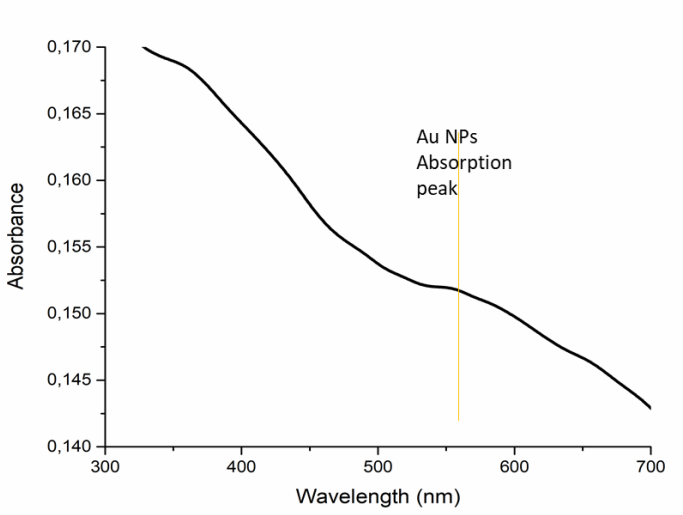

Figure 6. 19: UV-Vis of MPNPs-Au (first route), method C with initial pH=8.

6.1.3 MPNPs-Ag (first route)

In this paragraph the MPNPs-Ag nanocomposites coming from the first route synthesis are studied. As already done for MPNPs-Au, the three synthesis methods have been analyzed by using SEM and UV-Vis techniques; then the synthesis showing the best results has been selected as model synthesis for further investigation.

In the method A, the tannic acid and CA/APTES-functionalized SPIONs were firstly mixed together and subsequently the $AgNO_3$ has been added to allow the Ag NPs nucleation directly on SPIONs surface. The SEM images, reporting the morphological aspect of nanocomposites coming from this method, are showed in figure 6.20. Analyzing the images, it is possible to appreciate a large number of Ag

NPs on the SPIONs surface with a very good distribution in dispersion and size (which results to be around 20 nm). The high concentration of Ag NPs remained anchored to SPIONs surface is also confirmed by the UV-Vis analysis showed in figure 6.21. In the graph it is possible to observe a high signal in the Ag NPs absorbing window, with an absorbing peak at 460 nm; the peak at 290 nm instead, is the one related to the tannic acid.

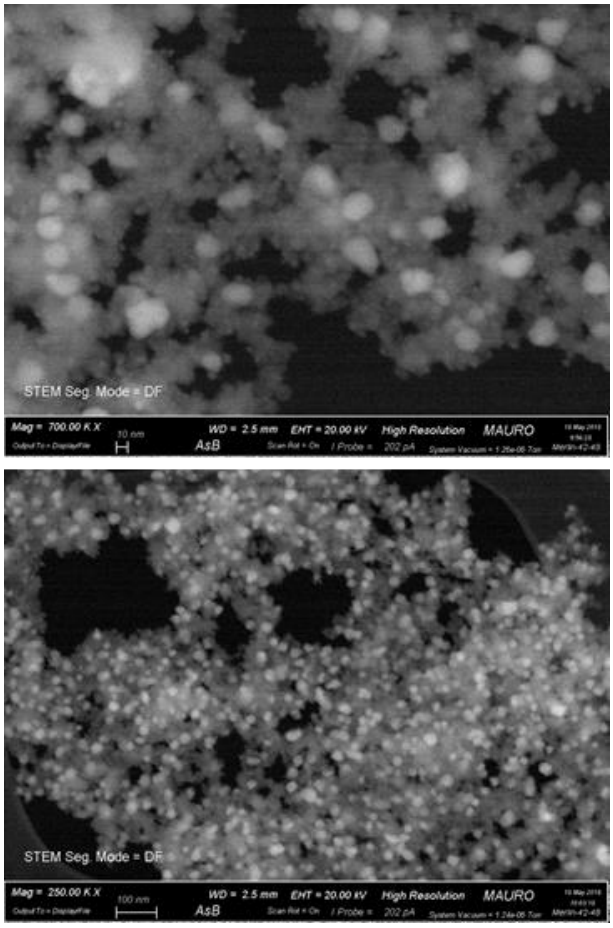

Figure 6. 20: SEM images of MPNPs-Ag (first route), method A.

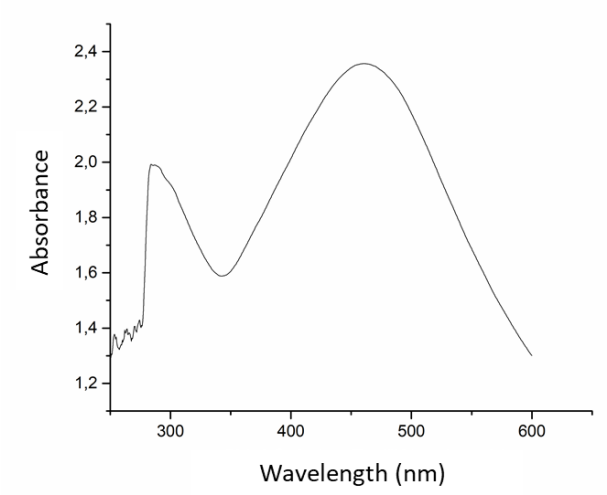

Figure 6. 21: UV-Vis of MPNPs-Ag (first route), method A.

In method B, the $AgNO_3$ was firstly dispersed with tannic acid, in order to reduce the silver salts and generate the Ag NPs, and subsequently added to the CA/APTES-functionalized SPIONs solution. Following this method, the Ag NPs should attach on SPIONs surface after being reduced by the tannic acid separately. In SEM images reported in figure 6.22, only few spots of Ag NPs are visible, this indicates that the nanoparticles do not adhere optimally to the SPIONs surface after being reduced separately from the tannic acid; moreover, some Ag NPs nanoparticles with much larger dimensions than the others, of about 50 nm, are evident. This is confirmed by the UV-Vis graph in figure 6.23, in which the curve does not present a sharp peak, but a wider curve probably given by the heterogeneity of the Ag NPs dimension in the sample.

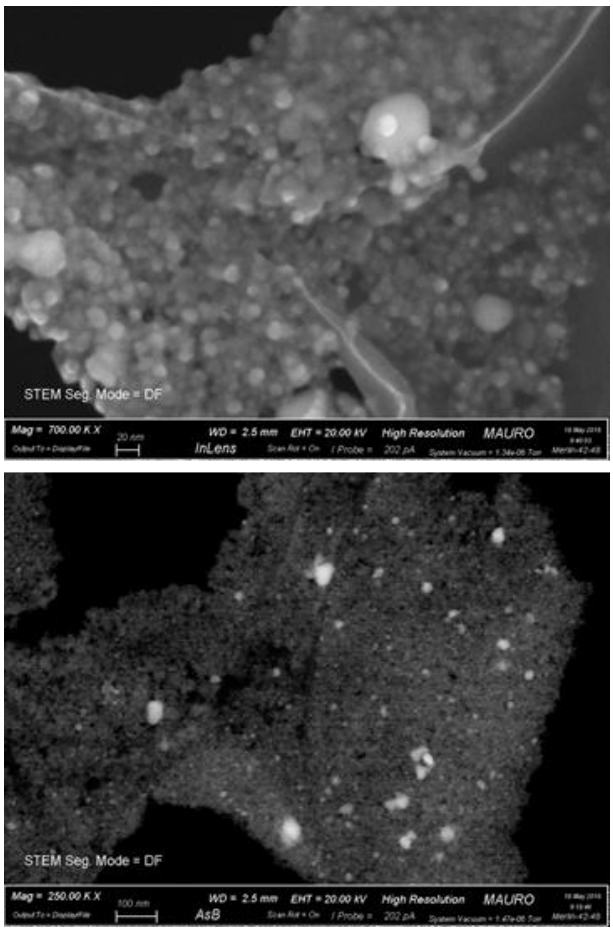

Figure 6. 22: SEM images of MPNPs-Ag (first route), method B.

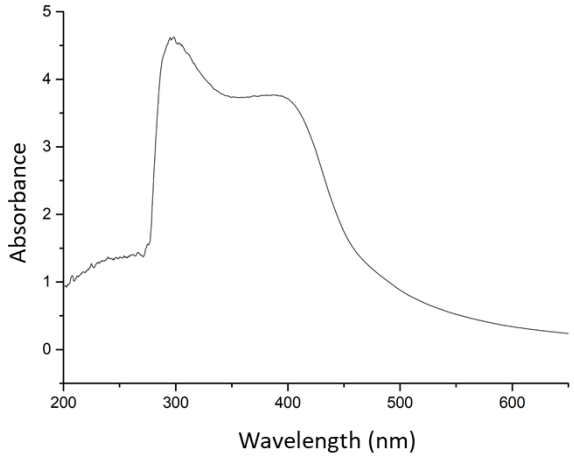

Figure 6. 23: UV-Vis of MPNPs-Ag (first route), method B.

In method C, $AgNO_3$ and CA/APTES-functionalized SPIONs solution were firstly mixed together in order to promote the silver salts adhesion on SPIONs surface and then the tannic acid was added to allow the $AgNO_3$ reduction. With this method, the Ag nanoparticles should generate only after the SPIONs surface grafting. Analyzing the SEM images (figure 6.24) it is possible to notice only a few bright spots ascribable to Ag NPs with very heterogeneous dimensions; in fact, as in method B, in the UV-Vis graph (figure 6.25) it is not possible to observe a well-defined peak but a wider curve.

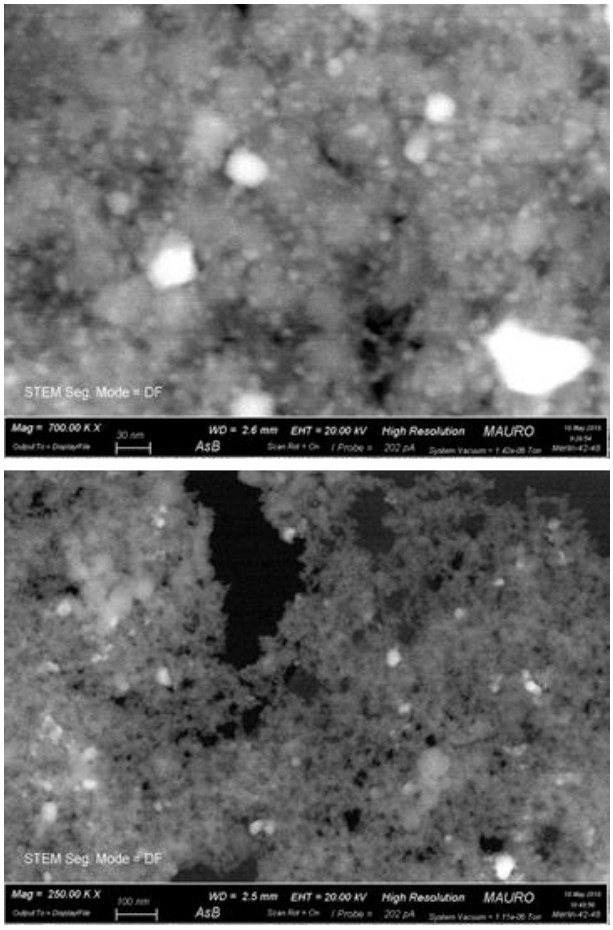

Figure 6. 24: SEM images of MPNPs-Ag (first route), method C.

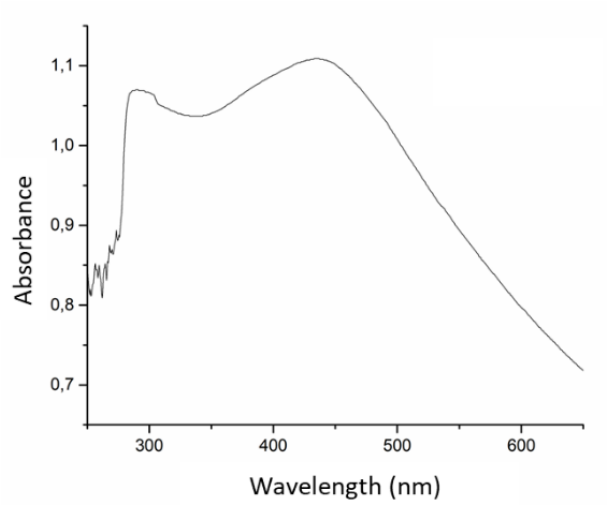

Figure 6. 25: UV-Vis of MPNPs-Ag (first route), method C.

Comparing the SEM images and UV-Vis analyses coming from the 3 presented methods, the synthesis coming from method A was selected as the best synthesis because it shows presents homogeneous and well-dispersed Ag NPs with a size of about 20 nm and a sharp absorption peak at 460 nm. For this reason, MPNPs-Ag (first route) synthetized following the method A has been used as model synthesis for further studies which will be presented in paragraph 6.3.

6.2 Second route synthesis characterization

In this paragraph the morphological, compositional and chemical characterization concerning the second route adopted to synthetize MPNPs-Au and MPNPs-Ag are described. In particular, in paragraph 6.2.1 the analyses confirming the correct binding of tannic acid on SPIONs surface, in the paragraphs 6.2.2 and 6.2.3 the preliminary characterization of the different methods used to synthetize MPNPs-Au and MPNPs-Ag are presented, in order to select best approaches to generate the NPs suspensions by using the tannic acid as reducing and stabilizing agent. Therefore, at the end of each paragraph the best synthesis method is selected for more in-depth characterization that will be presented in paragraph 6.3 together with the best results coming from the first route.

6.2.1 Tannic acid bond on SPIONs

In second route magnetic nanoparticles have been used without any prior functionalization or stabilization, in fact in these syntheses, it is tannic acid that acts as a reducing and stabilizing agent. In order to confirm the presence of the tannic acid on SPIONs surface, the FT-IR and UV-Vis analysis were performed as shown in figure 6.26 and 6.27 respectively.

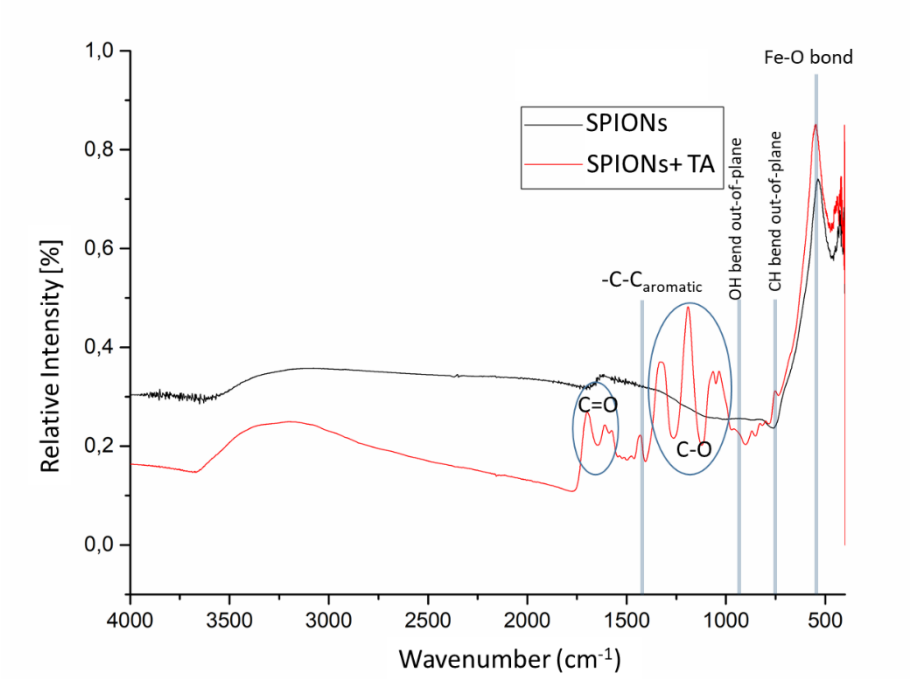

Figure 6. 26 FTIR spectra of SPIONs and SPIONs with tannic acid functionalization

From the FT-IR spectra are visible the main characteristic peaks of TA, in particular, the C=O stretching vibration at 1730-1705 cm^{-1} and C-O at 1100-1300 cm^{-1} [16], around 1452 cm^{-1} the stretching vibrations of -C-Caromatic groups appear, while at 923 cm^{-1} the peak indicate out of plane OH bending of acid groups, and the 758 cm^{-1} peak is referred to CH out of plane bending of phenyl groups. In the same spectra is still visible around 3400 cm^{-1} the broad peak of SPIONs which represents hydroxyl groups and surface-adsorbed water molecules and the vibrational modes of Fe-O bonds of magnetite, as confirmation of correct binding of tannic acid on SPIONs surface.

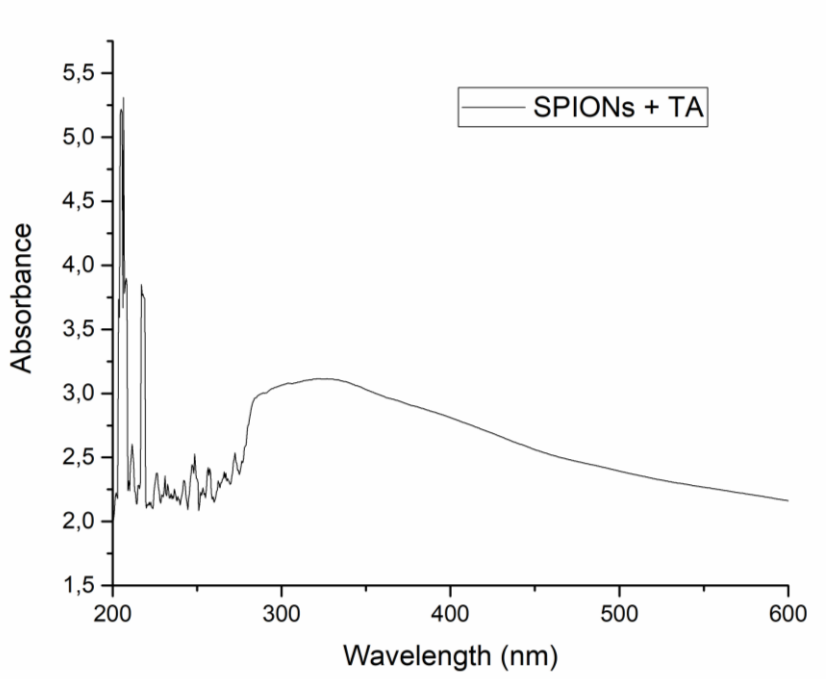

Figure 6. 27 UV-Vis spectra of SPIONs functionalized with TA

From UV-Vis analysis performed is visible the peak associated to the tannic acid around 300 nm. This corroborate the results from FT-IR which confirms the correct binding of tannic acid on SPIONs surface.

6.2.2 MPNPs-Au (second route)

In this paragraph the MPNPs-Au nanocomposites coming from the second route synthesis are studied in which tannic acid works as reducing and stabilizing agent.

Starting from method A, the tannic acid and bare SPIONs were firstly mixed together in order to avoid aggregation in SPIONs solution and subsequently the $HAuCl_4$ has been added to allow the Au nucleation directly on SPIONs surface. The SEM images reporting the morphological aspect of nanocomposites coming from this method is showed in figure 6.28. Analyzing the images, it is possible to

appreciate a large number of Au NPs on the SPIONs surface with a very good distribution in dispersion and size (the smallest particles result to be around 20 nm). The high concentration of Au NPs remained anchored to SPIONs surface is also confirmed by the UV-Vis analysis showed in figure 6.29. In the graph it is possible to observe a high signal in the Au NPs absorbing window with an absorbing peak at 620 nm.

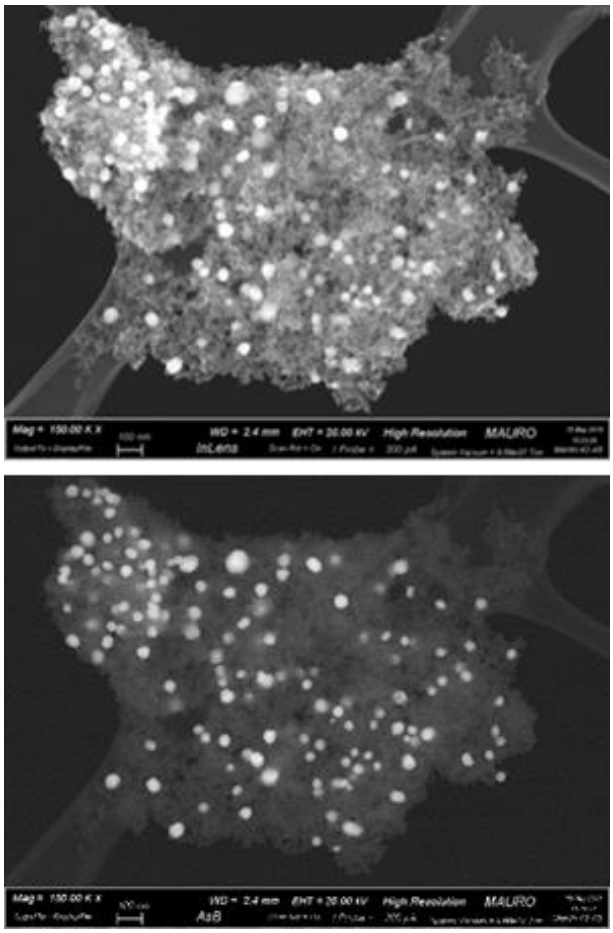

Figure 6. 28: SEM images of MPNPs-Au (second route), method A.

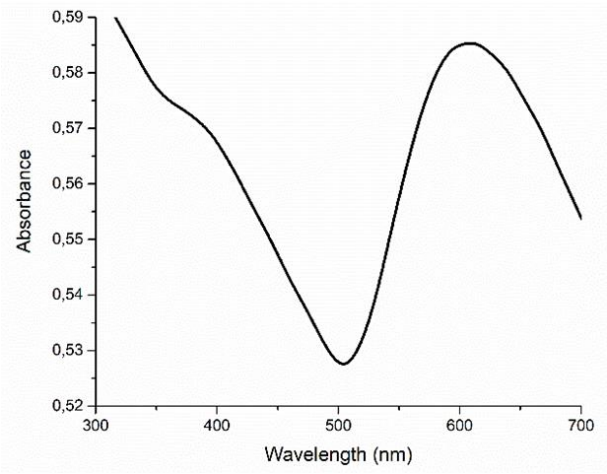

Figure 6. 29: UV-Vis of MPNPs-Au (second route), method A.

In method B, the $HAuCl_4$ was firstly dispersed with tannic acid, in order to reduce the gold salts and generate the Au NPs, and subsequently added to the SPIONs solution. The Au NPs should attach on SPIONs surface after being reduced by the tannic acid separately. In dark field and bright field SEM images reported in figure 6.30, some well-dispersed bright and dark spots ascribable to Au NPs with a size range around 20 nm are visible; this indicates that the nanoparticles stick to the SPIONs surface after being reduced separately from the tannic acid. But looking at UV-Vis graph (figure 6.31), the curve does not present a sharp absorption peak of Au NPs; this probably indicates that the number of Au NPs is not sufficient to produce a more intense signal in the Au absorption region.

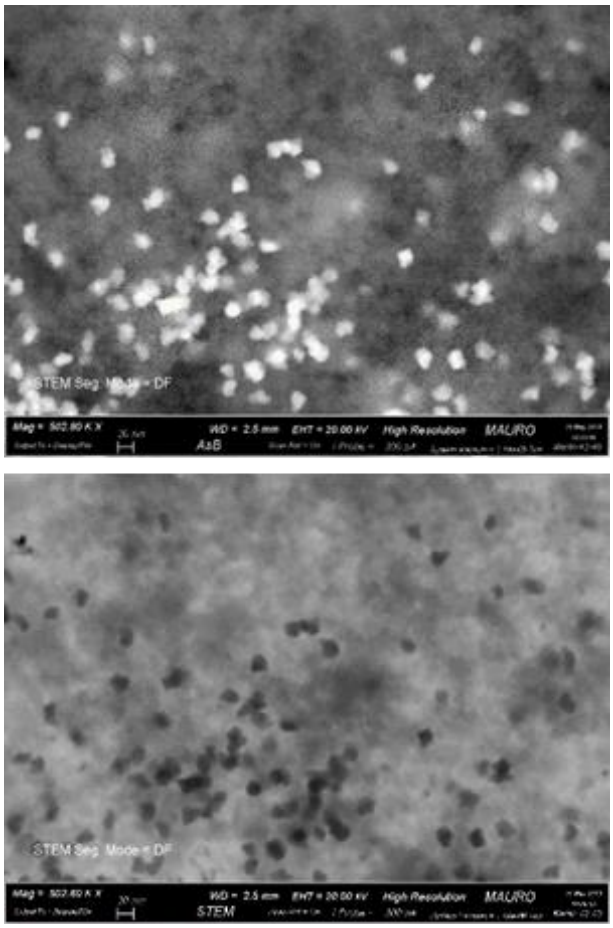

Figure 6. 30: SEM images of MPNPs-Au (second route), method B.

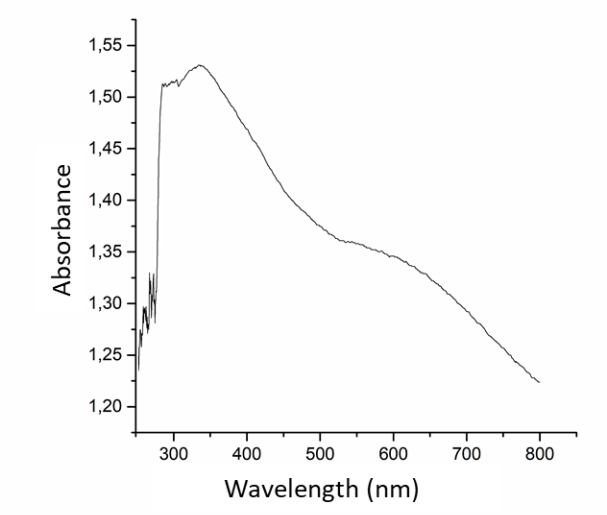

Figure 6. 31: UV-Vis of MPNPs-Au (second route), method B.

In method C, $HAuCl_4$ and bare-SPIONs were firstly mixed together in order to promote the gold salts adhesion on SPIONs surface and then the tannic acid was

added to allow the $HAuCl_4$ reduction and SPIONs stabilization. Analyzing the SEM images (figure 6.32) it is possible to notice only few spots of Au NPs with very heterogeneous dimensions; this is also confirmed by the UV-Vis graph (figure 6.33) which shown a wide absorbing curve instead of a peak, this is probably due to the heterogeneous dimension of NPs.

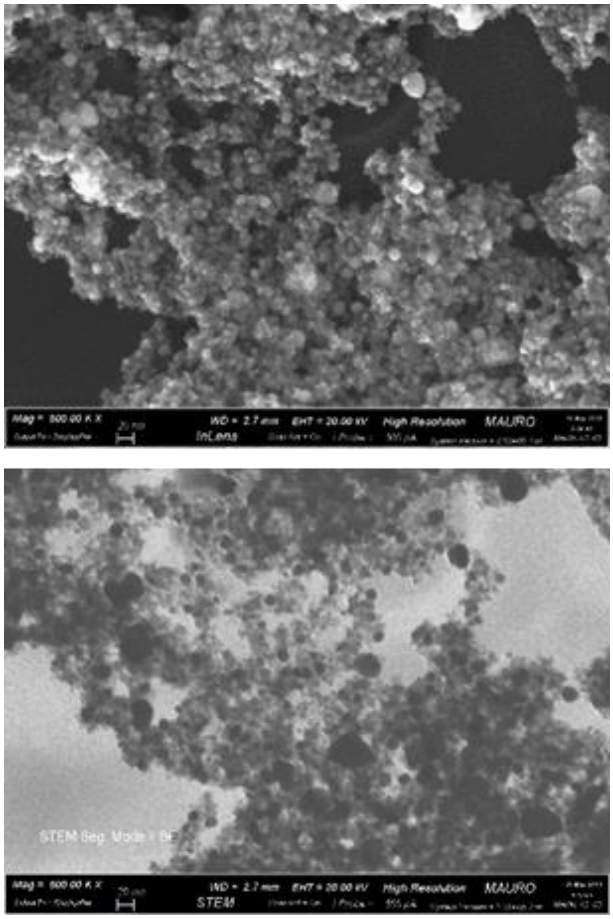

Figure 6. 32: SEM images of MPNPs-Au (second route), method C.

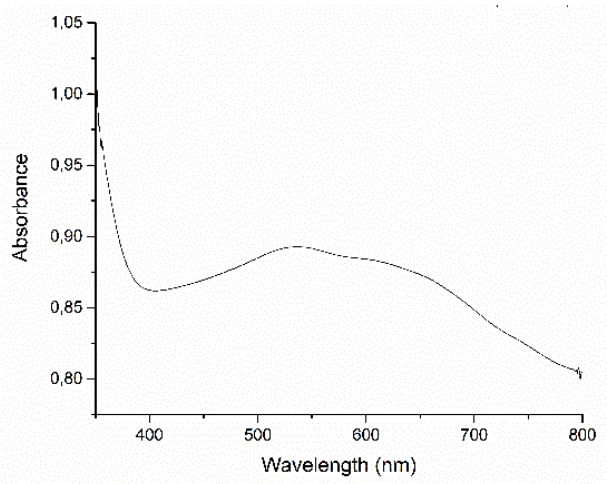

Figure 6. 33: UV-Vis of MPNPs-Au (second route), method C.

Analyzing the SEM images and UV-Vis graph of methods A, B and C, the synthesis selected as model for further studies is the MPNPs-Au (second route) synthetized following the method A. This because the SEM image shows a good distribution of Au NP with a dimensional homogeneity around 20 nm and UV-Vis analysis evidences a strong absorption peak at 620 nm if compared with UV-Vis analysis of method B and C.

Moreover, in order to identify functional groups present in the TA which are responsible for the stabilization and reduction, FT-IR measurement of MPNPs-Au were carried out as shown in figure 6.34. In the image is possible to observe an altered intensity and position of the peaks with respect to the FT-IR of SPIONs-TA (figure 6.26) as indication of the correct reduction of AuNPs. In particular, the shift of the broad peak from 3400 cm^{-1} to lower wavenumber suggest the involvement of OH functional groups as well as the altered intensity of CO groups and C-C aromatic rings which indicate the involvement of TA-SPIONs in immobilization of AuNPs[17]. On this data basis, it could be inferred that the TA remains bound to the MPNPs-Au surface and that the TA phenolic hydroxyls, as suggested from literature[18], may be responsible for the reduction of metal ions. In fact, at mild acidic/ basic conditions, the hydrolysis take place and the dissociation of the binding occur leading to the COO- groups exposure. These gropus, together with the rest of the polymer, can works as surfactant on the MPNPs-Au surface stabilizing them through electrosteric stabilization[18].

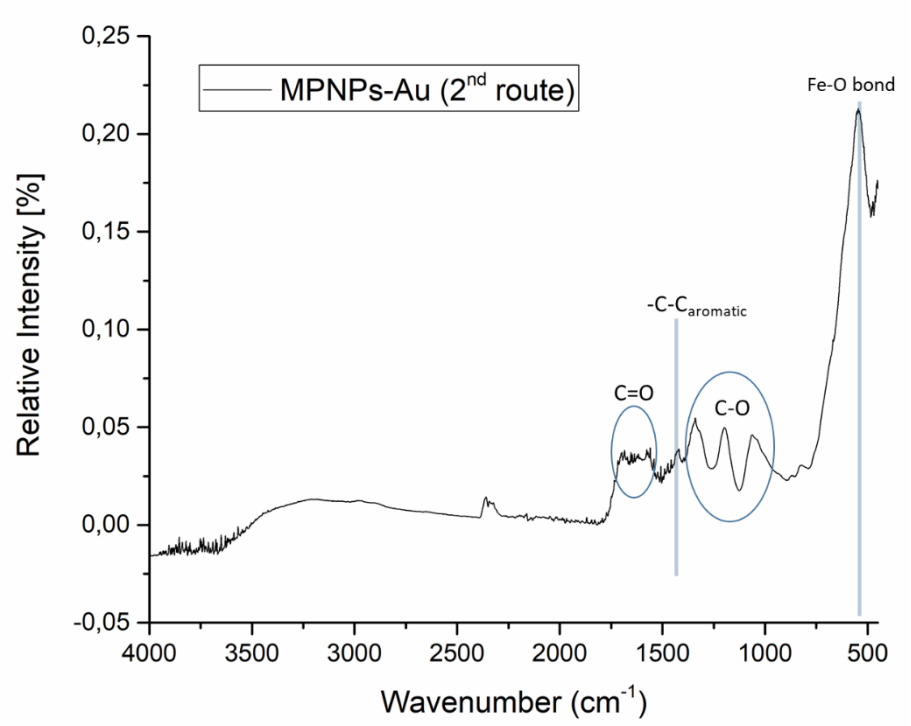

Figure 6. 34: FT-IR spectra of MPNPs-Au (second route)

6.2.3 MPNPs-Ag (second route)

In this paragraph the MPNPs-Ag nanocomposites coming from the second route synthesis are studied. As already performed for previous syntheses, the three methods have been analyzed by using SEM and UV-Vis techniques.

In the method A, the tannic acid and bare-magnetic NPs were firstly mixed together and subsequently the $AgNO_3$ was added to allow the Ag nucleation directly on SPIONs surface. Analyzing the SEM images (figure 6.35), it is possible to appreciate a large number of Ag NPs on the SPIONs surface with a good distribution and with a wide size range (between 20 and 100 nm). The high concentration of Ag NPs remained anchored to SPIONs surface is also confirmed by the UV-Vis analysis showed in figure 6.36. In the graph it is possible to observe a noticeable signal in the Ag NPs absorbing window with an absorbing peak around 430 nm.

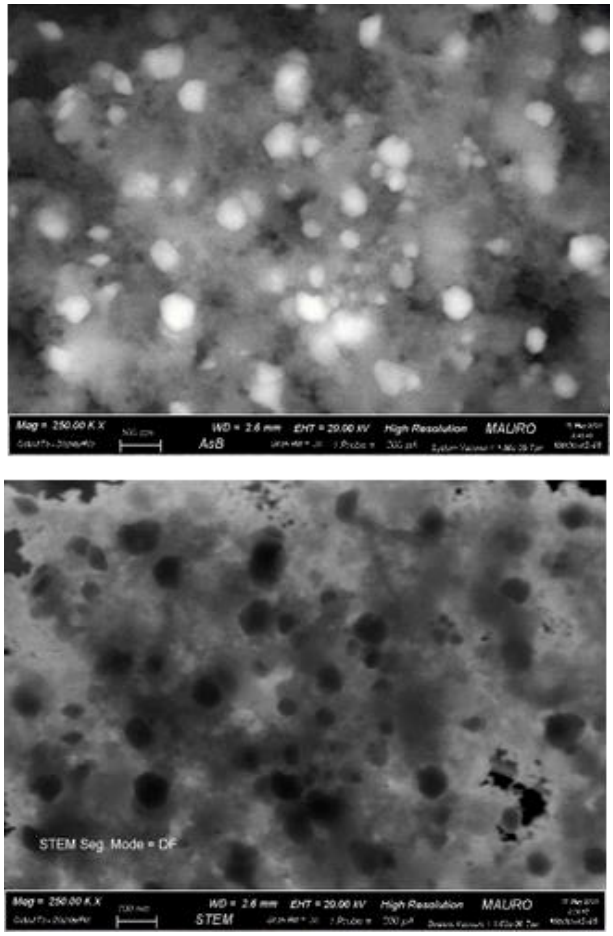

Figure 6. 35: SEM images of MPNPs-Ag (second route), method A. Scale bar: 100nm.

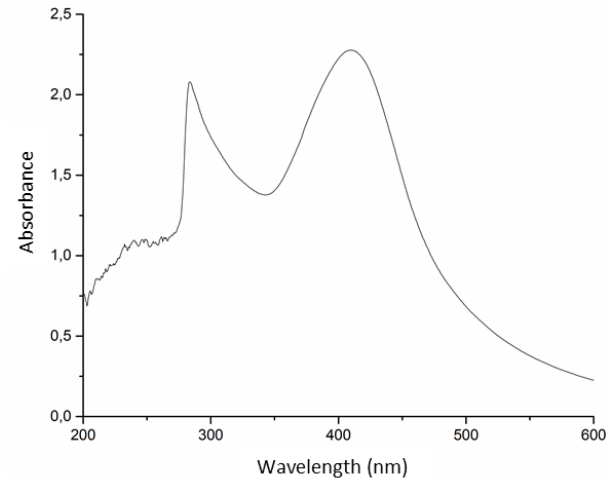

Figure 6. 36: UV-Vis of MPNPs-Ag (second route), method A.

Following the method B, the $AgNO_3$ and tannic acid were firstly mixed together, in order to promote the reduce the silver salts reduction, and subsequently added to the SPIONs solution. The SEM images reporting the morphological aspect of nanocomposites coming from this method is showed in figure 6.37: here a very large spots of Ag NPs with dimensions ranging from 50 nm to over 100 nm are visible. This is also evident from UV-Vis graph (figure 6.38) in which the curve is very wide and does not present a sharp absorption peak.

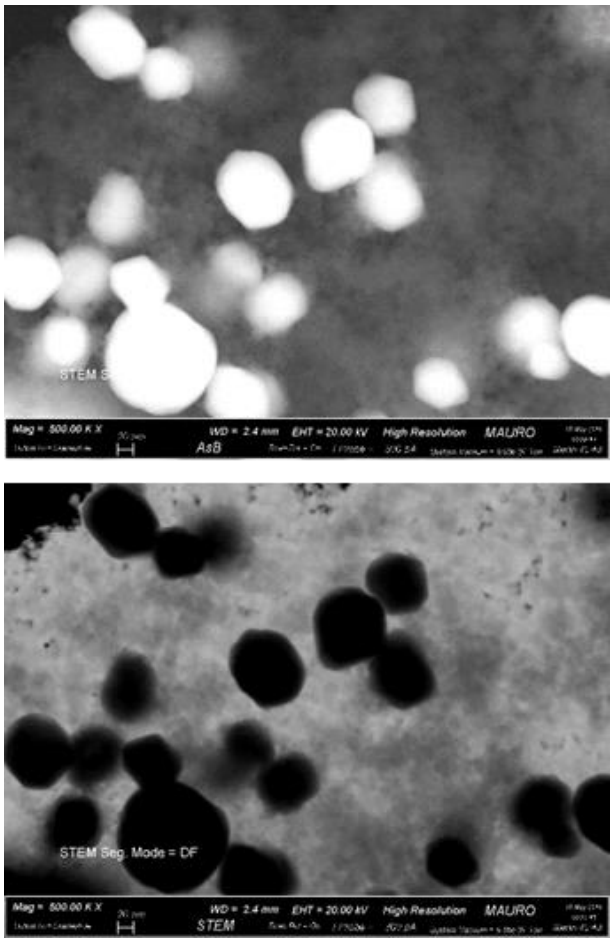

Figure 6. 37: SEM images of MPNPs-Ag (second route), method B.

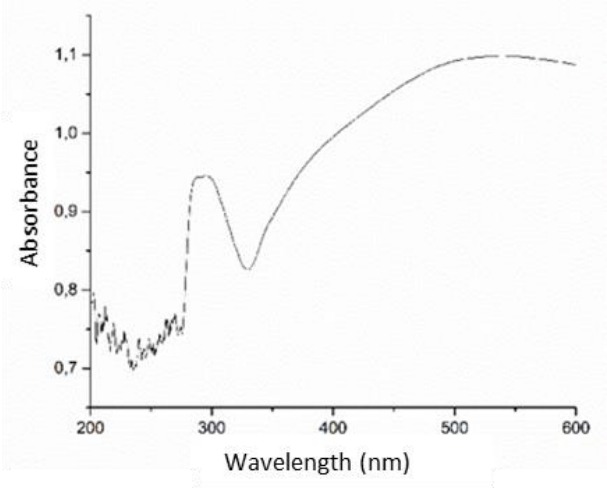

Figure 6. 38: UV-Vis of MPNPs-Ag (second route), method B.

In method C, $AgNO_3$ and bare-SPIONs were firstly mixed together in order to promote the gold salts adhesion on SPIONs surface and then the tannic acid was added to allow the $AgNO_3$ reduction and SPIONs stabilization. With this method, the Ag NPs are generated after the SPIONs surface grafting. Analyzing the SEM images (figure 6.39) numerous Ag NPs with a size range between 10 nm and 100 nm are visible. These heterogeneous dimensions are also confirmed by the UV-Vis graph (figure 6.40) which shows a wide absorbing peak if compared with absorbing peak generated from UV-Vis of method A.

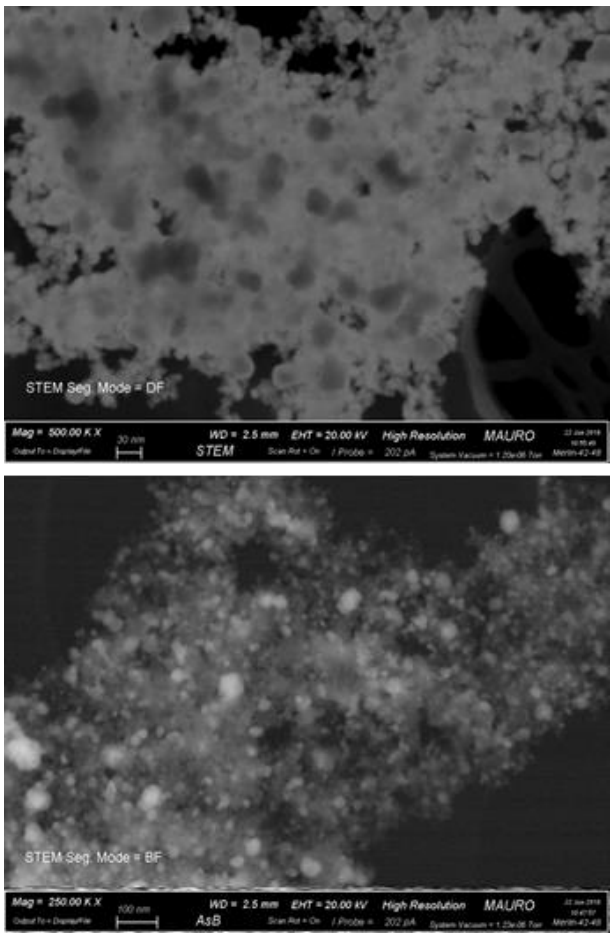

Figure 6. 39: SEM images of MPNPs-Ag (second route), method C.

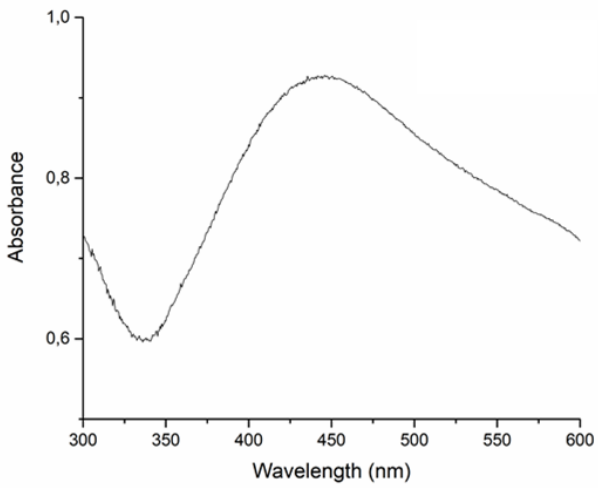

Figure 6. 40: UV-Vis of MPNPs-Ag (second route), method C.

Therefore, based on the SEM images and on the UV-Vis graphs, MPNPs-Ag (second route) synthetized following the method A was chosen as model synthesis and used for further studies presented in the following paragraphs. Moreover, in order to identify the functional groups present in the TA which are responsible for the stabilization and reduction, FT-IR measurement of MPNPs-Ag was carried out as shown in figure 6.41.

As already performed for MPNPs-Au (second route), also in this synthesis the FT-IR measurement of MPNPs-Ag (second route) were carried out in order to identify the TA functional groups responsible for the stabilization and reduction.

In the spectra is noticeable an altered position and intensity of the peaks with respect to the SPIONs-TA spectra (figure 6.26) as indication of the correct reduction of AgNPs. Again is possible to observe the shift of the broad peak from 3400 cm^{-1} to lower wavenumber, the altered intensity of CO groups and C-C aromatic rings which indicate the involvement of TA-SPIONs in immobilization of AgNPs[17] as discussed in previous paragraph. This indicates the correct role of the TA as reducing and stabilizing agent[18].

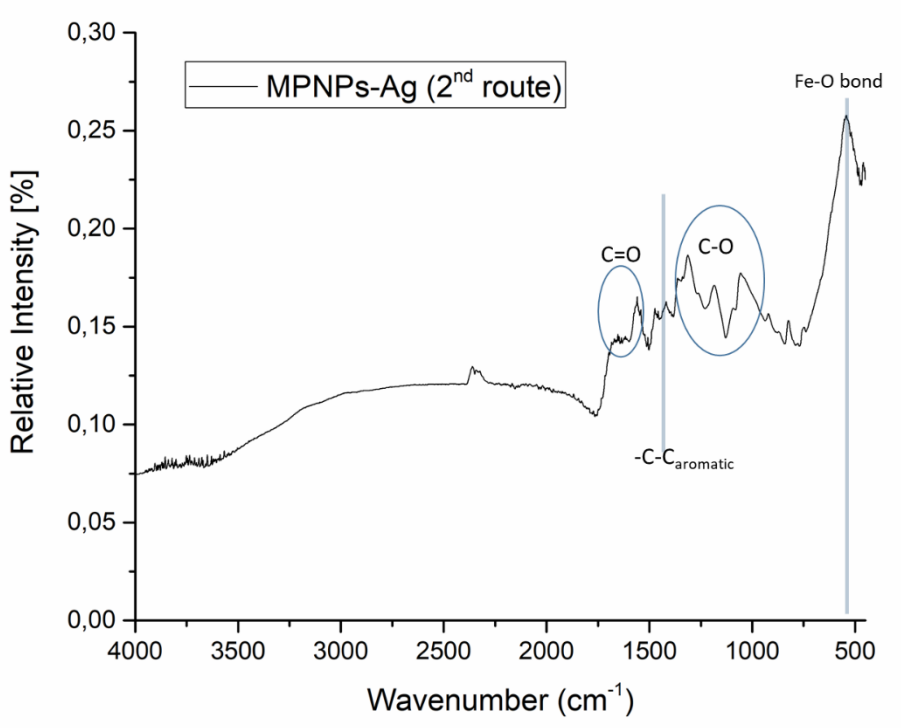

Figure 6. 41: FTIR spectra of MPNPs-Ag (second route)

6.3 Complete Characterization of selected synthesis

In this paragraph the model synthesis selected from first and second routes are analyzed more in depth through further characterization studies. In particular, the TEM images are firstly presented in order to evaluate the shape and the dimension on MPNPs, then the superparamagnetic behaviour and the magnetic saturation of the NPs are presented through the vibrating samples magnetometer graph. Moreover, in order to evaluate the ability of synthetized MPNPs to work as phototherapy system, the effect of the laser irradiation applied on the four different synthesis and the resulting graph are presented. Finally, to evaluate their ability in magnetic hyperthermia application, the graph related at the induction heating system are shown.

TEM images

In figure 6.42, the TEM images related to MPNPs-Au (first route) are shown, here it is possible to attest the Au-NPs round shape and Au-NPs size around 10 nm. As confirmation of SEM and UV-Vis analysis, not huge quantities of Au-NPs is present on SPIONs surface this is probably the cause of the low signal in gold absorbing window.

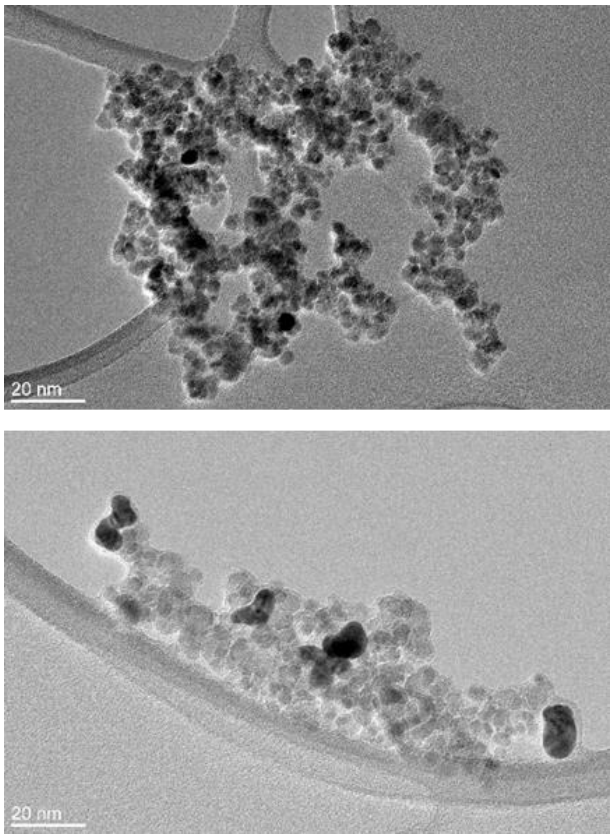

Figure 6. 42: TEM images of MPNPs-Au (first route)

The figure 6.43 shows the aspect of MPNPs-Ag (first route) in which the Ag NPs result to be homogeneous and well-dispersed in the solution. This corroborate the previous obtained results, in which a high concentration of Ag NPs with a dimension between 10 nm and 20 nm was observable, and a high signal in the Ag NPs absorbing window.

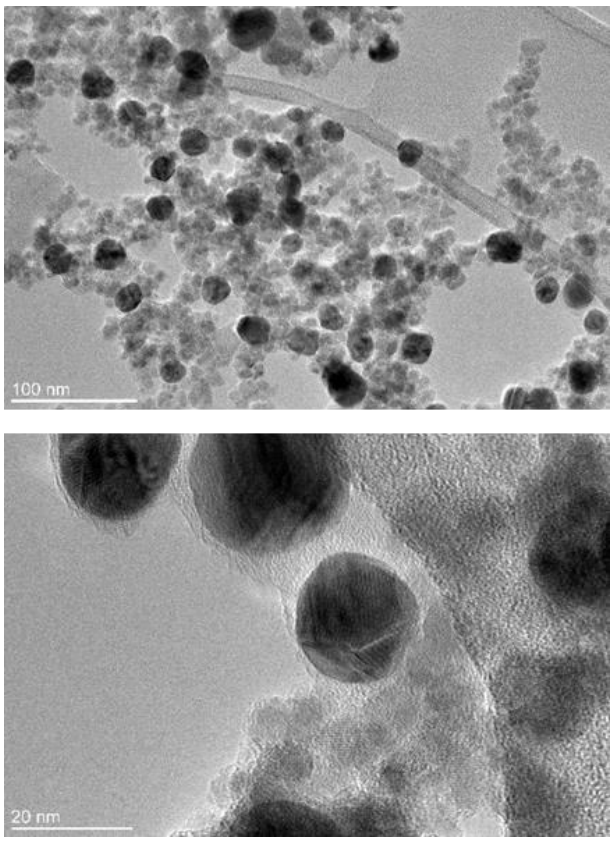

Figure 6. 43: TEM images of MPNPs-Ag (first route)

In figure 6.44 it is underlined the aspect of the MPNPs-Au (second route) solution. The Au NPs, as seen in previous paragraph, result to have a good distribution in the entire sample and a dimensional homogeneity around 10-20 nm, this is probably the reason for which the UV-Vis analysis in figure 6.29 showed a strong absorption peak at 620 nm.

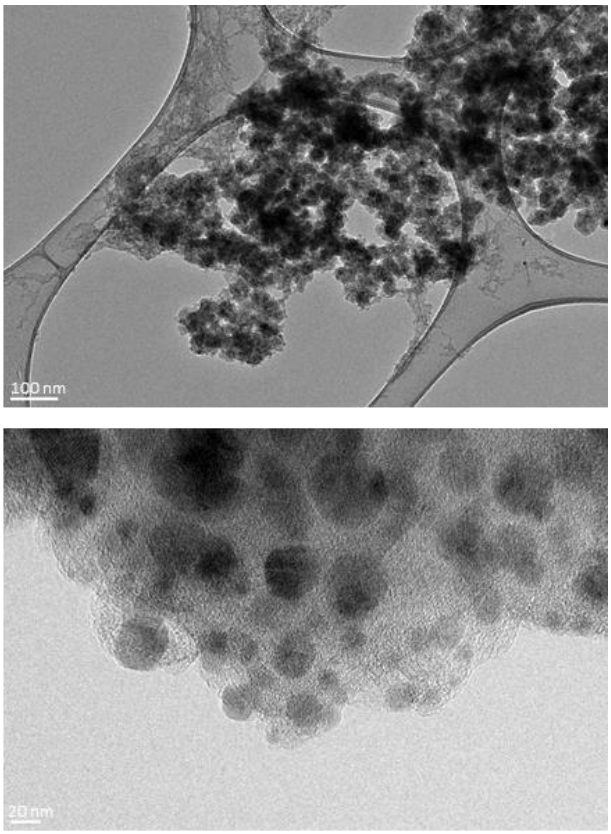

Figure 6. 44: TEM images of MPNPs-Au (second route)

In figure 6.45 it is possible to observe the MPNPs-Ag (second route) solution. In the images it is noticeable that the dimension of Ag NPs has a wide size range (between 20 and 100 nm) confirming the SEM images showed in previous paragraph.

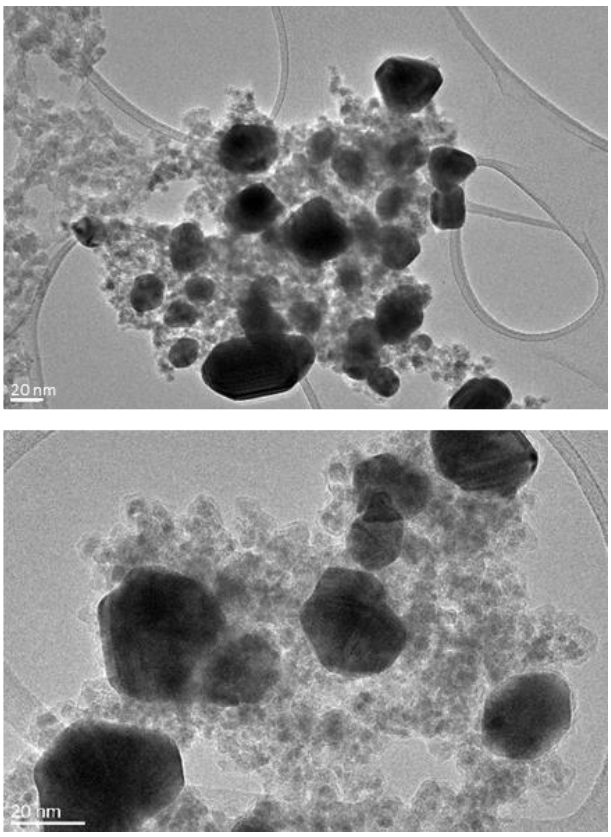

Figure 6. 45: TEM images of MPNPs-Ag (second route)

Vibrating Samples Magnetometer

In order to determine the magnetic properties of the suspensions, as functions of magnetic field, a Vibrating Samples Magnetometer has been used. In figure 6.46 the curves concerning the superparamagnetic behaviour and the magnetic saturation of the four selected synthesis with the addition of CA-capped magnetic NPs (CA-SPIONs), which are essential in order to have information on their magnetic response, are reported. Therefore, being able to manage these nanocomposites using a magnetic field is one of the main reasons for utilizing Fe_3O_4 NPs as support for noble metal nanoparticles. Hence, it is necessary to determine the effect that Au/Ag nanoparticles have on the magnetic properties of pure magnetite nanoparticles.

As it can be observed in the figure 6.46, all the samples exhibit the superparamagnetic behaviour as confirmed by the magnetization versus applied magnetic field characterizations obtained at room temperature. Moreover, looking at the graph, it is noticeable that CA-SPIONs shows higher magnetization in

comparison with the other samples, due to its lack of any external coating that lower these properties; in fact, the decrease in the saturation magnetizations of MPNPs-Ag/Au, could be linkable with the diamagnetic nature of silver and gold NPs anchored on SPIONs surface; moreover, out of the total quantity of particles used, the magnetite will be much lower in the samples in which gold and silver are also present.

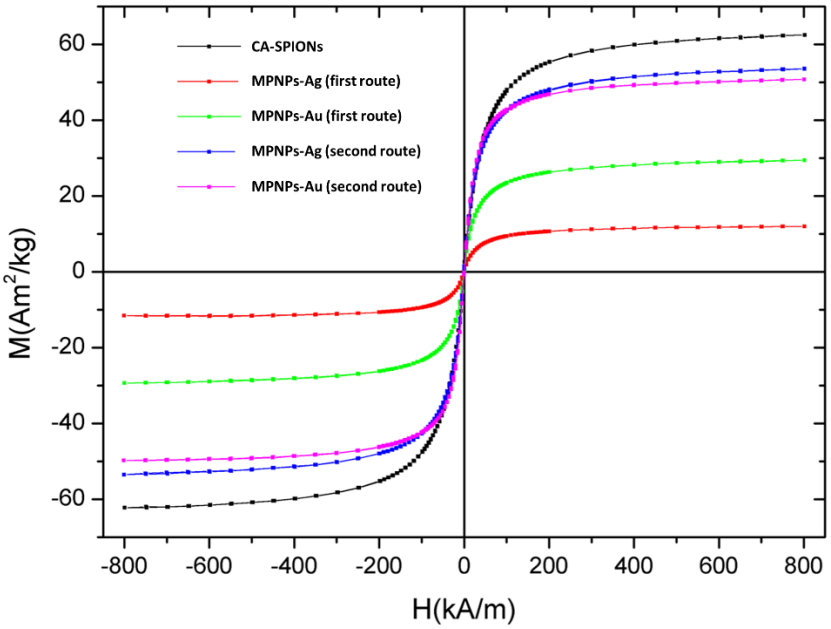

Figure 6. 46: Hysteresis loop of MPNPs-Au / MPNPs-Ag (first and second route) and CA-capped SPIONs at room temperature. The magnetic measurements show no coercivity and remanence at room temperature, suggesting their superparamagnetic behaviour.

Analysing the first and second route, it is possible to notice a difference in saturation magnetization between the MPNPs-Au/Ag synthetized by CA/APTES-SPIONs (first route) and those with only tannic acid (second route): this is probably due to the major amount of reagents that can generate a thick coating around SPIONs, which aggressively shields their magnetic response.

Despite this, all NPs show no hysteresis: the coercive field and remanence magnetization are absent at room temperature, above the blocking temperature for this material[19], this indicates that the metal NPs grafting on SPIONs does not influence excessively the magnetic properties of the precursor. The absence of

hysteresis is characteristic of superparamagnetic behaviour and confirms the nanometric size of SPIONs.

Laser irradiation

This analysis has been performed in order to detect ability of MPNPs to increase their temperature exploiting the SPR effect and to evaluate their ability to be used for photothermal treatment in cancer cells.

The results, expressed in matter of temperature difference, are shown in figure 6.47. The four different syntheses are compared both with CA-capped SPIONs than with water, in order to evaluate the difference between them in terms of ability to generate heat. In particular, it is possible to observe that the presence of noble metal nanoparticles, giving SPR properties to pure magnetite nanoparticles, granted higher heating rate to the nanocomposites. It is appreciable the MPNPs-Au (second route) sample, which is characterized by the highest heating rate among all the solutions: this can be attributed to higher absorption spectra at the characteristic wavelength of the irradiation showed in UV-Vis graph in figure 6.29.

In general, it is possible to notice that for all four syntheses there is an increase in temperature equal to at least 20°C (minimum value recorded for the MPNPs-Au - first route - curve) after 10 minutes of laser irradiation exposition.

Therefore, considering that the physiological temperature in the human body is equal to 37 ° C, each formulation, starting from this value, would potentially be able to cause a temperature rise between 42°C and 45°C in a few minutes and therefore be used for photothermal treatment in cancer cells.

Noticeable is the effect of CA-SPIONs which generates heat after laser irradiation. In fact, it has been shown that SPIONs are able to function as photothermal agents[20], but too high irradiation dose is required for the complete ablation of the tumor. For this reason, it is not one of the best candidates as a photothermal agent.

To be noted that in the results shown by laser irradiation test, no standard deviation values are reported, this limits the possibility to perform statistical analysis evidencing possible difference between the sample under investigation.

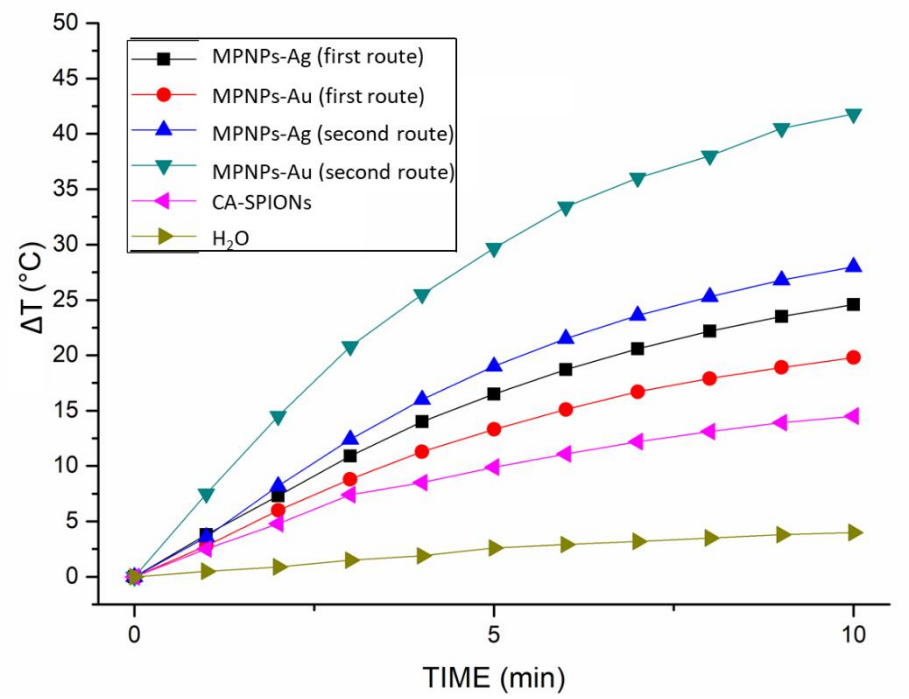

Figure 6. 47: Time-ΔT curve generated by laser irradiation

Induction heating system

Once attested the superparamagnetic behavior, the induction heating system has been used with the aim to evaluate the ability of synthetized NPs to work as therapy system in magnetic hyperthermia application. In particular, the ability of the nanoparticles to function as magnetic hyperthermia therapy system is assessed by measuring the temperature they produce in a period of time of 20 minutes. The results concerning the heat generation measured in the water in which the NPs are dispersed, are presented in figure 6.48, in which it is reported the time versus ΔT(C°).

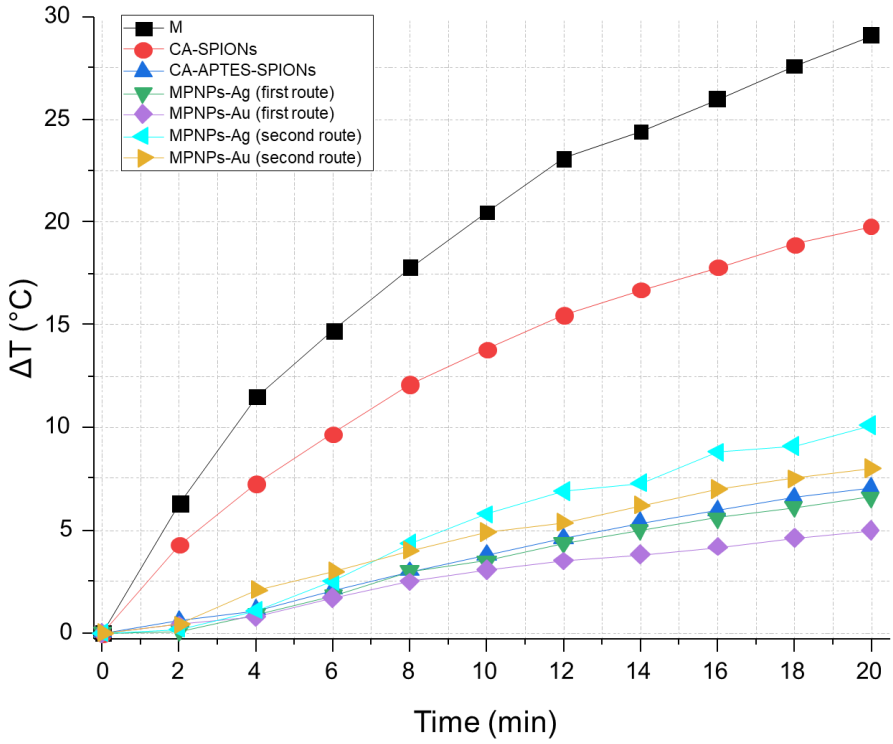

Figure 6. 48: Time-ΔT curve generated by induction heating system

In particular, it is possible to notice that bare-SPIONs (followed by CA-capped SPIONs) produce a significantly higher heating than all other formulations that have undergone stabilization, functionalization and decoration with silver or gold, which present a lower but very similar increase in temperature. The big difference lies in the fact that the concentration used is the same for all the samples, this means that out of the total quantity, the magnetite will be much lower in the samples in which gold and silver are also present. In fact, the concentration of NPs used for this analysis (1 mg/ml) was obtained from the whole sample (SPIONs + metal NPs) and therefore the exact amount of magnetite is not known. Furthermore, the functionalization carried out to obtain the MPNPs-Ag/Au involve the formation of superficial layers that surround the magnetite unit, worsening its ability to generate heat. In fact, is visible from the graph that the CA-APTES-SPIONs (blue curve) shows a very low heating with respect to the bare-SPIONs or CA-SPIONs, this means the presence of APTES strongly influence the heating rate of SPIONs.

Despite this, it is important to note that for hyperthermia treatments it is necessary to reach around 42°C - 45°C, this means that starting from a body temperature of about 37°C, at least 5°C more are required in order to observe some results. From the resulting graph it is noticeable that in 20 minutes, the samples prepared through the first route (with CA stabilization and APTES functionalization) barely reach the desired temperature (probably due to the major amount of reagents present on SPIONs surface), while the samples prepared through the second routes reach 10°C more in 20 minutes.

Observing the complete characterization of four produced syntheses, it is possible to analyze which one gives the best results in terms of SPR effect, size and dimension and ability to produce heat. In particular, in figure 6.49 the main characteristics of the syntheses are summarized.

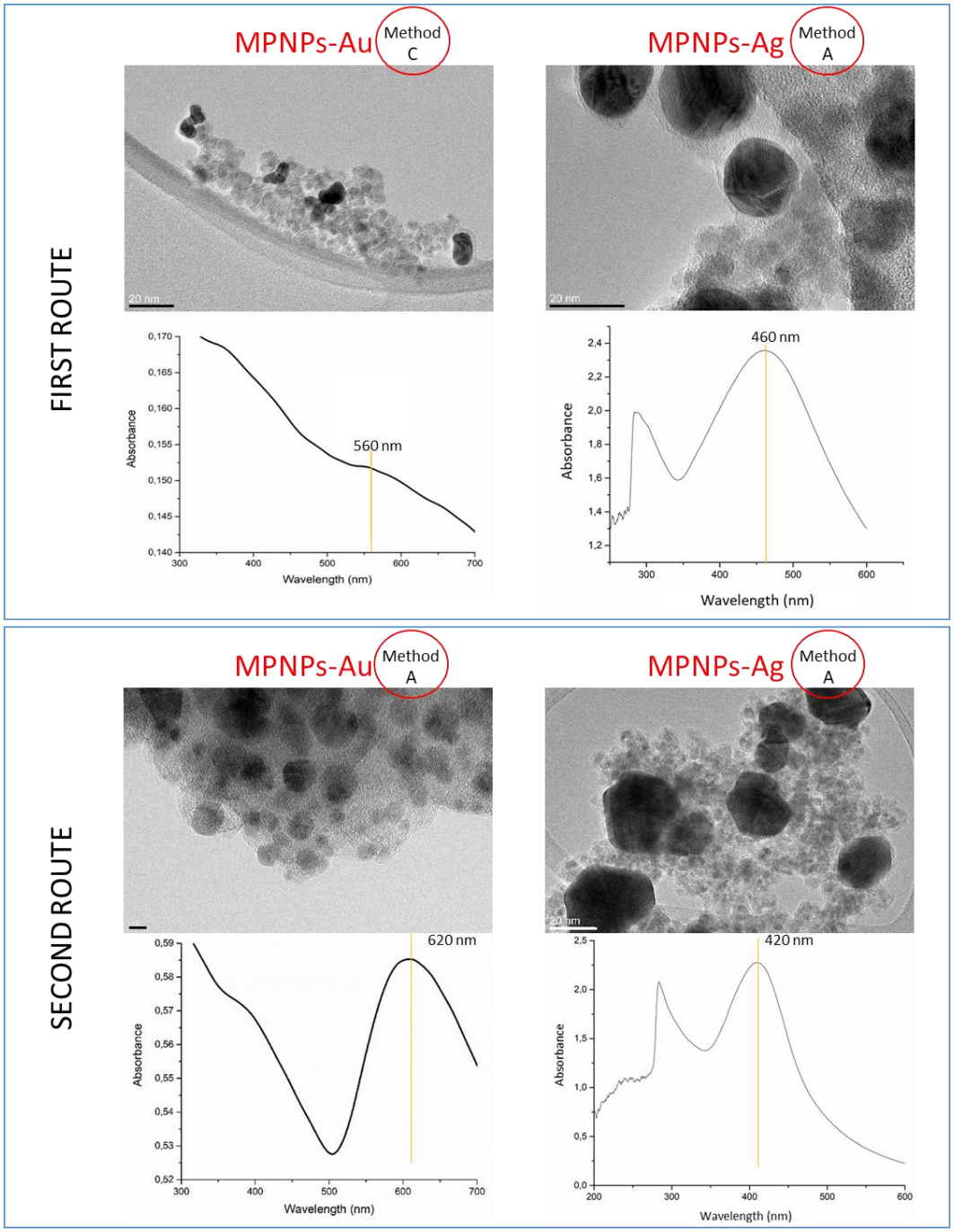

Figure 6. 49: main properties of the four selected syntheses. Scale bar for all figure is 20 nm.

Comparing the MPNPs-Au from first and second route, is noticeable that Au nanoparticles are correctly located on SPIONs surface and are characterized by uniform growth of metal nanoparticles in both syntheses with a range of dimension approximately between 20-40 nm. However, it is evident from TEM image -first

route-, that much lower amount of Au NPs are anchored on SPIONs with respect to the Au NPs from TEM image -second route-, this is also confirmed by the UV-Vis graph which shows a very high gold absorbing peak in case of MPNPs-Au synthetized from second route, while is quite low in the other one. Moreover, looking at hysteresis loop (figure 6.46), even if both NPs show no hysteresis, the MPNPs-Au from first route reduce the saturation magnetizations decreasing the nanocomposites magnetic response. This could be due to the presence of CA and APTES that influence the magnetic properties of the SPIONs, in fact, this influence is also confirmed by the heating curves generated by induction heating system: is evidenced a lower heating in the case of synthesis produced by the first way, while it turns out to be greater in the case of synthesis with only tannic acid (second route).

Another important difference between the two syntheses is evident in time-ΔT curve generated by the laser irradiation: the heating rate of the MPNPs-Au produced through second route is much higher than the ones generated through the first route; this is a very important parameter for applying the photothermal therapy.

By observing the MPNPs-Ag instead, it is evident for both syntheses, that a large number of Ag NPs are anchored on the SPIONs surface with a good distribution; the NPs size exceeds 20 nm, even reaching 100 nm in the second synthesis route. The high concentration of Ag NPs is also confirmed by the optical characterization, which show a high absorbing peak in both UV-Vis analyses. Furthermore, as already mentioned for MPNPs-Au, also the MPNPs-Ag show a lower magnetic response when CA-APTES functionalization is used. Regarding the time-ΔT curve generated by the laser irradiation instead, there are no obvious difference between the curves generated by the MPNPs-Ag of the first or second route which result to be very similar.

In general, it is possible to affirm that among the four syntheses used, the one that shows the best results in terms of physical, magnetic and optical characterization, is the MPNPs-Au synthesized using tannic acid as a reducing and stabilizing agent.

These results confirm that the synthesis optimization using tannic acid as a reducing and stabilizing agent has been successful: MPNPs-Au/Ag have been prepared by means of an innovative synthesis process using an ecofriendly agent with reducing and stabilizing ability[21] and with natural antioxidant, antimicrobial and antitumoral properties[19,22,23]. For this reason, further optimization with

Toluidine Blue (introduced in chapter 5.1.3) was applied to the synthesis MPNPs-Au synthetized by second route in order to enhance the gold absorbing peak. In fact, to increase the chances of success of the photothermal therapy, in addition to irradiating in the near infrared to ensure that the radiation penetrates deeply, it is preferable that the incident wave frequency is superimposed as the much as possible to the nanoparticles spectrum, so that the light absorption by the plasmonic unit is greater.

In figure 6.50 the normalized UV-Vis analyses of the diluted-MPNPs-Au before the TB addition, after the addition and after the washing step performed to remove all the unreacted compounds are presented.

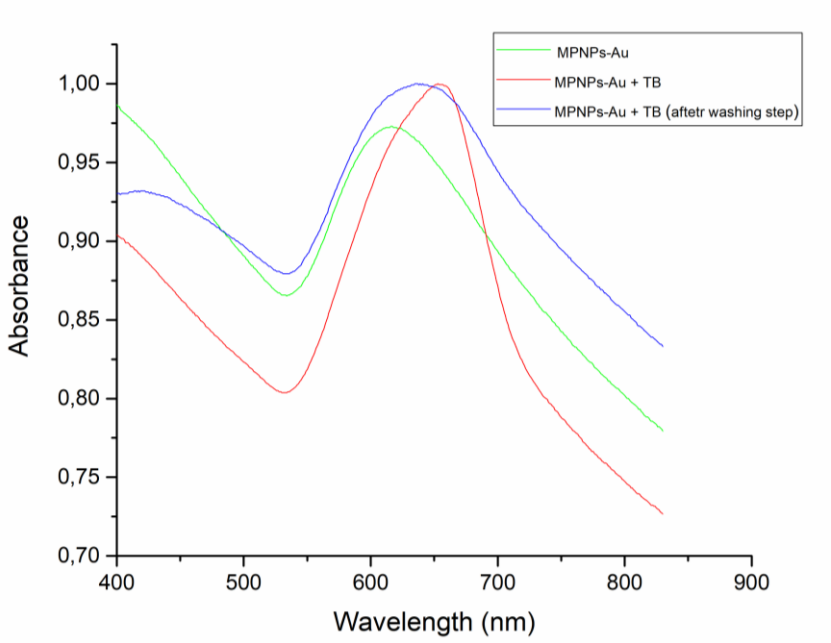

Figure 6. 50: UV-Vis analyses of the diluted-MPNPs-Au before the TB addition, after the addition and after the washing step

From the image, it is noticeable that the absorption peak shifts from a starting value of about 620 nm to 660 nm in the case of the solution in which the nanoparticles are at contact with toluidine blue. The final spectrum obtained after the washing step instead shows a peak at about 640 nm.

Therefore, the change persists even after the washing step. As suggested in the literature[24], the displacement of the peak could be due to the aggregation of the gold nanoparticles following the addition of the dye.

6.4 In vitro cytotoxicity evaluation

6.4.1 Hemotoxicological Analysis

The hemotoxicological properties were detected in order to evaluate the toxicological effect of the nanocomposites in contact with red blood cells (RBCs). The results concerning the RBCs hemolysis after incubation with 35 and 100 µg/mL concentration of MPNPs-Au/Ag synthetized by first and second routes, are shown in table 6.2.

Table 6. 2 Hemotoxicity Results

	SAMPLE	HEMOLYSIS (%)
First Route	MPNPs-Au (35 µg/mL)	1.9
	MPNPs-Au (100 µg/mL)	2.1
	MPNPs-Ag (35 µg/mL)	2.3
	MPNPs-Ag (100 µg/mL)	5.4
Second Route	MPNPs-Au (35 µg/mL)	5.5
	MPNPs-Au (100 µg/mL)	3.7
	MPNPs-Ag (35 µg/mL)	3.9
	MPNPs-Ag (100 µg/mL)	2.6
	Negative Control	2.8
	HBS Buffer	0
	Positive Control	100

.

From hemotoxicity results, it is possible to notice that after one day of incubation, the nanoparticles showed minimal hemotoxicity, comparable to that of the negative control sample. In fact, for each sample of RBC is founded that the hemolysis is very low (lower than 5.4% for all the samples), this means that the NPs toxicity at these concentrations is negligible and therefore they are potentially usable for biomedical applications[25,26]. In results shown by hemotoxicity test, no standard deviation values are reported, this limits the possibility to perform

statistical analysis evidencing possible difference between the sample under investigation.

6.4.2 Cytocompatibility on healthy and cancer cells

In order to test the cytotoxicity of NPs, human primary fibroblasts (HGF) and human skin-derived melanoma cells (A2058, CRL-11147 from ATCC) were selected as representative for physiological and pathogenic conditions, respectively. To test whether the NPs hold a selective target activity, cells were seeded at a defined number ($2x10^4$ cells/well) into multiwell plates and allowed to adhere and spread for 24 hs in the incubator (37°C, 5% CO_2). The day after, cells have been exposed to different concentration of MPNPs for 6 and 24 hours and the results are summarized in Figure 6.51 and Figure 6.52, respectively.

Looking at the HGF results, the toxic effect resulted as related to both the NPs concentration and the direct-exposure time. In fact, after 6 hs direct contact (Fig 6.51, left column), cells viability resulted as >60% for all the tested composition with the only exception of the MPNPs-Ag (first route) 100 μg/ml. After 24 hs of direct contact, a general decrease in cells viability was observed for all the tested NPs, thus suggesting that the contact-time can be a factor in influencing cells behavior (Fig 6.51, right column). Likewise to the results obtained after 6 hs, a further worsening was observed when NPs concentrations was improved: in fact, the 100 μg/ml resulted as the most toxic condition with particular emphasis for the MPNPs-Ag (first route) and MPNPs-Ag (second route). Images from light microscopy (Fig. 6.53) offer a possible explanation of such time and dose-dependent toxic effect: in fact, a massive debridement of single NPs as well as the formation of numerous aggregates was noticed for the 100 μg/ml concentration in comparison with the 25 and 50 μg/ml ones. Therefore, it can be speculated that the HGF cells were sensitive to the NPs aggregates impairing nutrients uptake and oxygen distribution thus resulting toxic for cells metabolism. Moreover, the Ag-doped NPs reported a higher toxicity in comparison to the Au-doped ones applied

in the same conditions and concentrations; therefore, HGF cells demonstrated to be more prone in tolerating gold rather than silver which can be an interesting result for the future application of the laser-induced phototherapy for biomedical purposes.

Moving to the melanoma A2058 cells results (Fig. 6.52), it was noticed that those kinds of cells were much more resistant to the NPs in comparison with the HGF. In fact, none of the metabolic results were >90% in comparison with untreated control at both the tested time-points and by applying all the concentrations. However, light microscopy images (Fig. 6.54) showed again the presence of dispersed particles and aggregates within the wells containing cells (a typical phenomenon of tumor cells grown in vitro is that they do not grow as single cells but tend to aggregate and form clusters); therefore, despite a similar trend in NPs deposition, melanoma cells demonstrated a higher intrinsic ability to well tolerate the presence and the effects due to the NPs in respect to the HGF ones. Of course, these results can be ascribed to the higher ability of the tumorigenic cells to skip toxic effects due to the lack of apoptotic check points that are still presents in the HGF cells that are non-tumorigenic nor immortalized cells. However, the possibility to exploit in the future the laser-induced phototherapy by the NPs response, open for the possibility to compare such results with the effects coming from the photo-activation.

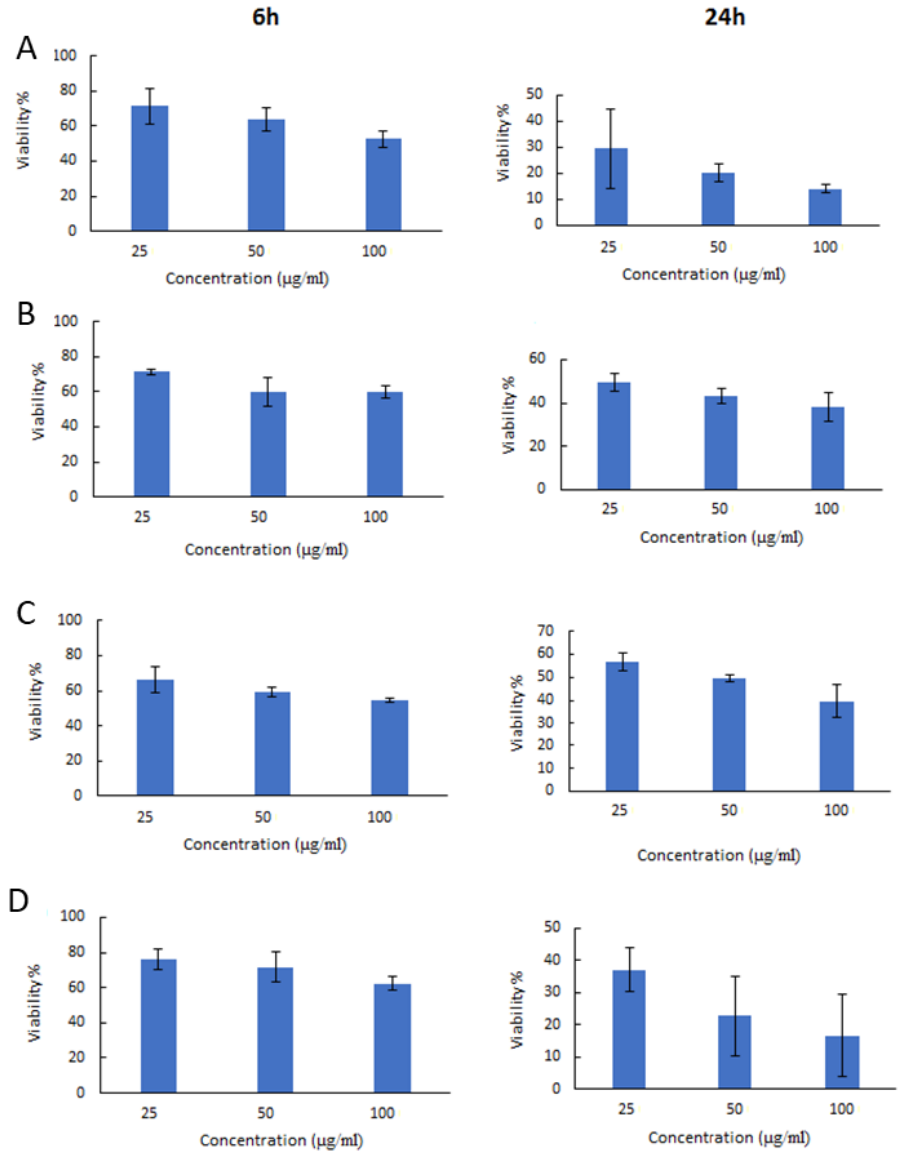

Figure 6. 51: Cytotoxicity test towards HGF cell. A) MPNPs-Ag (first route) B) MPNPs-Au (first route); C) MPNPs-Au (second route); D) MPNPs-Ag (second route).

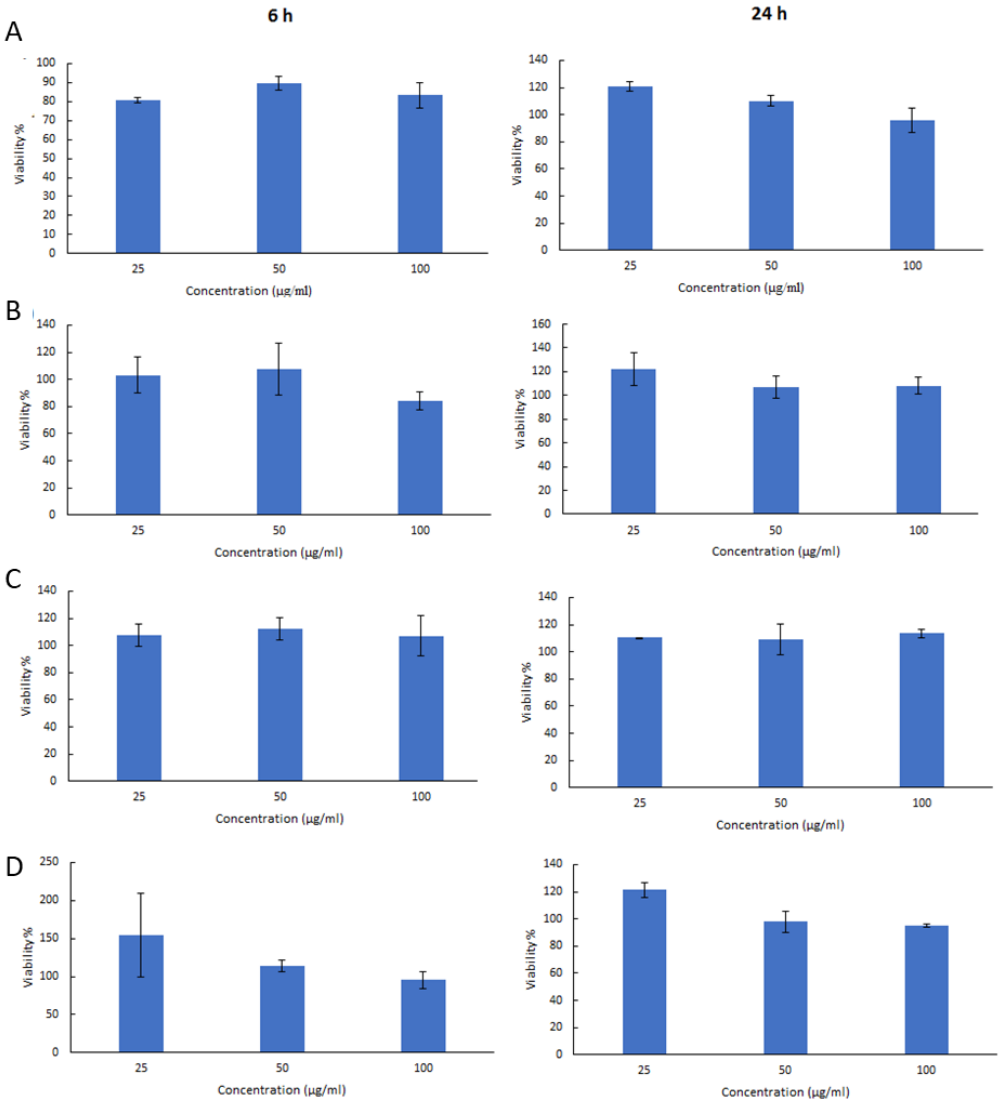

Figure 6. 52: Cytotoxicity test towards A2058 cell. A) MPNPs-Ag (first route) B) MPNPs-Au (first route); C) MPNPs-Au (second route); D) MPNPs-Ag (second route).

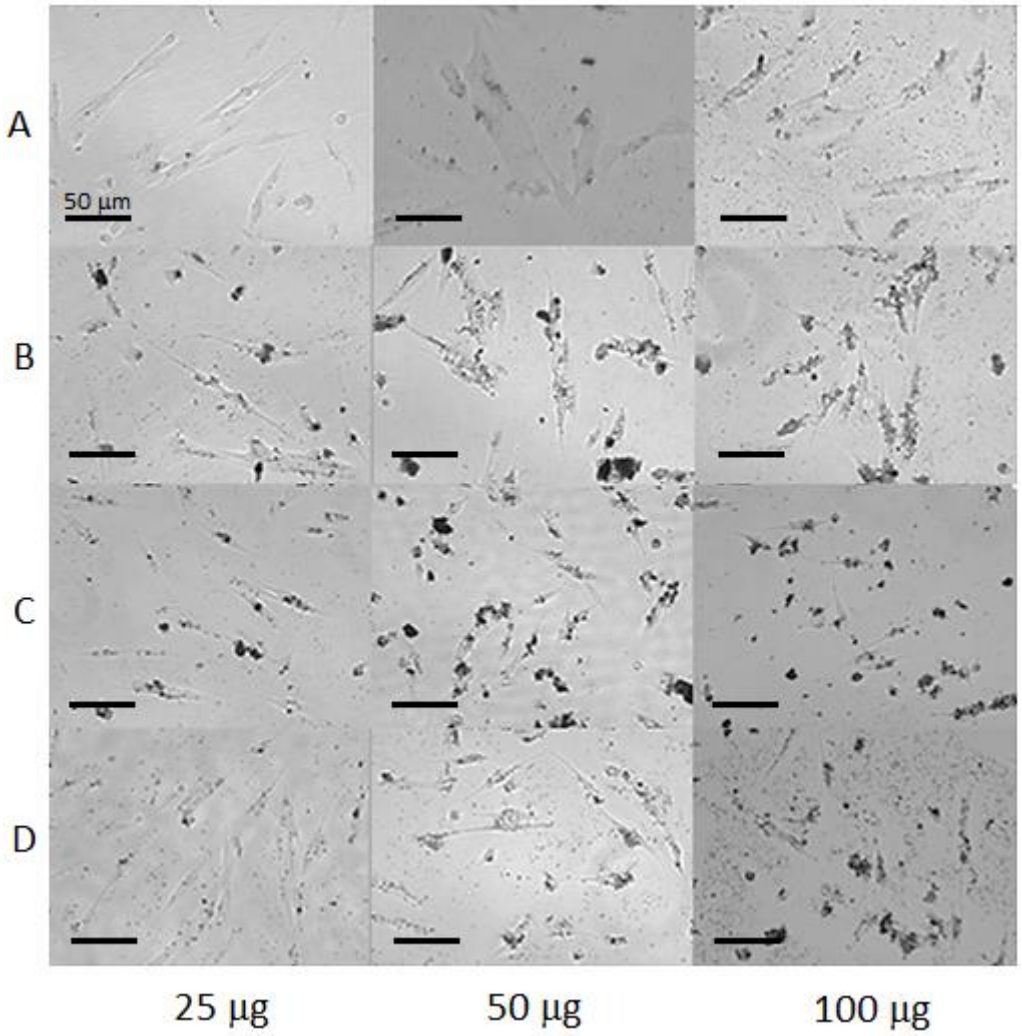

Figure 6. 53: NPs internalization onto HGF cell after 24 hs direct contact. A) MPNPs-Ag (first route) B) MPNPs-Au (first route); C) MPNPs-Au (second route); D) MPNPs-Ag (second route).

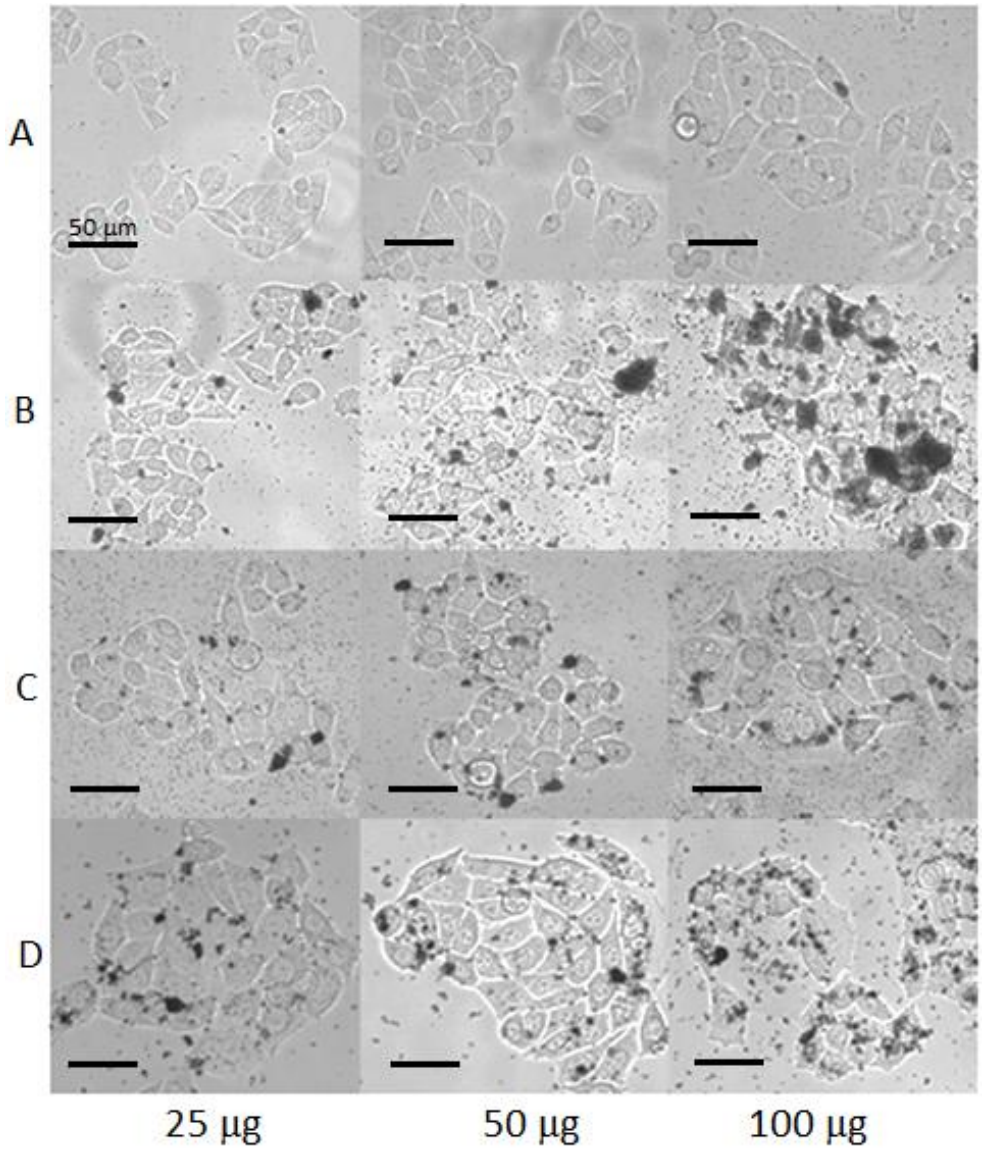

Figure 6. 54: NPs internalization onto A2058 cell after 24 hs direct contact. A) MPNPs-Ag (first route) B) MPNPs-Au (first route); C) MPNPs-Au (second route); D) MPNPs-Ag (second route).

6.5 Laser induced phototherapy

In this paragraph the results concerning the laser induced phototherapy are discussed. This will be useful to understand if the NPs are able to be used as tool for photothermal therapy by converting the received light into thermal energy and to establish the MPNPs' ability to induce apoptosis in cancer cells without affecting the viability of healthy ones when irradiated with laser source. Accordingly, a

comparison between the intrinsic toxicity of the NPs and the light-activated ones will be useful to understand whether the photo-activation can be useful in improving the NPs activity towards tumorigenic cells. The NPs used are MPNPs-Au coming from the first synthesis route because before performing the synthesis optimization using the TA as reducing and stabilizing agent, preliminary studies were conducted in order to have information on their ability to produce heating through laser irradiation in direct contact with cells.

The first analysis is achieved by using the fluorescence microscope in which the resulting images give information about the cellular status. In fact, thanks to the different staining used, it is possible to understand whether cells are damaged or not. Three different concentrations of MPNPs-Au (5, 25 and 50 μg/ml) were tested, both on HGF and HO-1-N-1 cells, in order to evaluate the difference between them in terms of viability. Figure 6.55 shows the images depicting which cells are exposed to the different MPNP concentrations and then irradiated for five minutes with a laser light. The control, without any nanoparticle exposure, is shown as well. It is easy to see that any important damage occurs when cells are treated with 5 and 25 μg/ml, both HGF and HO-1-N-1 cells and both when laser irradiation is applied or not. On the contrary, when 50 μg/ml of NPs concentration is used, it is possible to see that only HO-1-N-1 cells undergo apoptosis. This happens only when the laser irradiation is applied; it is clear that the same MNNP-Au concentration is not having any detrimental effect if the sample is not irradiated.

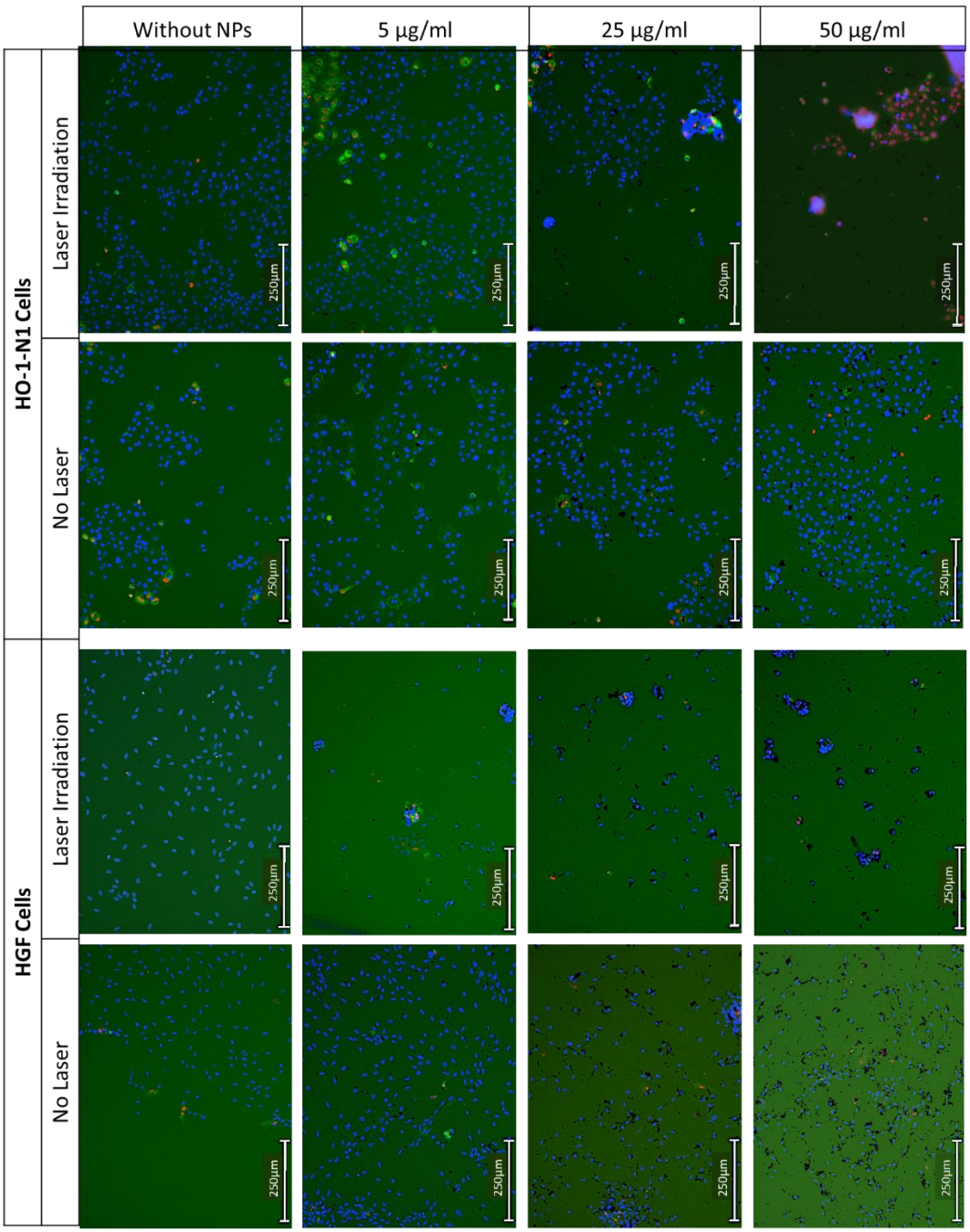

Figure 6. 55: Fluorescence microscope images of HGF cells and HO-1-N1 exposed to different NPs concentration. The test shows the difference between cells exposed to MPNPs and irradiated with laser light and the cells exposed to MPNPs without irradiation. Staining used: Red: PI; Blue: Hoechst; Green: Annexin. Scale bar: 250 µm

The second analysis performed is the WST assay, which indicates the number of viable cells that can be quantified by measuring the absorbance given from their metabolic activity. For this test only the MPNP concentration of 5 and 50 µg/ml were tested. In figure 6.56 B, WST assay on HO-1-N1 cells shows an important

decrease of intensity by raising the concentrations of MPNPs-Au, mostly when the cells are exposed to five minutes of laser irradiation (in red), which means that cell viability is negatively affected by the contact with MPNPs-Au, which is clearly amplified by laser irradiation. On the contrary, figure 6.56 A related to HGF cells, shows only a slight decrease in cell viability for MPNP-Au concentration of up to 50 μg/ml, both when they are irradiated or not irradiated. This result is relevant for the hypothesis that a synergistic effect of MPNPs-Au and irradiation can be selective on tumouriogenic cells, while preserving physiological cell viability.

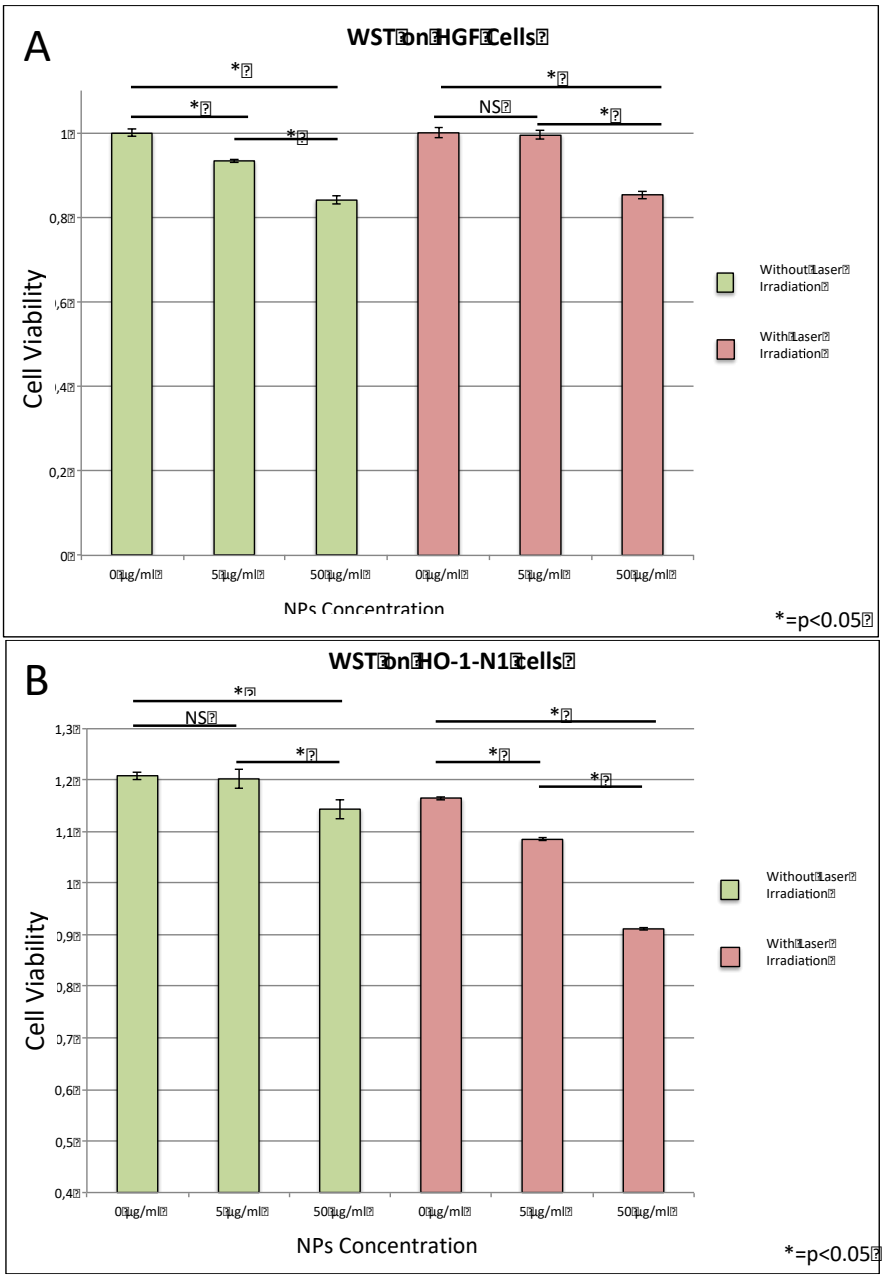

*Figure 6. 56: WST assay of HGF cells (A) and HO-1-N1 (B) exposed to 0, 5 and 50 µg/ml of MPNPs. The red columns are related to the samples irradiated with 5 minutes' laser light. p-values (Student's t-test) indicated above bars; NS: non-significant; *: significant for p<0.05.*

In figure 6.57 and 6.58 the Raman spectra registered on HGF and HO-1-N-1 cell lines are reported respectively. For this test the concentration of 50 µg/ml was used, since the WST assay and fluorescence microscope indicated that at this concentration the best performance has been achieved. The graphs report (in green) the spectra acquired from cells not exposed to laser irradiation, while the spectra acquired after five minutes of continuous laser irradiation has been applied is shown

in red. In a Raman shift, when the laser beam hits a cell, chemicals within the cell can absorb and reflect or scatter the light waves. This scattering generates a marker at various wavelengths that can be used to identify specific molecules, which depends on the molecule type and the chemical bonds present within its structure[27].

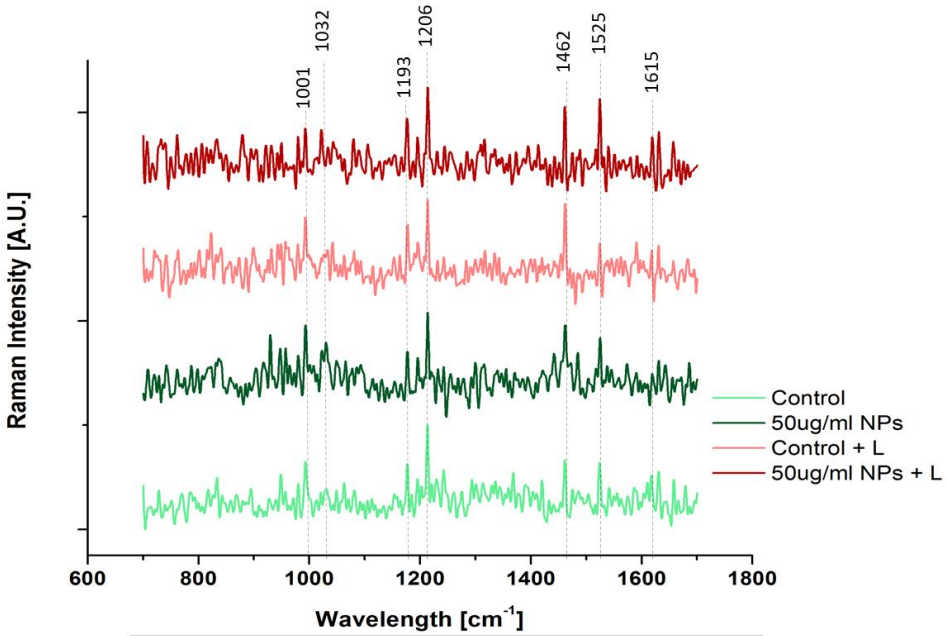

1001 cm^{-1}	Symmetric ring breathing mode of Phenylalanine, C-C skeletal stretch.
1032 cm^{-1}	CH_3 CH_2 bending modes of collagen and phospholipids, phenylalanine of collagen, proline
1193 cm^{-1}	Ring stretch, in-plane CH bend, CH2 twist
1206 cm^{-1}	Hydroxyproline, tyrosine (collagen assignment)
1462 cm^{-1}	CH2 bending mode of proteins and lipids
1525 cm^{-1}	Carotenoids
1615 cm^{-1}	Tyrosine, tryptopan, C=C (protein)

Figure 6. 57: Raman spectra of HGF cells with corresponding peaks.

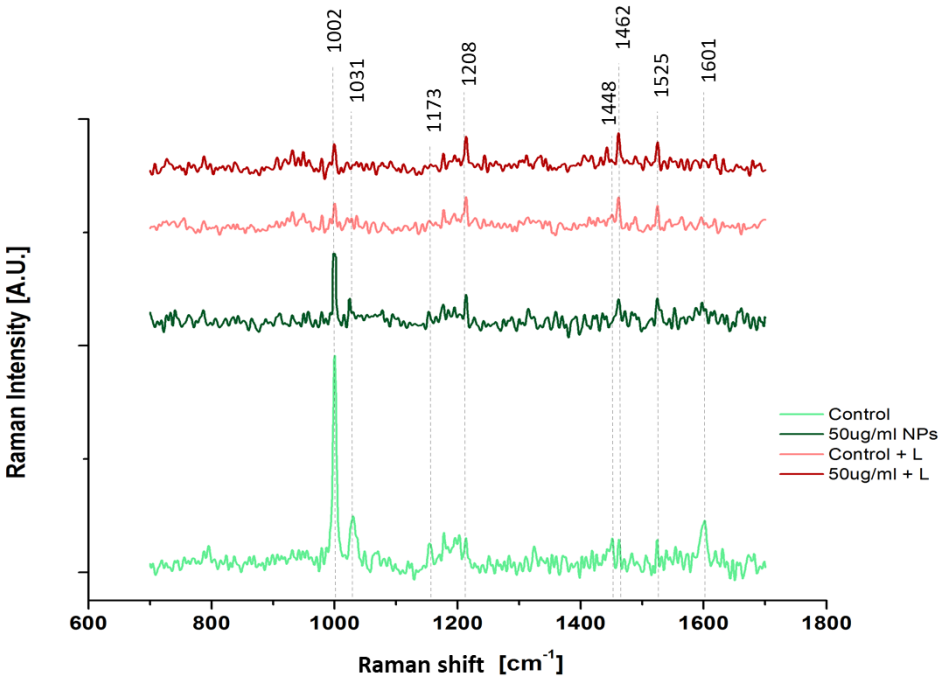

1002 cm^{-1}	Symmetric ring breathing mode of Phenylalanine, C-C skeletal stretch.
1031 cm^{-1}	CH_3 CH_2 bending modes of collagen and phospholipids, phenylalanine of collagen, proline. C-H in-plane banding mode of phenylalanine C-H stretching of protein.
1173 cm^{-1}	Cytosine, guanine, Tyrosine (collagen type I)
1208 cm^{-1}	Tryptophan, phenylalanine (protein assignment)
1448 cm^{-1}	CH_2 CH_3bending mode in malignant tissue
1462 cm^{-1}	CH2 bending mode of proteins and lipids
1525 cm^{-1}	Carotenoids
1601 cm^{-1}	Tyrosine, phenylalanine ring vibration (proteins)

Figure 6. 58: Raman spectra of HO-1-N1 cells with corresponding peaks

As regard the HGF cells (Figure 6.57), there aren't important differences between four spectra, it seems that NPs and laser doesn't have any important effect on cells. The presence of carotenoid (1525 cm^{-1}) in all spectra of healthy cells means that inflammatory pathway is occurring. Regarding HO-1-N1 cells instead (figure 6.58), the major difference among the four spectra is that the phenylalanine level (peak at 1002 cm^{-1}), an important indicator of cellular vitality[28], is really high in the cells not exposed to the laser (with a slight decrease in the case of exposition to MPNPs-Au, as already observed in the WST assay) and become lower when laser irradiation is applied, both with and without exposition to MPNPs-Au. This test reveals that irradiation could cause metabolic alterations to HO-1-N1 cells but the

synergistic effect of MPNPs-Au and irradiation is more difficult to show with this test. Other information regarding the alteration of cellular condition is given from the peaks at 1031 cm^{-1} and 1601 cm^{-1} (again referring to phenylalanine) which decreases with laser irradiation.

These results are consistent with the results obtained from the fluorescence microscope and the WST assay; in fact, both analyses confirm that when cells are exposed to a concentration of 50 μg/ml of MPNPs-Au and irradiated with laser light, HO-1-N1 cells undergo apoptosis and have metabolic alteration.

Thanks to the results obtained through the laser induced phototherapy analysis, is possible to assume that the correct concentration of MPNPs-Au is significantly important to allow the laser irradiation be effective on tumouriogenic cells, in fact is visible that when the synergistic effect of MPNPs-Au and 5 minutes of laser irradiation take place, the apoptosis in cancer cell is induced while no effect is shown on healthy ones. This means that the MPNPs-Au are able to convert the received light into thermal energy when irradiated with laser source and to start apoptosis only in cancer cells due their higher sensitivity to heat with respect to the healthy ones.

1. Miola, M. *et al.* Reductant-free synthesis of magnetoplasmonic iron oxide-gold nanoparticles. *Ceram. Int.* **43**, 15258–15265 (2017).
2. Multari, C. *et al.* Magnetoplasmonic nanoparticles for photothermal therapy. *Nanotechnology* **30**, 255705 (2019).
3. Ormelli, C. Magnetoplasmonic nanoparticles for photothermal therapy. (Politecnico di Torino, 2019).
4. Li Quadri, T. Sintesi e caratterizzazione di nanoparticelle magnetoplasmoniche per applicazioni biomediche= Synthesis and characterization of magnetoplasmonic nanoparticles for biomedical applications. (Politecnico di Torino, 2019).
5. Bruce, I. J. *et al.* Synthesis, characterisation and application of silica-magnetite nanocomposites. *J. Magn. Magn. Mater.* **284**, 145–160 (2004).
6. Singh, R. K., Kim, T.-H., Patel, K. D., Knowles, J. C. & Kim, H.-W. Biocompatible magnetite nanoparticles with varying silica-coating layer for use in biomedicine: Physicochemical and magnetic properties, and cellular compatibility. *J. Biomed. Mater. Res. Part A* **100A**, 1734–1742 (2012).
7. Răcuciu, M., Creanga, D. & Airinei, A. Citric-acid-coated magnetite nanoparticles for biological applications. *Eur. Phys. J. E. Soft Matter* **21**, 117–121 (2006).
8. Liu, Y., Li, Y., Li, X.-M. & He, T. Kinetics of (3-Aminopropyl)triethoxylsilane (APTES) Silanization of Superparamagnetic Iron Oxide Nanoparticles. *Langmuir* **29**, 15275–15282 (2013).
9. Mohammad-Beigi, H., Yaghmaei, S., Roostaazad, R., Bardania, H. & Arpanaei, A. Effect of pH, citrate treatment and silane-coupling agent concentration on the magnetic, structural and surface properties of functionalized silica-coated iron oxide nanocomposite particles. *Phys. E Low-dimensional Syst. Nanostructures* **44**, 618–627 (2011).
10. Bacri, J.-C., Perzynski, R., Salin, D., Cabuil, V. & Massart, R. Ionic ferrofluids: A crossing of chemistry and physics. *J. Magn. Magn. Mater.* **85**, 27–32 (1990).
11. Klein, N. D., Hurley, K. R., Feng, Z. V. & Haynes, C. L. Dark field transmission electron microscopy as a tool for identifying inorganic nanoparticles in biological matrices. *Anal. Chem.* **87**, 4356–4362 (2015).
12. Islam, N. U. *et al.* A multi-target therapeutic potential of Prunus domestica

gum stabilized nanoparticles exhibited prospective anticancer, antibacterial, urease-inhibition, anti-inflammatory and analgesic properties. *BMC Complement. Altern. Med.* **17**, (2017).

13. Young, J. *et al.* Size-controlled synthesis of monodispersed gold nanoparticles via carbon monoxide gas reduction. *Nanoscale Res. Lett.* **6**, 428 (2011).
14. Min, J., Metals, N. & Metals, N. Section B : Metallurgy KINETICS AND MECHANISM OF THE REACTION OF GOLD (III) CHLORIDE COMPLEXES WITH FORMIC ACID. **51**, 133–142 (2015).
15. Ojea-jime, I. & Campanera, J. M. Molecular Modeling of the Reduction Mechanism in the Citrate- Mediated Synthesis of Gold Nanoparticles. (2012).
16. Pantoja, M. & González-Rodríguez, H. Study by infrared spectroscopy and thermogravimetric analysis of Tannins and Tannic acid. *Rev. Latinoam. química* **39**, 107–112 (2010).
17. Veisi, H., Moradi, S. B., Saljooqi, A. & Safarimehr, P. Silver nanoparticle-decorated on tannic acid-modified magnetite nanoparticles (Fe3O4@TA/Ag) for highly active catalytic reduction of 4-nitrophenol, Rhodamine B and Methylene blue. *Mater. Sci. Eng. C* **100**, 445–452 (2019).
18. Aromal, S. A. & Philip, D. Facile one-pot synthesis of gold nanoparticles using tannic acid and its application in catalysis. *Phys. E Low-dimensional Syst. Nanostructures* **44**, 1692–1696 (2012).
19. Correa, J. R. *et al.* Structure and superparamagnetic behaviour of magnetite nanoparticles in cellulose beads. *Mater. Res. Bull.* **45**, 946–953 (2010).
20. Estelrich, J. & Busquets, M. A. Iron Oxide Nanoparticles in Photothermal Therapy. *Molecules* **23**, (2018).
21. Ahmad, T. Reviewing the Tannic Acid Mediated Synthesis of Metal Nanoparticles. *J. Nanotechnol.* **2014**, 954206 (2014).
22. Gali-Muhtasib, H. U., Yamout, S. Z. & Sidani, M. M. Tannins protect against skin tumor promotion induced by ultraviolet-B radiation in hairless mice. *Nutr. Cancer* **37**, 73–77 (2000).
23. Zhang, J. *et al.* Tannic acid mediated induction of apoptosis in human glioma

Hs 683 cells. *Oncol. Lett.* **15**, 6845–6850 (2018).

24. Kitching, H., Kenyon, A. J. & Parkin, I. P. The interaction of gold and silver nanoparticles with a range of anionic and cationic dyes. *Phys. Chem. Chem. Phys* **44**, 6050–6059 (2014).
25. Ajdary, M. *et al.* Health Concerns of Various Nanoparticles: A Review of Their in Vitro and in Vivo Toxicity. *Nanomater. (Basel, Switzerland)* **8**, 634 (2018).
26. Yao, Y., Zang, Y., Qu, J., Tang, M. & Zhang, T. The Toxicity Of Metallic Nanoparticles On Liver: The Subcellular Damages, Mechanisms, And Outcomes. *Int. J. Nanomedicine* **14**, 8787–8804 (2019).
27. Shen, Y., Xu, F., Wei, L., Hu, F. & Min, W. Live-Cell Quantitative Imaging of Proteome Degradation by Stimulated Raman Scattering. *Angew. Chemie Int. Ed.* **53**, 5596–5599 (2014).
28. Huang, X. & El-Sayed, M. A. Gold nanoparticles: Optical properties and implementations in cancer diagnosis and photothermal therapy. *J. Adv. Res.* **1**, 13–28 (2010).

Chapter 7

Conclusions and perspectives

The main objective of the activities conducted during the present PhD work, was aimed to prepare new hybrid nanoplatforms (MPNPs) for a potential use in photothermal therapy of cancer.

In particular, the first aim of this thesis was to produce a facile and reproducible synthesis useful to develop the hybrid nanoplatforms composed of a magnetic core and an external gold or silver NPs decoration, maintaining the peculiar properties of both nanomaterials.

Another important objective was to find the best synthesis procedure in terms of materials, properties, scalability and cost-efficiency by means of the innovative use of tannic acid (TA). In fact, many strategies were tried in order to obtain the best synthesis method by means of TA, which was also proposed as stabilizing and reducing agent to create a new, simple and green synthesis method.

An additional aim of the work was to investigate the cytotoxicity of the as-prepared MPNPs in contact with different cells in order to evaluate their potential use for biomedical application and to study the ability of the nanoplatforms to work as phototherapy system in contact with cancer cells.

In detail, MPNPs-Au and MPNPs-Ag were prepared through different synthesis methods in order to obtain nanoplatforms composed of a magnetic core and an external AuNP or Ag NPs decoration, which maintains the peculiar properties of both nanomaterials and characterized by homogeneous size and distribution. An optimization process of the synthesis procedure was performed in order to identify the best route in terms of size, morphology, structure, composition, magnetic response and plasmonic properties for generating the hybrid nanoplatforms.

Specifically, with the aim to reduce the gold and the silver salts directly on SPIONs surface, the innovative use of TA was selected as reducing agent; moreover, an optimization process was performed by using TA as reducing and stabilizing agent, which successfully allowed to remove all other chemicals.

The synthesis selection process leds to identify the best synthesis route among the first route in which CA was used as stabilizing, APTES as functionalizing and TA as reducing agent; and second route in which TA was used as the sole reagent to work as a stabilizing and reducing agent both for MPNPs-Au and MPNPs-Ag, selecting the second synthesis route as the most promising ones in both cases. In fact, with second synthesis route TA was used as reducing and stabilizing agent, this allow to synthetize the nanoplatforms with a new green synthesis method, able to reduce the synthesis step and costs by avoiding the use of other reagents as citric acid and APTES instead used in first synthesis route. Moreover, it shows promising results in terms of reproducibility, structural results, dimension and dispersion of NPs as well as magnetic response and plasmonic properties.

In fact, regarding MPNPs-Au the second route allows to generate nanocomposites composed by a large number of Au NPs on the SPIONs surface with a very good distribution in dispersion and size (around 20 nm); moreover, thanks to this process synthesis, it is possible to appreciate a high concentration of Au NPs anchored to SPIONs surface which is not visible on the images coming from the first route. This is also confirmed by the UV-Vis analysis, which shows an important gold absorbing peak with respect to the ones coming from the first route. The same happens for MPNPs-Ag, which shows a very good distribution with an Ag NPs size ranging from 20 to 100 nm, the high distribution of Ag NPs on SPIONs is confirmed by the absorbing peak at 420 nm. In both syntheses, the

magnetic and optical properties show better results in terms of saturation magnetization and heat generation respectively, as discussed in chapter 6.3.

On the base of the results obtained from the physical, chemical, magnetic and optical characterizations, it can be affirmed that the use of TA as reducing and stabilizing agent, significantly affect the morphology and the properties of the MPNPs-Au and MPNPs-Ag, showing better results for MPNPs-Au, which was identified as the most promising synthesis in terms of structural results, reproducibility and optical properties.

Based on this choice, the synthesis was further optimized with toluidine blue and the gold absorbing peak was successfully enhanced to higher wavelength increasing the chances of success of the photothermal therapy by shifting the peak, which ensure deep penetration of the radiation in the tissues.

The cytotoxicity assessment was performed in all the four syntheses in order to evaluate the difference among them. The analyses evidenced that in case of RCBs hemolysis the NPs toxicity at 35 and 100 μg/mL concentrations, is negligible and therefore they are potentially usable for biomedical application. Looking at the cytocompatibility performed on healthy and cancer cells, we observed that in HGF cells after 6 hours of exposition, the cells viability resulted as >60% but after 24 hours of direct contact, a general decrease in cells viability was observed for all the tested concentration, while the melanoma A2058 cells results, show much more resistance to the NPs due to their higher ability to skip toxic effects with respect to HGF cells. Moreover, the Ag-doped NPs reported a higher toxicity in comparison to the Au-doped ones applied in the same conditions and concentrations; therefore, HGF cells demonstrated to be more prone in tolerating gold rather than silver which can be an interesting result for the future application of the laser-induced phototherapy for biomedical purposes.

With the aim to obtain a preliminary evaluation of the photothermal power of the as synthetized NPs, the MPNPs-Au were used to accomplish the analyses and the tests provided information on the best MPNP concentration to bring HO-1-N-1 cells to apoptosis without having a negative effect on HGF cells, the result being 50 μg/mL. Upon laser irradiation, any detrimental effect on HGF cells were shown, while the tumoral ones underwent apoptosis and show metabolic alteration.

This confirmed the ability of Au NPs to be used as tool for photothermal therapy by converting the received light into thermal energy and to induce apoptosis in cancer cells without affecting the viability of healthy ones when irradiated with a laser source.

In conclusion, with this work a facile and reproducible synthesis method was designed and used to develop new hybrid nanoplatforms (MPNPs) composed of a magnetic core and an external Au NPs or Ag NPs decoration, which maintains the peculiar properties of both nanomaterials. The tannic acid was successfully used as reducing and stabilizing agent able to reduce the metal NPs directly on SPIONs surface and to stabilize the suspension, optimizing the synthesis and creating an innovative green synthesis method, which allows to remove all other chemicals.

The synergy and the combined effect of SPIONs and Au NPs allows us to maintain the possibility of precisely driving the MPNPs to a specific tumour site using an external magnetic field, due to their superparamagnetic response, and to produce heat by converting the light received from laser irradiation into thermal energy, due to the Au NPs' decoration.

Thus, these hybrid nanoplatforms have great potential for use in photothermal therapy in cancer.

Moreover, the characterization results of the as obtained MPNPs colloids may help to improve knowledge about magnetic and plasmonic nanoparticles used in biomedical applications. Further studies will attempt to obtain nanoplatforms that can be used in deeper areas of the body. In fact, by changing the shape of Au NPs (ie. Au Nanorods), it is possible to shift the absorption peak in the NIR region, this would be useful to allow a better absorption of laser irradiation even in deeper tissues. In this way, we will be able to get multifunctional colloids with great potential for nanoparticle based diagnostic and therapeutic applications, such as magnetic photothermal therapy treatments, useful not only for superficial areas of the body, but also to treat more deeply tumors.